國立臺灣大學生命科學院植物科學研究所

博士論文

Institute of Plant Biology

College of Life Science

National Taiwan University

Doctoral Dissertation

地錢細胞色素P450受tasiRNA及微型核酸雙調控機制研究及大岩桐花瓣原生質體暫時性表達系統之建立

Dual regulation of cytochrome P450 expression by tasiRNA and microRNA in *Marchantia polymorpha* and the establishment of *Sinningia* petal protoplast transient expression system

洪育翎

Yu-Ling Hung

指導教授：王俊能、林詩舜、鄭石通 博士

Advisors: Chun-Neng Wang, Shih-Shun Lin, Shih-Tong Jeng Ph.D.

中華民國 113 年 5 月

May 2024

doi:10.6342/NTU202404007

致謝

攻讀博士是條漫漫長路，驀然回首，居然也走過了七年的時光，其間無數次的迷惘、懷疑這條道路、徘徊在放棄與堅持之間，最終，總算是完成了這段蛻變的旅程。在這段旅程中，我由衷的感謝指導教授王俊能教授、林詩舜教授和鄭石通教授。謝謝王老師帶領著我的研究從開花植物大岩桐一路做到蘚苔類植物地錢，到日本京都大學交換學習新的技術，在這其間我在研究的學海中迷航，找不到方向，甚至一度陷入一片黑暗，看不見任何希望的曙光，我也因此休學，停下腳步，重新審視自己未來的道路。而林老師就像是上天給的禮物，我們僅在國際研討會中有過一次交流，林老師卻記住了我們的研究，在隔年的國際研討會中，他們最新發表的分析資料居然與我們的停滯的研究相關，在得知我休學的消息後，關心的詢問我是否想重啟博士班的研究，這份分析資料就像是曙光，林老師就是指路明燈，為我的研究從黑暗中開闢出一條全新的道路，對林老師的感謝無法言喻。鄭老師則是在學術領域上給了我最大的自由度及支持。三位指導教授就是我研究生涯中的領航人，帶領著我前進，指引我方向，謝謝老師們，我的博士旅途才能完成!此外，感謝口試委員 Aino Komatus 博士、Ryuichi Nishihama 博士、吳素幸博士、邱子珍博士、陳荷明博士審閱我的論文並給予寶貴的建議，讓我將博士論文修繕的更加完整。

在博士班的生涯中，要感謝許多人的幫助，才能完成這本論文。謝謝京都大學 Takayuki Kohchi 教授讓我在他的實驗室學習技術，也謝謝這期間元琦一起分擔龐大的工作量及孫芮協助我們建築所有需要的載體，因為有你們，我在日本度過了一段忙碌但愉快的時光。謝謝冠霆學長人生道路上的建議，讓我更全面的去思考，下每個重要的決定。謝謝盈綺在實驗室帳務處理上多方的幫忙，在你身上我學會堅定自我，還有實驗之餘偶爾要小小的放風，例如去送個公文，體驗實驗以外的業務。謝謝 Abigail、Veny、Thanh ha、Pookiie、欣平、如瑩、薇倫、瑄斐、芊燕、芳英、炳男、昭慈、鄭璇、俞如、亮合、詠丞、佳蓁大家一起分擔實驗室的工作，一起舉辦派對，411 真的是一個有愛的實驗室，很開心能與你們共事。特別感謝昭君學姊從碩士到博士一路上的幫忙，不管是實驗設計、實驗問題排除、論文寫作、文章投稿等疑難雜症，學姊的經驗與建議總是讓我受益良多!

最後的感謝獻給鼓勵、陪伴我的家人們，有你們我才能堅持住，尤其是先生宜倫在最後論文撰寫及準備口試期間一肩擔下照顧幼嬰芸析的重任，讓我可以專心的完成這最後一哩路。

doi:10.6342/NTU202404007

摘要

植物的微型核酸 (miRNAs) 在後轉錄層級調控目標基因的表現，控制著植物生長發育的過程。其中，保守性的 miRNAs 在植物發育的所有方面幾乎都發揮了至關重要的作用。本論文的研究展示保守的 miR390 在基礎陸地植物地錢中的分子調控機制及功能並建立了開花植物中花瓣原生質體暫時性轉殖系統，為研究 miR390 調控開花相關基因提供了一個技術平台。在第二章中，研究顯示在地錢中 miR390 透過裁切 *TAS3* 轉錄本產生轉導性短干擾 RNAs (tasiRNAs)，從中找到一個大量表現的 tasiRNA，tasi78A，並預測到其目標基因為一個細胞色素 P450 基因，Mp*CYP78A101*。同時還預測到 Mp*CYP78A101* 受到另一個 miRNA, miR11700 共同調控。透過暫時性轉殖系統驗證了 tasi78A 及 miR11700 負向調控 Mp*CYP78A101*，並且可能通過調控生長素訊息來影響地錢的無性生殖器官孢芽 (gemma) 以及有性生殖器官的生長發育。第三章則是建立了開花植物苦苣苔屬中大岩桐的花瓣原生質體暫時性轉殖系統，將切成條狀的花瓣浸泡在 1.5%纖維素酶 (cellulase) 和 0.4% 離析酶 (macerozyme) 的酵素溶液中六小時，可獲得高產量的花瓣原生質體，並達到 41.4%的轉殖效率。本論文對於保守的 miR390 從基礎陸地植物到開花植物在演化上、基因調控機制及功能性將有更全面的了解。

關鍵字：miR390/*TAS3*、tasiRNA 生合成、生長素訊息、Mp*CYP78A101*、地錢、大岩桐、原生質體

doi:10.6342/NTU202404007

Abstract

Plant microRNAs (miRNAs) regulate target gene expression at the post-transcriptional level and control the growth and development of plants. Among them, conserved miRNAs play key roles in plant development, with functions spanning almost all aspects. This study unveils the molecular regulatory mechanisms and functions of the conserved miR390 in the basal land plant, *Marchantia polymorpha*. Moreover, a petal protoplast transient transformation system in flowering plant was established, providing a technical platform for investigating miR390 regulation of flowering-related genes. In Chapter 2, we demonstrated that miR390 generates trans-acting short-interfering RNAs (tasiRNAs) by cleaving *TAS3* transcripts in *M. polymorpha*. Among these tasiRNAs, one highly expressed tasiRNA, tasi78A, was identified, and its target gene was predicted to be a cytochrome P450 gene, Mp*CYP78A101*. Moreover, we further predicted that Mp*CYP78A101* is co-regulated by another miRNA, miR11700. Using a transient transformation system, we validated that tasi78A and miR11700 negatively regulate Mp*CYP78A101* and potentially affect the development of asexual reproductive organs (gemmae) and sexual organs through auxin signaling. In Chapter 3, we established a petal protoplast transient transformation system in the flowering plant Gloxinia (*Sinningia speciosa*). By immersing petal strips in an enzyme solution containing 1.5% cellulase and 0.4% macerozyme for 6 hours, we obtained high yields of petal protoplasts and achieved a transformation efficiency of 41.4%. This study provides a further understanding of the evolution, gene regulatory mechanisms, and functional roles of conserved miR390 from basal land plants to flowering plants.

Keywords: miR390/*TAS3*, tasiRNA biogenesis, auxin signaling, Mp*CYP78A101*, *Marchantia polymorpha*, *Sinningia speciosa*, protoplast

doi:10.6342/NTU202404007

Content

doi:10.6342/NTU202404007

doi:10.6342/NTU202404007

doi:10.6342/NTU202404007

doi:10.6342/NTU202404007

doi:10.6342/NTU202404007

Chapter 1

Literature review

doi:10.6342/NTU202404007

1.1 Introduction

In plants, endogenous small RNAs, including micro RNAs (miRNAs) and short-interfering RNAs (siRNAs), serve as negative regulators for gene expression in the post-transcriptional level (Bartel, 2004). Small RNAs are loaded into ARGONAUTE (AGO) proteins to form RNA-induced silencing complexes (RISCs), which then silence mRNAs that are complementary to the sRNA sequence. This silencing can take the form of degradation of the mRNA transcripts or inhibition of their translation into proteins (Pratt and MacRae, 2009; Axtell, 2013). Increasingly, studies demonstrate that small RNAs play a crucial role in plant development processes by regulating transcription factors and contributing to plant responses to stress, environmental adaptation, and morphological diversity (Bonnet et al., 2006; Chen, 2009; D'Ario et al., 2017). Some small RNAs are conserved across land plants and play a key role in most aspects of developmental control in plants (Axtell et al., 2007; Chen, 2009; Axtell, 2013; You et al., 2017), highlighting their importance. Chapter 1 summarizes the current understanding of the molecular regulatory mechanisms and functional studies of conserved small RNAs, as well as how to establish a transient transfection system to validate the molecular mechanisms of small RNAs.

1.2 RNA silencing

1.2.1 Biogenesis and types of small RNAs

Regulatory small RNAs refer to a group of nucleotide (nt) molecules ranging from 20 to 30 in length, which govern RNA-level regulation and influence plant morphogenesis, stress response, auxin response, and other processes (Chen, 2009; Chuck et al., 2009; Axtell, 2013). Small RNAs can be divided into two major categories based on their biogenesis process (Axtell, 2013). One category is miRNAs, which are formed from single-stranded RNA with hairpin structures. The other category is

doi:10.6342/NTU202404007

siRNAs, which are derived from double-stranded RNA (dsRNA) precursors.

MiRNAs are approximately 21-nts in length and are transcribed from *MIR* genes by RNA polymerase II (Pol II) into single-stranded primary miRNAs (pri-miRNAs) (Xie et al., 2005). Pri-miRNAs then fold into hairpin structures and are recognized by the DICER-LIKE1 (DCL1), zinc finger protein SERRATE (SE) and the dsRNA-binding protein HYPONASTIC LEAVES1 (HYL1), processing them into precursor-miRNAs (pre-miRNAs) (Han et al., 2004; Yang et al., 2006; Song et al., 2007). Next, DCL1 continues to cleave pre-miRNAs to produce miRNA/miRNA* duplexes (Axtell et al., 2011). In contrast, siRNAs originate from single-stranded RNAs (ssRNAs) produced endogenously by plants via RNA polymerase IV (Axtell, 2013) or acquired from viral infections. These single-stranded RNAs are then used as templates by RNA-dependent RNA Polymerases (RdRps) to generate dsRNAs (Carthew and Sontheimer, 2009; Axtell, 2013). Subsequently, DICER cleaves the dsRNAs into siRNA duplexes (Henderson et al., 2006; Voinnet, 2008). Both miRNA and siRNA duplexes are loaded into AGO proteins to form RISC and regulate downstream genes (Takeda et al., 2008).

1.2.2 The conservation of miRNA

MiRNAs are more conserved than siRNAs. The individual miRNAs being conserved across different plant species, along with their target genes (Zhang et al., 2006; Willmann and Poethig, 2007; Jones-Rhoades, 2012). In contrast, individual siRNAs may not necessarily be conserved among closely related species because their positions often overlap with transposons (Axtell, 2013). Therefore, new siRNAs may be generated or lost during evolution due to changes in transposon position or copy number. Consequently, regarding the evolutionary history of small RNAs in plants, miRNAs have a stronger advantage. Currently, ten miRNA families are known to have high conservation to all land plants. These ten miRNA families are miR156, miR160,

doi:10.6342/NTU202404007

miR166, miR171, miR319/159, miR390, miR395, miR396, miR408, and miR535 (Alaba et al., 2015). Among these conserved miRNAs, miR390 is particularly notable as it can generate secondary siRNAs by loading into the AGO7 protein (Allen et al., 2005; Axtell et al., 2006; Montgomery et al., 2008a). These secondary siRNAs, which originate from specific genomic loci in a phased pattern and direct the cleavage of protein-coding transcripts in trans, referred to as trans-acting short interfering RNAs (tasiRNAs) (Vazquez et al., 2004; Allen et al., 2005; Yoshikawa et al., 2005).

1.3 The knowledge of miR390

1.3.1 miR390 specifically loads into AGO7

In plants, most miRNAs are loaded into AGO1 (Vaucheret et al., 2004; Mi et al., 2008; Liang et al., 2023) to regulate target mRNAs negatively, but miR390 is specifically loaded into AGO7 (Montgomery et al., 2008a). While most miRNAs have a 5' terminal U, miR390 has a 5' terminal A. Additionally, AGO7 exhibits a preference for 5' terminal A and specifically recognizes the central region (G-A mismatch, guide position 11) and seed region (G-U wobble, guide position 3) of the miR390/miR390* duplex (Endo et al., 2013). These factors contribute to the specific loading of miR390 into AGO7, rather than into AGO1, which prefers 5' terminal U (Kim, 2008; Mi et al., 2008).

1.3.2 The regulatory mechanism and function of miR390

In Arabidopsis, miR390 cooperates gene silencing components, including DICER-LIKE 4 (DCL4), HUA ENHANCER 1 (HEN1), RNA-DEPENDENT RNA POLYMERASE 6 (RDR6), SUPPRESSOR OF GENE SILENCING 3 (SGS3), DOUBLE-STRANDED RNA BINDING (DRB) and ARGONAUTE 7 (AGO7) (Allen et al., 2005; Pegler et al., 2019), to cleave a non-coding transcript, *TRANS-ACTING*

doi:10.6342/NTU202404007

SIRNA 3 (*TAS3*), and generates tasiRNAs. The transcript of *TAS3* bears two recognition sites for miRNA390 targeting and the biogenesis of tasiRNAs followed the "two-hit" mechanism (Axtell et al., 2006; de Felippes et al., 2017). The AGO7-miR390 RNA-induced silencing complex (RISC) triggered cleavage at the 3' target site, while the 5' target site contained a central mismatch that interfered with the AGO7 cleavage (Montgomery et al., 2008a). Therefore, the 'two-hit and one-cleavage' configuration ensured that the production of tasiRNAs was phased in relation to their specific position with 21-nt (Axtell et al., 2006; Montgomery et al., 2008a; Fei et al., 2013; de Felippes et al., 2017). Among these tasiRNAs, there are two tandem tasiRNAs, known as tasiARFs, as they guide the degradation of *AUXIN RESPONSIVE FACTOR* (*ARF*) genes, which is crucial for auxin signals (Allen et al., 2005; Axtell et al., 2006). This molecular mechanism is called miR390/*TAS3*/*ARF* module. The miR390/*TAS3*/*ARF* module is evolutionarily conserved among both dicots and monocots (Xia et al., 2017; Luo et al., 2021). Many conserved miRNAs are abundantly expressed, and they regulate the transcript factors involved in the development control (Axtell and Bowman, 2008). Indeed, in angiosperm, this conserved miR390/*TAS3*/*ARF* pathway plays an important role in developmental progression, including reproductive development (Ding et al., 2020), root architecture (Marin et al., 2010), and adaxial-abaxial polarity of leaf and flower (Chitwood et al., 2009; Braybrook and Kuhlemeier, 2010; Nien, 2018).

1.3.3 The conservation of miR390/*TAS3* module

To date, four *TAS* gene families were defined in Arabidopsis (Allen et al., 2005; Axtell et al., 2006; Rajagopalan et al., 2006), but only the *TAS3* family is present among the land plants, including monocots (Williams et al., 2005; Heisel et al., 2008), fern (Berruezo et al., 2017) and non-vascular land plants(Axtell et al., 2006; Axtell et al., 2007; Tsuzuki et al., 2016; Morozov et al., 2018). The presence of miR390 and *TAS3*

doi:10.6342/NTU202404007

can be traced back to the transition from charophyte algae to the earliest common ancestor of land plants (Morozov et al., 2018). Moreover, compared to the highly conserved miR390, *TAS3*-like loci are divergent into varied classes along with the main taxa of *Bryopsida*, *Marchantiophyta*, and *Sphagnopsida* among non-vascular plants (Morozov et al., 2018). Six *TAS3* genes have been identified in moss, *Physcomitrium patens* (Axtell et al., 2007; Arif et al., 2012), while only one *TAS3* gene has been detected in liverwort, *Marchantia polymorpha* (Xia et al., 2017; Lin and Bowman, 2018). While *TAS3* genes exhibit remarkable evolutionary diversity, they all share a common requirement for miR390 target sites to initiate tasiRNA biogenesis. Interestingly, tasiRNAs production occurs through diverse mechanisms. The simplest mode only requires a single miR390 targeting event to produce tasiRNAs (de Felippes et al., 2017). In Arabidopsis, it follows a 'two-hit and one-cleavage' model, with tasiRNAs generated from the cleaved 3' miR390 target site. In contrast, bryophytes, such as *P. patens* and *M. polymorpha*, possess two miR390 target sites. *P. patens* generates tasiRNAs from both ends of these sites (Axtell et al., 2007), while *M. polymorpha* shows evidence of degradation at both sites (Lin and Bowman, 2018), implying a similar bidirectional tasiRNA production. These examples indicate that bryophytes might employ a 'two-hit and two-cleavage' model. Although the miR390/*TAS3* module is conserved, the subsequent generation of tasiRNAs differs significantly between flowering plants and bryophytes. Flowering plants predominantly produce tasiRNAs from a single cleavage site, while bryophytes may tend to produce a greater variety of tasiRNAs bidirectionally from both cleavage sites.

1.4 The miR390/*TAS3* module in bryophytes

1.4.1 The possible diverse function for miR390/*TAS3* module in bryophytes

The miR390/*TAS3* module is a conserved regulatory mechanism in the land plants

doi:10.6342/NTU202404007

(Xia et al., 2017), but its regulatory mechanisms and functional aspects in bryophytes remain largely unexplored. In *P. patens*, overexpression of miR390 leads to tasiRNAs accumulation and delays the transition from young protonemata to adult leafy gametophores (Cho et al., 2012). However, this phase transition is not only regulated by miR390 but also by miR156. In *P. patens*, miR156 not only targets downstream genes *SQUAMOSA PROMOTER BINDING PROTEIN-LIKE* (*SPL*) genes but also cleaves *TAS6* to generate tasiRNAs and suppresses tasiRNAs produced from miR390-cleaved *TAS3*. The phase transition in moss is coordinately regulated by the miR156 and miR390 regulatory network (Cho et al., 2012). In bryophytes, miR390 cleaves *TAS3* to generate not only tasiARF but also tasiAP2 (Axtell et al., 2007; Krasnikova et al., 2013; Morozov et al., 2018). TasiAP2 has been identified to target mRNAs containing AP2 domains, while tasiARF targets mRNAs containing B3 and ARF domains (Talmor-Neiman et al., 2006; Axtell et al., 2007). While tasiAP2 sequences are conserved in bryophytes, the tasiARF sequences are distinct in *P. patens* and *M. polymorpha* (Axtell et al., 2007; Xia et al., 2017; Morozov et al., 2018). Moreover, tasiAP2 exhibits relatively low abundance in *M. polymorpha* small RNAs profile, and its potential target genes has not been identified in the current literature (Xia et al., 2017; Lin and Bowman, 2018). These findings suggest potential divergence in the regulatory mechanisms of the miR390/*TAS3* module between *P. patens* and *M. polymorpha*.

1.4.2 Advantages of studying *M. polymorpha*

M. polymorpha is a dioecious haploid liverwort, its life cycle is mainly dominated by the haploid gametophyte, and it also exhibits low genetic redundancy in most regulatory pathways (Bowman et al., 2017). These characteristics are helpful for functional genetic analyses. In addition, the nuclear and organellar genomes of *M. polymorpha* has been sequenced (Ohyama et al., 1988; Ohyama, 1996; Shimamura,

doi:10.6342/NTU202404007

2016; Bowman et al., 2017), the sequence, structure, annotation, promoter sequence, the copy number of genes, miRNAs information (Lin et al., 2016; Tsuzuki et al., 2016) can be available on the website: Marpolbase (http://marchantia.info/). Moreover, *Agrobacterium*-mediated transformation system, CRISPR/Cas9 knockout system, and transient transformation system have been well developed in *M. polymorpha* (Ishizaki et al., 2008; Shen et al., 2014; Tsuboyama and Kodama, 2014; Tsuboyama-Tanaka and Kodama, 2015; Iwakawa et al., 2021), the transformants could be available within one month. A series of Gateway binary vectors designed for transgenic experiments on *M. polymorpha* are also well development (Ishizaki et al., 2015). All of these advantages promote the *M. polymorpha* to be an excellent model to investigate the conservation and diversification of miR390/*TAS3* module during land plant development and evolution.

1.4.3 Recent study of small RNA-mediated gene silencing pathway and miR390/*TAS3* module in *M. polymorpha*

In *M. polymorpha*, a set of components involved in RNA-mediated gene silencing including MpDCL1a (Mp1g02840), MpDCL1b (Mp7g12090), MpHYL1 (Mp7g08450), MpHEN1 (Mp3g16010), MpDCL4 (Mp7g11720), MpAGO1 (Mp1g18110), MpAGO4a (Mp1g23190), MpAGO4b (Mp6g20400), MpAGO9 (Mp8g08610), and MpRDR6 (Mp8g14970) were defined (Lin et al., 2016; Bowman et al., 2017), suggests the presence of a functional RNA silencing pathway in this organism. The biochemical functions of these proteins have not yet been reported, and some of them lack some functional domains comparing to that in Arabidopsis (Pietrykowska et al., 2022). However, the newly discovered miR11707.1 and miR11707.2 in *M. polymorpha* have been shown to target MpAGO1, confirming the existence of small RNA-mediated gene silencing in *M. polymorpha* (Lin et al., 2016).

doi:10.6342/NTU202404007

Seven conserved miRNAs have been identified in liverworts, including miR160, miR166, miR171, miR319/miR159, miR390, miR408, and miR529/miR156 (Lin et al., 2016; Tsuzuki et al., 2016; Pietrykowska et al., 2022). Most of these miRNAs negatively regulate transcription factors(Lin et al., 2016; Pietrykowska et al., 2022), highlighting their importance in plant growth and development.

As a basal land plant, *M. polymorpha* exhibits low genetic redundancy (Bowman et al., 2017), only single miR390 gene and single *TAS3* gene has been identified (Krasnikova et al., 2013; Lin et al., 2016; Tsuzuki et al., 2016; Xia et al., 2017; Lin and Bowman, 2018). It is well known that miR390 is specifically loaded into AGO7 to form an RISC to cleave the *TAS3* transcripts and produce tasiRNAs in Arabidopsis (Montgomery et al., 2008a). However, no *AGO7* gene has been identified in *M. polymorpha* (Bowman et al., 2017), and the ancestor of the AGO7 emerged from seeds plants based on the phylogenetic analysis (Xia et al., 2017). The miR390 should be loaded into other AGO proteins for tasiRNA biogenesis in *M. polymorpha*.

To data, only four AGO-like proteins have been found in *M. polymorpha*, one is MpAGO1, and the other three are MpAGO4a and MpAGO4b, and MpAGO9 (Tsuzuki et al., 2016; Bowman et al., 2017). In Arabidopsis, AGO1 and AGO4 respond to miRNA post-transcriptional gene silencing (PTGS) and the RNA-directed DNA methylation (RdDM) pathway, respectively. In contrast, AGO9 exhibits a preference for binding to 24-nucleotide small RNAs derived from transposable elements (TEs) (Duran-Figueroa and Vielle-Calzada, 2010; Olmedo-Monfil et al., 2010). This raises a critical question: which AGO protein is responsible for cleaving *TAS3* in response to miR390, leading to the generation of tasiRNAs? In addition, the RNA silencing components including MpDCL1a (Mp1g02840), MpDCL1b (Mp7g12090) MpDCL4 (Mp7g11720), MpAGO1 (Mp1g18110), and MpRDR6 (Mp8g14970), might contribute to tasiRNA biogenesis for the miR390/*TAS3* module. While Xia et al. (2017) suggested that the

doi:10.6342/NTU202404007

primary function of the conserved miR390/*TAS3* module is the regulation of *ARF* genes in *M. polymorpha* (Xia et al., 2017), degradome data revealed only five reads at the cleavage site of *ARF* in tasiARF. Thus, the regulation of *ARF* by tasiARF in *M. polymorpha* remains unclear. In addition, the tasiARF in flowering plants specifically regulates the auxin pathway; the function or target interaction of the tasiARF sequence in *M. polymorpha* still requires validation.

In contrast to the tasiARF/*ARF* module's role in regulating auxin signaling in angiosperms, Jiang et al. (2021) found that CYP78A, a cytochrome P450 monooxygenase, activates cytokinin signaling, thereby stimulating auxin biosynthesis and increasing auxin levels (Jiang et al., 2021). The role of CYP78A in auxin accumulation or distribution has been highlighted across various plant species, including moss, monocot rice, wheat, and dicot rapeseed (Miyoshi et al., 2004; Katsumata et al., 2011; Guo et al., 2022; Zhou et al., 2022), suggesting a potential link between CYP78A and auxin. There are six members (CYP78A5-10) of the CYP78A subfamily in Arabidopsis with functional redundancy (Bak et al., 2011). In contrast, bryophytes such as *P. patens* and *M. polymorpha* have only two CYP78A members. *P. patens* possesses PpCYP78A27 and PpCYP78A28 (Katsumata et al., 2011), while *M. polymorpha* has MpCYP78A101 (Mp3g23930) and Mp1g14150. In *P. patens*, these two CYP78A members also exhibit redundant functions, as a double mutant is required to observe increased auxin levels (Katsumata et al., 2011). Given the close phylogenetic relationship between *P. patens* and *M. polymorpha*, the CYP78A members in *M. polymorpha* may also be involved in auxin-related functions and show redundant functions. While the regulatory relationship between tasiARF and *ARF* remains unclear, the conserved miR390/*TAS3* module might influence the auxin signaling pathway through tasiARF/*ARF* module or alternative mechanisms.

A transient transformation system offers a rapid and efficient method to validate

doi:10.6342/NTU202404007

the relationship between sRNAs and their target genes. Agroinfiltration, a common transient transformation technique involving the injection of *Agrobacterium* into plant tissues, is frequently used in tobacco. However, due to the thick and brittle nature of thallus of *M. polymorpha*, this method has not been applied in *M. polymorpha*. Two primary transient transformation methods have been reported in *M. polymorpha*: agropenetration and biolistics. Agropenetration involves vacuum-infiltrating *Agrobacterium* into the thallus (Iwakawa et al., 2021). Biolistics denotes coating DNA-coated gold particles and delivering them into 4-5-day-old gemmalings using a particle bombardment (Ghosh et al., 2016). Agropenetration is a more cost-effective and accessible approach for transient transformation in *M. polymorpha* compared to biolistics, which requires expensive gold particles and specialized equipment.

In Chapter 2, we focus on elucidating the regulatory mechanisms and functional roles of the miR390/*TAS3* module in *M. polymorpha*. Based on the current literature, we know that the miR390, *TAS3*, *ARF* genes, and RNA silencing-related proteins are all present in *M. polymorpha*. It is highly likely that miR390 also regulates downstream genes by cleaving *TAS3* and interacting with RNA silencing components to produce tasiRNAs in *M. polymorpha*. Besides the well-characterized downstream target gene *ARF*, we are particularly interested in studying the functions of other previously unidentified high-abundance tasiRNAs. Moreover, we aim to optimize the transient transformation system in *M. polymorpha*, as reported by Iwakawa et al. (2021), to quickly validate the regulatory mechanisms between sRNAs and their target genes.

1.5 MiR390/*TAS3* module in floral symmetry

1.5.1 Recent study of miR390/*TAS3* module in *Sinningia speciosa*

Sinningia speciosa (Lodd.) Hiern, commonly known as the florist's gloxinia, is a member of the Gesneriaceae family and a popular ornamental plant. This species is

doi:10.6342/NTU202404007

famous for its beautiful and diverse flowers, exhibiting bilateral (zygomorphic) and radial (actinomorphic) symmetry. Beyond its unique symmetry, *S. speciosa* has a remarkable range of floral characteristics, including vibrant colors, diverse shapes, and varying sizes. *Sinningia speciosa*, with its small and easy-to-cultivate genome, has recently emerged as a model plant for studying flower symmetry and diversity variations (Dong et al., 2018; Hasing et al., 2019). MiRNAs also play a role in this process, with miR159 involved in regulating flowering time, and our lab's discovery that miR390 has been co-evolved in floral zygomorphy (Li et al., 2013; Nien, 2018). Our research revealed high expression of miR390 in the ventral petal, where it likely degrades its downstream target gene, *AUXIN RESPONSIVE FACTOR3/4* (*ARF3/4*). This finding was validated through transcriptome, degradome, and qRT-PCR analyses. Conversely, *ARF3/4* was highly expressed in the dorsal petals, promoting their growth. This differential expression pattern of miR390 and *ARFs* likely contributes to developing zygomorphy (bilateral symmetry) in the flower (Nien, 2018). This miR390/*TAS3*/*ARF* module in controlling the adaxial-abaxial polarity of leaf (Chitwood et al., 2009; Braybrook and Kuhlemeier, 2010) has been co-opted in floral zygomorphy (Nien, 2018).

1.5.2 Transient transformation system

Protoplast transformation system is a powerful tool for transient expression assays (Yoo et al., 2007). This system, widely adopted for research projects requiring high-throughput analysis, has also been applied to examine signal transduction (Cao et al., 2014; Lin et al., 2013), protein-protein interaction (Andrea et al., 2006), and subcellular localization. Protoplasts maintain the cell and transcriptome identity, exhibiting regulatory activity similar to the responses observed in original tissues and plants (Faraco et al., 2011; Lin et al., 2013; Sheen, 2001; Yoo et al., 2007). Moreover, the

doi:10.6342/NTU202404007

transient expression system using protoplasts offers high efficiency and sensitivity, allowing the detection of most regulatory responses within 2-10 hours after foreign gene transformation (Yoo et al., 2007). Moreover, this system enables foreign DNA transfer independently of *Agrobacterium*, overcoming the challenge of *Agrobacterium* infection in *S. speciosa*. Therefore, we prioritize establishing a protoplast transformation system.

The protoplast transformation system can be divided into two parts: protoplast isolation and DNA transfection. To establish an efficient system, the conditions affecting protoplast isolation and DNA transfection need to be optimized. After protoplast releasing from plant tissue, the first problem is proper osmotic pressure for preventing protoplast lysis. The osmotic pressure can be adjusted with inorganic salts (KCl, NaCl, and $MgSO_4$) and/or non-metabolizable sugar (mannitol, most commonly used) (Huang et al., 2013). In addition, the suitable osmotic pressure for protoplast depends on the species, cultivar, and material source (Nanjareddy et al., 2016; Yoo et al., 2007). The osmotic pressure firstly adjusted in this study. The enzyme combination and the enzymolysis (cell wall digestion) time are important factors, which affect protoplast yield. Higher concentration of enzyme and longer enzymolysis time increase the protoplast yield, however, they also decrease cell viability (Wu et al., 2017). For protoplast isolation, the osmotic pressure, enzyme combination and enzymolysis time should be optimized in *S. speciosa* for achieving the high protoplast yield with high cell viability.

DNA transfection, there are many methods to transfer plasmid DNA into protoplast, *e.g.*, PEG-mediated, electroporation, heat shock, and microinjection. Therein, the PEG-mediated method shows the highest cell viability after plasmid DNA transformation and has the highest transformation efficiency (Nanjareddy et al., 2016; Sheen, 2001). By contrast, the electroporation and heat shock methods damage

doi:10.6342/NTU202404007

protoplast and reduce cell viability. Therefore, they have the lowest transformation efficiency (Nanjareddy et al., 2016). Based on transformation efficiency, the PEG-mediated method was used in this study. The concentration of PEG (40% PEG is commonly used), the transferring plasmid DNA/protoplast ratio, the quality of plasmid DNA, and the transfection time also need to be optimized to achieve the highest transformation efficiency (Cao et al., 2014; Lin et al., 2014; Wu et al., 2017). In Chapter 3, we aim to optimize conditions for protoplast yield and transformation efficiency to establish a transient expression system in petal protoplasts in *S. speciosa*.

1.6 Aim of this study

This study elucidates the molecular regulatory mechanisms and functional roles of the miR390/*TAS3* module in *M. polymorpha*, a basal land plant. By employing CRISPR/Cas9 gene-editing and genetic transformation techniques, we generated transgenic plants harboring Mp*mir390*^{ge} mutants and Mp*MIR390* plants. The small RNA profiles of the transgenic plants were used to assess the importance of miR390 in tasiRNA production. Interestingly, while the miR390/*TAS3* module is conserved, flowering plants and *M. polymorpha* utilize different mechanisms, 'two-hit and one-cleavage' and 'two-hit and two-cleavage', respectively, to generate siRNAs. Therefore, this study explored the differences and similarities in tasiRNA production between these two plant groups. In addition, we investigated the potential downstream genes and regulatory relationships of other highly abundant tasiRNAs in *M. polymorpha*. To further understand the involvement of the miR390/*TAS3* module in the growth and development in *M. polymorpha*, we employed promoter-reporter assays to examine its expression patterns. Notably, the miR390/*TAS3* module has co-evolved to participate in petal bilateral symmetry development in *S. speciosa*. To validate this regulatory relationship, we are developing a transient expression system using petal protoplasts.

doi:10.6342/NTU202404007

This study provides the new insights in the evolution, regulation, and function of miR390/*TAS3* module from basal land plants to flowering plants.

doi:10.6342/NTU202404007

Chapter 2

Dual regulation of cytochrome P450 gene expression by two distinct small RNAs, a novel tasiRNA and miRNA, in *Marchantia polymorpha*.

This article has been published in the Plant Cell Physiology journal.

Hung, Y. L., Hong, S. F., Wei, W. L., Cheng, S., Yu, J. Z., Tjita, V., ... & Lin, S. S. (2024). Dual regulation of cytochrome P450 gene expression by two distinct small RNAs, a novel tasiRNA and miRNA, in *Marchantia polymorpha*. Plant and Cell Physiology, 65:1115-1134.

doi:10.6342/NTU202404007

2.1 Abstract

The miR390-derived *TAS3* trans-acting short-interfering RNAs (tasiRNAs) module represents a conserved RNA silencing pathway in the plant kingdom; however, its characterization in the bryophyte *Marchantia polymorpha* is limited. This study elucidated that MpDCL4 processes Mp*TAS3* double-stranded RNA (dsRNA) to generate tasiRNAs, primarily from the 5'- and 3'-ends of dsRNA. Notably, we discovered a novel tasiRNA, tasi78A, can negatively regulate a cytochrome P450 gene, Mp*CYP78A101*. Additionally, tasi78A was abundant in MpAGO1, and transient expression assays underscored the role of tasi78A in repressing Mp*CYP78A101*. A microRNA, miR11700, also regulates Mp*CYP78A101* expression. This coordinate regulation suggests a role in modulating auxin signaling at apical notches of gemma, influencing the growth and sexual organ development of *M. polymorpha* and emphasizing the significance of RNA silencing in Mp*CYP78A101* regulation. However, phylogenetic analysis identified another paralog of the *CYP78* family, Mp1g14150, which may have a redundant role with Mp*CYP78A101*, explaining the absence of noticeable morphological changes in loss-of-function plants. Taken together, our findings provide new insights into the combined regulatory roles of miR390/Mp*TAS3*/miR11700 in controlling Mp*CYP78A101* and expand our knowledge about the biogenesis and regulation of tasiRNAs in *M. polymorpha*.

Keywords: *Marchantia polymorpha,* miR11700, miR390/Mp*TAS3*, Mp*CYP78A101*, tasi78A, tasiRNA biogenesis, auxin-signaling

doi:10.6342/NTU202404007

2.2 Introduction

Trans-acting short-interfering RNA (tasiRNA) is a unique RNA silencing mechanism in the plant kingdom. In Arabidopsis, the *TAS* transcript undergoes cleavage by a microRNA (miRNA)-AGO1 complex. Subsequently, RNA-DEPENDENT RNA POLYMERASE 6 (AtRDR6) was used to transcribe the cleaved *TAS* fragments into double-stranded RNA (dsRNA). The dsRNAs are then processed by DICER-LIKE 4 (AtDCL4), leading to the generation of 21-nucleotide (nt) tasiRNAs in a head-to-tail arrangement (Allen et al., 2005; Yoshikawa et al., 2005). In particular, *TAS3* is conserved throughout land plants (Xia et al., 2017). Studies in Arabidopsis indicate that the main components involved in *TAS3* tasiRNA biogenesis include microRNA390 (miR390), AGRONAUTE 7 (AtAGO7), AtDCL4, HUA ENHANCER1 (AtHEN1), and AtRDR6 (Allen et al., 2005; Pegler et al., 2019). The *TAS3* transcript is characterized by the presence of two miR390 target sites located at its 5'- and 3'-ends, a configuration described in the “two-hit” model (Xia et al., 2017). This unique arrangement of miR390 target sites on the *TAS3* transcript suggested that, over the course of evolution, *TAS3* loci might have developed a bidirectional processing mechanism involving these two sites (Xie et al., 2005; Axtell et al., 2006). Studies have shown that the miR390-AtAGO7 complex binds to the 5'-end target site without cleavage, while the 3'-end target site is bound and cleaved by the complex (Allen et al., 2005; Montgomery et al., 2008a). Both binding to these target sites and the 3'-end cleavage must be specifically carried out by AtAGO7 to initiate subsequent tasiRNA production (Allen et al., 2005; Montgomery et al., 2008a). The combination of miR390-AtAGO7 for *TAS3* tasiRNA production cannot be replaced by other miRNAs or AtAGO1 (Allen et al., 2005; Montgomery et al., 2008a).

In Arabidopsis, the *TAS1* and *TAS2* transcripts are activated by miR173 cleavage, while the *TAS4* transcripts are activated by miR828 cleavage (Allen et al., 2005;

doi:10.6342/NTU202404007

Rajagopalan et al., 2006; Montgomery et al., 2008b; Cuperus et al., 2010; Luo et al., 2012). Both miR173 and miR828 are 22-nt in length miRNAs and are loaded into AtAGO1 to initiate tasiRNA biogenesis. In contrast, miR390 is 21-nt in length, indicating that the mechanism of *TAS3* tasiRNA production differs from that of other TASs. The genome of *Marchantia polymorpha*, a bryophyte, encodes miR390 but does not contain AGO7, raising the question of whether MpAGO1 carries miR390. Additionally, degradome data revealed evidence of cleavage at both the 5'- and 3'-ends of the miR390 cleavage sites of Mp*TAS3* (Xia et al., 2017; Lin and Bowman, 2018), suggesting that the generation of tasiRNAs from Mp*TAS3* might adopt a two-cleave strategy.

In angiosperms, *TAS3*-derived tasiARF targets the clade B *AUXIN RESPONSIVE FACTOR* (*ARF*) family (tasiARF/*ARF* module), which plays a pivotal role in downregulating the auxin signaling pathway (Allen et al., 2005; Axtell et al., 2006; Garcia et al., 2006; Douglas et al., 2010; Yan et al., 2010; Xia et al., 2017). Additionally, the tasiARF/*ARF* module enhances the auxin response in *Physcomitrium patens*, leading to increase sensitive and stable expression of auxin-responsive genes (Plavskin et al., 2016). However, in *M. polymorpha*, the role of Mp*TAS3*-derived tasiARF in Mp*ARF2* regulation is currently unclear.

Instead of the tasiARF/*ARF* module regulating auxin signaling in angiosperms, Jiang et al. (2021) reported that a cytochrome P450 monooxygenase (CYP) superfamily member, CYP78A, can activate cytokinin signaling to promote the activation of auxin biosynthesis genes, increasing auxin content. In Arabidopsis, there are six members of the *CYP78A* subfamily (Bak et al., 2011). In bryophytes, *P. patens* has two *CYP78As* (Pp*CYP78A27* and Pp*CYP78A28*), both of which have redundant functions affecting colony size, gametophore formation, and hormone signaling during protonema growth and gametophore development (Katsumata et al., 2011). *M. polymorpha* also contains

doi:10.6342/NTU202404007

two proteins, Mp*CYP78A101* (Mp3g23930) and Mp1g14150, but their functions remain unclear (Nelson, 2018). In angiosperms, the regulation of *CYP* genes by miRNAs plays a pivotal role. For instance, in *Jatropha curcas*, *CYP86A8* and *CYP94A2* are regulated by Jcu-miR156f, while in wheat, *CYP450* is under the regulatory control of miR9773 (Li et al., 2017; Yang et al., 2019). These results indicate the importance of miRNA-mediated modulation in maintaining the stability of *CYP* expression.

The genome of *M. polymorpha* encodes genes involved in RNA silencing based on sequence similarity (Bowman et al., 2017). Given the haploid chromosome set of *M. polymorpha*, mutations in essential genes could lead to lethal mutant strains, complicating functional studies. Additionally, due to the regulatory role of miR390, overexpression of the *TAS3* transcript may not necessarily increase the yield of tasiRNAs. Moreover, a gain-of-function in the *TAS3* transcript might result in an overproduction of tasiRNAs, which poses challenges for the specific analysis of individual tasiRNAs. All these factors make studying *TAS3* tasiRNAs in *M. polymorpha* particularly challenging. Therefore, studies related to RNA silencing component genes have not been reported. In this study, we successfully knocked out the Mp*DCL4* and *MIR390* genes using gene editing technology, confirming that MpDCL4 and miR390 are involved in *M. polymorpha TAS3* tasiRNA production. We also identified a highly expressed tasiRNA, tasi78A, and demonstrated that tasi78A coordinately regulates Mp*CYP78A101* with miR11700 via the artificial miRNA (amiRNA) approach. Through gain-of-function and loss-of-function studies, we demonstrated that the miR390/tasi78A/miR11700 module regulates the expression of Mp*CYP78A101*, affecting the sensitivity of *M. polymorpha* to auxin and controlling plant development.

doi:10.6342/NTU202404007

2.3 Materials and Methods

2.3.1 Plant materials and growth conditions

Tak-1 (male) and Tak-2 (female) *M. polymorpha* plants were cultured in half-strength Gamborg's B5 medium supplemented with 1.0~1.2% agar. The asexual growth of plants was maintained under continuous light at 50–60 µmol photons m^{-2} s^{-1} at 20°C. For reproductive growth induction, mature gemma were transferred to white light conditions and supplemented with far-red light (30 µmol photons m^{-2} s^{-1}).

2.3.2 Gene construction

Guide RNAs (gRNAs) were designed by using the CasFinder tool of MarpolBase (https://marchantia.info/tools/casfinder/). The primer sets containing the *Bsa*I restriction site were used for gRNA cloning and ligated to the entry vector pMpGE_En03 (Sugano et al., 2018). To overexpress the Mp*MIRs*, the precursors of miR390 and miR11700 were amplified and cloned into pENTR/D-TOPO (Invitrogen). For artificial miRNA construction, we followed the standard protocol (Stemmer et al., 1995) to assemble *amiR-TASI78A* within the miR159 precursor of Arabidopsis (agroinfiltration in *N. benthamiana*) or the miR160 precursor of *M. polymorpha* (agropenetration in *M. polymorpha*). For the reporter assay, we amplified a 120-nt fragment of target DNA containing the miRNA target site ($78ARep^{YFP}$, $11700Rep^{YFP}$, and $11689Rep^{YFP}$) and cloned it into the pENTR/D-TOPO vector (Invitrogen). The entry vector with gRNA was subsequently transformed into the pMpGE010 or pMpGE011 binary vector (Sugano et al., 2018), and the pENTR vectors with the precursor of miRNA or amiRNA were further transformed into the pMpGWB103 or pMpGWB303 (Ishizaki et al., 2015) or pBA-DC-myc binary vector via the LR Clonase (Invitrogen). The reporter clones were further subcloned into pBA-DC-YFP vector through an LR reaction. *MIR390*, Mp*TAS3*, *MIR11700*, and Mp*CYP78A101* promoter-

doi:10.6342/NTU202404007

reporter constructs were constructed by amplifying 5~5.5 kb of the sequence upstream of the transcription start site of the target gene. The promoter regions of *MIR390*, Mp*TAS3*, *MIR11700*, and Mp*CYP78A101* were amplified from *M. polymorpha* gDNA, ligated into the entry vector pENTR1a and recombined into the pMpGWB115 (Citrine-NLS reporter) vector (Ishizaki et al., 2015). All primer sets used gene construction can be found in Supplementary Table S1.

2.3.3 Plant transformation and gene knock-out

Agrobacterium-mediated transformation of *M. polymorpha* was conducted following the thallus transformation method (Kubota et al., 2013). The *Agrobacterium* strain GV2260 harboring a binary vector (pMpGE010-gRNA-miR390, miR11700 or dcl4) was used to generate the *mir390*^{ge}, *mir11700*^{ge}, and *dcl4*^{ge} mutants. The *mir390*^{ge} mutant line #21 was used as a genetic background to generate the *mir390/11700*^{ge} double mutant. All the gRNAs were designed based on the PAM site on the *M. polymorpha* genome sequence and are listed in Supplementary Table S1. In addition, a binary vector (pMpGWB103-MIR390 or MIR11700) was used to construct the *MIR390*^{OE} and *MIR11700*^{OE} plants. After cocultivation with *Agrobacterium*, the transformants were washed with sterile water 3 to 5 times and selected on medium supplemented with 100 mg/mL cefotaxime and antibiotics (10 mg/mL hygromycin or 0.5 μM chlorsulfuron) depending on the selection of the marker in the binary vector. Regenerating transformants (T1) were transferred to a new selective medium until gemmae (G1) was produced. Further asexual generation from G1 was used for all the experiments performed in this study.

2.3.4 Small RNA detection

Northern blot analysis was conducted for sRNA detection. Total RNA (10~20 μg)

doi:10.6342/NTU202404007

was separated on a 15% polyacrylamide/1×TBE/8 M urea gel and transferred to a Hybond-N+ membrane. The antisense DNA probes for miRNA were end-labeled with [γ-^{32}P] ATP using T4 polynucleotide kinase (New England Biolabs). A Mimi Quick Spin Oligo Column (Roche) was used to purify the free radioisotopes. The UV cross-linked membrane was prehybridized with ULTRAhyb®-Oligo hybridization buffer (Ambion) for 1 h at 42°C. Then, the labeled probe was added to the hybridization buffer to hybridize the immobilized RNA for 16 h at 42°C, and the signal was detected using X-ray film (GE Healthcare) at –80°C for 16 h to 7 days, depending on the miRNA expression level.

2.3.5 MpAGO1-IP

For the MpAGO-IP experiment, homemade polyclonal antibodies against MpAGO1 (α-MpAGO1) were utilized at a working concentration of 1 mg/mL. Prior to conducting MpAGO1-IP, a mixture of 15 μL of IgG and 30 μL of protein A beads (Bio-Rad) was mixed and pre-incubated for a minimum of 30 minutes. Fresh 0.5 g fresh samples were ground into a fine powder and then extracted using 500 μL of AGO1-IP buffer (composed of 50 mM Tris-HCl, pH 7.5, 150 mM NaCl, 5 mM MgCl2, 0.1% Nonidet P-40, and 10% glycerol). The tissue lysate was centrifuged at 13,000 rpm for 10 minutes, followed by a 2-hour supernatant incubation with pre-cultured IgG beads at 4°C. The MpAGO1 precipitate was washed with AGO1-IP buffer twice and resuspended in 1× PBS buffer. The IP products were further subjected to RNA extraction using TRIzol reagent (Invitrogen) to construct a cDNA library.

2.3.6 Small RNA deep sequencing

Thirty-day-old thalli of the wild-type Tak-1, *mir390^{ge}* mutant, *MIR390^{OE}* plant, and *dcl4^{ge}* mutant were used for cDNA library construction. The sRNAs from 0.2 g of

doi:10.6342/NTU202404007

fresh thalli were extracted with a miRNA isolation kit (Geneaid) and used for cDNA library construction following the manufacturer's instructions for the RNA Library Prep Kit (Invitrogen Thermo Fisher Scientific). The sRNA sequencing was accomplished through single-read (1×50) strand-specific HiSeq sequencing (Illumina) by next-generation sequencing (NGS) at the High Throughput Genomics Core of Academia Sinica. The raw reads were trimmed to filter out the adapters and the low-quality reads by using CLC Genomic Workbench (Qiagen, Hilden, Germany). The expression of miRNAs of interest was normalized by counting reads per million (RPM) in different samples. The metadata of the cellular and MpAGO1-IP profiles were deposited in the National Center for Biotechnology Information (NCBI) under the SRA accession numbers SRR27497907, SRR27497909, SRR27497905, and SRR27497906, respectively.

2.3.7 Promoter-reporter assays

Sporelings (for *MIR390* and Mp*TAS3*) or thalli (for *MIR11700* and Mp*CYP78A101*) were transformed with *Agrobacterium* strain GV2260 harboring the binary vectors. Next, the transformants were selected with 10 mg/L hygromycin. The Critrine-NLS signal in the G2 generation of transformants was detected via a Leica TCS SP5 confocal microscope (TechComm, College of Life Science, National Taiwan University).

2.3.8 Small RNA target identification

The candidate sRNAs and Tak-1 mRNA file (v5.1) were employed as queries for identifying potential miRNA targets using psRNAtarget with the default settings from the 2017 release. The prediction outcomes were subsequently cross-referenced with the degradome profile. Potential target sites were determined based on substantial degradome reads, specifically the specific accumulation of more than 20 reads at the

doi:10.6342/NTU202404007

10th and 11th positions of the predicted site.

2.3.9 Real-time RT–PCR and stem-loop qRT-PCR

qRT-PCR was performed to detect the expression level of mRNA. The obtained total RNA was treated with TURBO™ DNase (Ambion) to remove genomic DNA contamination. Then, first-strand cDNA was synthesized by SuperScript™ III Reverse Transcriptase (Invitrogen). The primer sets 5'- GAAGTTCCAGCAATCGTCGG-3' and 5'-GCGGTGTGAGATGTAGCAAG-3' were used for the detection of Mp*ARF2*. The primer sets 5'-CTCGACTCTCAACGAGCAAG-3' and 5'-AGCCCAAAACAGAAGCAGAA-3' and 5'- ATTGCTCTGTGGAAGTTTGAGACT-3′ and 5'- GTGGTTGAGTCGATGATGAGAAC-3' were used to amplify Mp*CYP78A101* and the internal control gene *EF1α*, respectively. qRT-PCR was performed using the KAPA SYBR FAST qPCR kit (KAPA Biosystems) in a Bio-Rad CFX real-time PCR machine (Bio-Rad). Three biological replicates and three technical repeats were included in the qRT-PCR assay.

Stem-loop qRT-PCR was performed to detect the expression levels of mature miRNAs. Stem-loop RT primers bind to the 3' portion of miRNA molecules and are reverse-transcribed by Supersucript™ IV (Invitrogen). Next, the RT product was quantified using the miRNA-specific forward primer and a universal reverse primer with the universal probe library (UPL) system. The RT primers 5'-GTTGGCTCTGGTGCAGGGTCCGAGGTATTCGCACCAGAGCCAACGACGCT-3' and 5'-GTTGGCTCTGGTGCAGGGTCCGAGGTATTCGCACCAGAGCCAACAAAAAT-3' were used for reverse transcription of MpmiR390 and Mp*U6*, respectively. Then, the primer 5'- GTTGAAGCTCAGGAGGGAT-3' and the universal reverse primer 5'-GTGCAGGGTCCGAGGT-3' were used for the amplification of Mp*MIR390*. The

doi:10.6342/NTU202404007

primers 5'-GATACAGAGAAGATTAGCATGG-3' and the universal reverse primer 5'-GTGCAGGGTCCGAGGT-3' were used to amplify the internal control Mp*U6*.

2.3.10 Transient expression by agroinfiltration

The *Agrobacterium tumefaciens* strain ABI harboring the expression binary vector was incubated in LB medium supplemented with 100 µg/mL spectinomycin and 50 µg/mL kanamycin for 24 h at 28°C. Then, the cultures were subcultured at 1/10 volume in LB medium supplemented with 10 mM MES (pH 5.6), 40 µM acetosyringone, 100 µg/mL spectinomycin, and 50 µg/mL kanamycin and incubated at 28°C for 16 h. The *Agrobacterium* were collected by centrifugation, and the resulting pellet was resuspended in inoculation buffer (ddH$_2$0 supplemented with 10 mM MgCl$_2$ and 150 µM acetosyringone). For the appropriate infection conditions, the absorbance of the inoculation buffer with *Agrobacteria* was adjusted to OD600=1.0, and the cultures were incubated at room temperature for 3 h (Lin et al., 2013). Next, the *Agrobacteria* containing the Mp*MIR* gene or target fragment fused with YFP were mixed equally and co-infiltrated into 4-week-old *N. benthamiana* plants. After 2- or 3-days of culture, the YFP fluorescence of the infiltrated leaves was detected by using a Leica TCS SP5 II confocal laser-scanning microscope (Joint Center for Instruments and Research, College of Bioresources and Agriculture, National Taiwan University), and the expression level of the miRNAs was validated by northern blotting.

2.3.11 Transient expression by agropenetration in *M. polymorpha*

Iwakawa et al. (2021) reported a transient transformation method for *M. polymorpha*, we referred to a pervious study (Iwakawa et al., 2021) and used 14-day-old thalli as the material, with some optimization based on our experimental needs. First, we utilized the *Agrobacterium* strain GV2260 for the transformation. Second, we substituted 2%

doi:10.6342/NTU202404007

sucrose in all media with 2% glucose to improve the transformation efficiency. Third, the pH of the co-culture medium was adjusted to 5.2~5.3 to increase the transformation efficiency. Fourth, the *Agrobacterium* infection concentration for *M. polymorpha* was adjusted according to different transformation vectors: the concentrations for *78ARep*^{YFP} and *11689Rep*^{YFP} were diluted to be at OD$_{600}$ = 0.02, and that for *11700Rep*^{YFP} was diluted to be at OD$_{600}$ = 0.04. The co-culture time was three days, during which vacuum penetration was applied on the first day (two times for 5 minutes each) and the second day (two times for 3 minutes each) to facilitate *Agrobacterium* entry into *M. polymorpha*. Notably, the construct expressing 11*689Rep*^{YFP} without the target site used as an internal control. The YFP signals of transformed thalli *were detected using* a Leica TCS SP5 II confocal laser-scanning microscope (Joint Center for Instruments and Research, College of Bioresources and Agriculture, National Taiwan University).

2.3.12 Auxin sensitivity assay

For the assessment of auxin sensitivity, 9 gemmae per plate of WT and gemma from *dcl4*^{ge} mutant, *mir390*^{ge} mutant, *mir390/11700*^{ge} mutant, and *amiR-TASI78A*^{OE} plants were cultured on plates on 1/2 Gamborg's B5 media supplemented with/without 0 μM, 0.25 μM, or 0.5 μM NAA for a duration of 14 days. Photographic records of the plates were captured, and plant categorization was performed at the end of the 14-day period. The thallus area was collected by quantifying the pixel values. The ratio of the cell area (with NAA/without NAA) was calculated and classified as extremely sensitive (ratio < 0.025), sensitive (ratio 0.025-0.2), or less sensitive (ratio > 0.2) to reflect the effects of NAA on plant growth. The percentage of thalli for various plants in the three levels of the NAA effect was calculated.

doi:10.6342/NTU202404007

2.3.13 Cell size quantification

Staining gemma with fluorescein diacetate (FDA) was conducted according to the field protocol established by Westermann et al. (Westermann et al., 2020). Following staining, the gemmae were examined via fluorescence microscopy, and images of the cells were captured. Specifically, epidermal cells in the central region of the gemma (approximately 31-129 cells/gemma) were manually identified and delineated. The area of these cells was then quantitatively analyzed from 9 to 12 gemmae by measuring the pixel values in the image.

2.3.14 Phylogenetic tree of *CYP78* and *CYP98* families

We searched for the 47 homologous genes of *CYP78* and *CYP98* from the MarpolBase and Phytozome (https://phytozome-next.jgi.doe.gov/) databases across the genomes of *Ceratodon purpureus*, *Physcomitrium patens*, *Ceratopteris richardii*, *Diphasiastrum complanatum*, *Amborella trichopoda*, *Oryza sativa*, and *Arabidopsis thaliana*. Multiple sequence alignment of these *CYP78* and *CYP98* genes was performed using the Muscle algorithm with default parameters in MEGAX software (Kumar et al., 2018). The resulting phylogenetic tree was constructed using both neighbour-joining (NJ) (Tamura et al., 2004) and maximum likelihood (ML) algorithms with default settings. Bootstrapping (1000 replicates) was applied for both the ML and NJ analyses. The phylogenetic trees obtained through the ML and NJ methods are highly similar; hence, we present the ML tree in our findings.

2.4 Results

2.4.1 miR390/*TAS3*/Mp*ARF2* pathway in *M. polymorpha*

We investigated whether the conserved regulatory mechanism of the miR390/Mp*TAS3* module also exists in *M. polymorpha*. Degradome profiling from the

doi:10.6342/NTU202404007

vegetative stage was employed to verify the specific sites where miRNA targets are cleaved in the RNA molecules (Lin et al., 2016). Two degradome-supported processing sites were previously assigned to Mp*TAS3* (Fig. 1A) (Lin et al., 2016). Fifty-nine degradome reads (2.09 RPM) were present at the 5'-end of the miR390 target site of Mp*TAS3* (Fig. 1B), while only 9 degradome reads (0.32 RPM) were observed at the 3'-end of the target site (Fig. 1C). Additionally, we identified a target site of tasiARF at 136-nt from the start codon of Mp*ARF2*, with 5 degradome reads (0.18 RPM) at the cleavage site (Fig. 1D).

To verify the loading of miRNAs and tasiRNAs into MpAGO1, we conducted an immunoprecipitation experiment using α-MpAGO1 antibodies and sequenced the small RNAs bound to MpAGO1. Then, we compared the abundance of these small RNAs between the cellular small RNA-Seq profile (cellular profile) and the MpAGO1-immunoprecipitated small RNA-Seq profile (MpAGO1-IP profile) from the vegetative stage. The cellular and MpAGO1-IP profiles exhibited 10.8 RPM and 55.9 RPM of miR390, respectively (Fig. 1E), indicating enrichment of miR390 in MpAGO1. In contrast, we observed low RPM values for tasiARF (1.5 RPM) in the MpAGO-IP profile (Fig. 1E).

In Arabidopsis, AtDCL4 is the major component involved in tasiRNA processing. We investigated the role of MpDCL4 by performing CRISPR/Cas9 editing of the Mp*DCL4* genome (Fig. 1F) and obtained five *dcl4*^{ge} mutants, all of which exhibited INDELs located on exon 7 of the Mp*DCL4* genome sequence (Appendix 1A and B, data from Ms. Veny's master thesis). Specifically, we used the male *dcl4*^{ge} mutant line #7-10, which carries an insertion causing a frameshift mutation (Appendix 1C and D, data from Ms. Veny's master thesis), for small RNA analysis. We compared the composition of *TAS3* tasiRNAs in Tak-1 plants and *dcl4*^{ge} mutants. Our results showed the presence of tasiRNAs in Tak-1 plants but not in *dcl4*^{ge} mutants (Fig. 1F).

doi:10.6342/NTU202404007

Furthermore, the RPM values of miRNAs in both Tak-1 plants and *dcl4^{ge}* mutants were similar (Fig. 1F), indicating that MpDCL4 specifically affects the generation of tasiRNAs and functions like AtDCL4 in tasiRNA biogenesis. Overall, these findings provide evidence for the conserved regulatory mechanism of the miR390/Mp*TAS3* module in *M. polymorpha*, highlighting the role of MpAGO1 and MpDCL4 in small RNA processing and target cleavage.

2.4.2 Mp*TAS3*-derived tasiRNAs are mainly processed from the 3'-end phasing positions 1 and 2 of Mp*TAS3* transcripts

To further explore the biogenesis of Mp*TAS3*-derived tasiRNAs, we mapped 21-nt small RNAs from the cellular and MpAGO1-IP profiles to Mp*TAS3* transcripts. Our analysis revealed that Mp*TAS3*-derived phased 21-nt tasiRNAs could be initiated from different positions of Mp*TAS3* in a phased pattern, indicating the influence of MpDCL4 on tasiRNA production. However, whether MpDCL4 can cleave both directions of double-strand Mp*TAS3* remains unknown. Thus, the directionality of MpDCL4, whether it starts from the 5'-end and/or 3'-end, still requires further investigation. Given that AtAGO7-miR390 does not cleave the 5'-end of At*TAS3*, the generation of tasiRNAs in Arabidopsis initiates from the 3'-end of the At*TAS3* transcript. To maintain a uniform comparative basis between *M. polymorpha* and Arabidopsis, the 3'-end of the Mp*TAS3* transcript has also been selected as the initiation point for tasiRNA production.

To define the potential phasing positions, we assigned the 10th nt of the 3'-end of the miR390 cleavage site as position 1, with subsequent positions having a 1-nt shift toward the 5'-end, denoted as position 2, position 3, and so on (Fig. 2A). In the different positions analyzed, the tasiRNAs initiated from the 3'-end at position 2 (3'-end P2), which are equivalent to those initiated from the 5'-end at position 4 (5'-end P4), were identified as the most abundant among the Mp*TAS3*-derived tasiRNAs (Fig. 2B, panel

doi:10.6342/NTU202404007

i; Supplementary Fig. S1). Overall, position 2 exhibited the highest proportion of tasiRNAs, accounting for more than 60% of the tasiRNAs in both the cellular and MpAGO-IP profiles (Fig. 2B, panel ii; Supplementary Fig. S1), indicating that tasiRNAs derived from Mp*TAS3* are predominantly generated from phasing position 2 and efficiently loaded into MpAGO1. Additionally, approximately 5-15% of tasiRNAs can also be loaded into MpAGO1 from phasing position 1 (3'-end P1 or 5'-end P5) (Fig. 2B, panel ii; Supplementary Fig. S1). The results indicate that the tasiRNAs loaded into MpAGO1 primarily originate from phasing positions 1 and 2. In Arabidopsis, tasiRNAs are also primarily produced and loaded into AtAGO1 from phasing positions 1 and 2 (Fig. 2B, panels iii and iv). These observations highlight the similarity in tasiRNA biogenesis mediated by MpDCL4 in *M. polymorpha* compared to Arabidopsis.

Moreover, we analyzed the 5'-end nucleotide composition of the tasiRNAs derived from the phasing positions 1 and 2. Notably, most of these tasiRNAs (62.83%) had a 5'-end 1^{st}-U (Fig. 2C, panel i). When tasiRNAs were loaded into MpAGO1, the paired strands of Mp*TAS3*-derived tasiRNAs exhibited unequal amounts. Consequently, 90.28% of the MpAGO1s loaded with Mp*TAS3*-derived tasiRNAs from phasing positions 1 and 2 were 5'-end 1^{st}-U, 6.41% were 5'-end 1^{st}-A, 3.24% were 5'-end 1^{st}-C, and 0.07% were 5'-end 1^{st}-G (Fig. 2C, panel ii). In Arabidopsis, the 5'-end nucleotides of tasiRNAs are primarily composed of U (72.48%) and A (23.58%) (Fig. 2C, panel iii), but when they are loaded into AtAGO1, they are mainly composed of U (97.71%) (Fig. 2C, panel iv). These findings provide valuable insights into the preferential loading and potential regulatory role of specific tasiRNAs mediated by MpAGO1 and AtAGO1.

2.4.3 A novel tasi78A regulates Mp*CYP78A101*

To further understand the role of tasiRNAs in RNA silencing, we examined the abundance of Mp*TAS3*-derived tasiRNAs from the 3'-end phasing position 2 in the

doi:10.6342/NTU202404007

MpAGO1-IP profile. Our analysis revealed that a novel tasiRNA, tasi78A (660.1 RPM), was significantly enriched (Fig. 2D). Moreover, the degradome data revealed 747 degradome reads (26.89 RPM) at the target site (138 nt) in the Mp*CYP78A101* transcript (Fig. 2E), indicating that Mp*CYP78A101* is the primary target of tasi78A. Based on small RNA target identification, tasi78A exhibited 14 putative target genes; however, the other genes displayed only a few degradome reads (fewer than 5 reads, Supplementary Fig. S2), further supporting the primary target role of tasi78A on Mp*CYP78A101*. Furthermore, we observed enrichment of four other Mp*TAS3*-derived tasiRNAs, namely tasi2-3'D6(+) (79.4 RPM), tasi2-3'D9(+) (185.3 RPM), tasi2-3'D10(+) (61.9 RPM), and tasi2-3'D4(-) (29.5 RPM) (Fig. 2D). However, none of these tasiRNAs cleave putative target transcripts based on the prediction and degradome profiles (Supplementary Fig. S3). Notably, the very weak degradation of Mp*ARF2* (Fig. 1D) was supported by the low abundance of tasiARF (0.7 RPM in the cellular profile and 1.5 RPM in the MpAGO1-IP profile) (Fig. 2D). Additionally, tasi78A, the reverse and complementary sequence to tasiAP2, originated from the phasing position 4 (Fig. 2F). A previous study suggested that the tasiAP2 sequence is unique to non-vascular plants (Morozov et al., 2018). Therefore, it is reasonable to infer that the reverse complemented tasi78A may also be conserved in non-vascular plants.

2.4.4 miR390 leads to the production of tasiRNAs in *M. polymorpha*

To further investigate the miR390/Mp*TAS3* regulatory pathway, we generated transgenic lines overexpressing the *MIR390* gene under the control of the EF1α promoter ($MIR390^{OE}$ plant) and created *MIR390* knockout mutants ($mir390^{ge}$ mutant). In the $mir390^{ge}$ mutants, the structure of the miR390 precursor showed a conformational change in either the miR390 mature strand or the star strand (Fig. 3A), implying the absence of miR390 production. Northern blot analysis revealed that the

doi:10.6342/NTU202404007

levels of miR390 were significantly increased in the *MIR390*^{OE} plants than in the Tak-1 plants; however, the levels of tasiARF and tasi78A only show slightly increased (Fig. 3B). The small RNA profile also confirmed the expression of miR390, tasiARF, and tasi78A in the *MIR390*^{OE} plants (Fig. 3C). In contrast, no detectable miR390 was detected in the four mutants when we checked their small RNA-Seq profiles (Fig. 3C). Furthermore, tasiARF and tasi78A were not detected in the *mir390*^{ge} mutants, indicating the loss of Mp*TAS3*-derived tasiRNA generation in these mutants (Fig. 3C). Notably, we unexpectedly detected a 24-nt variant of miR390 (5'-ACAAAGCUCAGGAGGGAUAGCGUC-3'), in the *MIR390*^{OE} plants, the reason for which remains unknown (Fig. 3B and C).

2.4.5 Mp*CYP78A101* was regulated by both tasi78A and miR11700

In addition to tasi78A, we identified a miRNA target site on Mp*CYP78A101* (Fig 4A). The target site is at position 237 nt and is targeted by miR11700, which exhibited 338 degradome reads (12.17 RPM) with a prominent peak at the targeting position (Fig. 4A). Moreover, tasi78A (660.1 RPM) and miR11700 (354.7 RPM) were significantly enriched in the MpAGO1-IP profile (Fig. 2D; and 4B).

To further examine the regulatory relationship between small RNAs (tasi78A and miR11700) and Mp*CYP78A101*, transient expression reporter assays were performed in *Nicotiana benthamiana*. To ectopically express tasi78A, we constructed an amiRNA for tasi78A (amiR-tasi78A) (Fig. 4C). The chimeric construct of *YELLOW FLUORESCENT PROTEIN* (*YFP*) fused with the tasi78A target site of Mp*CYP78A101* (*78ARep*^{YFP}) exhibited fluorescent signals in the cytoplasm (Fig. 4D, panel i). Interestingly, co-expressing *78ARep*^{YFP} with amiR-tasi78A (*78ARep*^{YFP}+amiR-tasi78A) reduced the YFP fluorescence (Fig. 4D, panel i). In contrast, there was no difference in YFP fluorescence between YFP alone and YFP co-expressing amiR-tasi78A

doi:10.6342/NTU202404007

(YFP+amiR-tasi78A) (Fig. 4D, panel i). Moreover, the presence of amiR-tasi78A was confirmed by northern blotting in the samples co-expressing amiR-tasi78A (Fig. 4D, panel ii). These data suggested that amiR-tasi78A can cleave the RNA substrate containing the tasi78A target site within Mp*CYP78A101*.

Similarly, when the substrate *11700Rep*^{YFP} was co-expressed with miR11700, a decrease in YFP fluorescence was observed compared to that of the YFP control (Fig. 4E, panel i). However, no difference in YFP fluorescence was detected between samples expressing YFP alone and those co-expressing YFP and miR11700 (Fig. 4E, panel i). Northern blotting confirmed the high expression of miR11700 in the samples expressing miR11700 (Fig. 4E, panel ii). In addition, all YFP fluorescence intensities were quantified (Supplementary Fig. S4). The results indicated that the expression of both *78ARep*^{YFP} and *11700Rep*^{YFP} decreased by less than 0.2-fold in the amiR-tasi78A and miR11700 samples, respectively (Supplementary Fig. S4). These findings indicated that both tasi78A and miR11700 can target Mp*CYP78A101*.

2.4.6 Promoter assay for *MIR390*, Mp*TAS3*, *MIR11700*, and Mp*CYP78A101*

A promoter assay was conducted to investigate the expression patterns of *MIR390*, Mp*TAS3*, *MIR11700*, and Mp*CYP78A101*. Robust signals of *MIR390*$_{pro}$*:Citrine-NLS* and Mp*CYP78A101*$_{pro}$*:Citrine-NLS* signals were detected at the apical notch, the site of the apical meristem, in gemma (Fig. 5A and B). Additionally, signals of Mp*TAS3*$_{pro}$*:Citrine-NLS* and *MIR11700*$_{pro}$*:Citrine-NLS* signals were also observed at the apical notch of the gemma, although the signals were relatively weak (Fig. 5C and D). The overlapping expression patterns observed in the promoter assays suggested that the miR390/Mp*TAS3* module and *MIR11700* may regulate Mp*CYP78A101* at the apical notch area in the gemma. Furthermore, signals of *MIR390*$_{pro}$*:Citrine-NLS* and Mp*TAS3*$_{pro}$*:Citrine-NLS* were also detected in the gemma cup (Fig. 5A and C),

doi:10.6342/NTU202404007

indicating that the miR390/Mp*TAS3* module may influence the development of the gemma cup. Notably, Tak-1 plants served as a negative control in the promoter assay, where no citrine fluorescence was observed (Fig. 5E).

2.4.7 Tasi78A negatively regulates Mp*CYP78A101* in *M. polymorpha*

Our observations revealed that *MIR390*^{OE} plants and *mir390*^{ge} mutants exhibited no noticeable phenotypic differences from Tak-1 plants, including differences in gemma cup formation, thallus morphology, and sexual organ development (Supplementary Fig. S5A and B). Notably, upregulation of Mp*CYP78A101* was observed exclusively in the *mir390*^{ge} mutants (Supplementary Fig S5C). However, overexpression of miR390 in *MIR390*^{OE} plants did not significantly reduce the expression of Mp*CYP78A101* because of only slightly increased tasi78A (Fig. 3B and C; Supplementary Fig. S5D and E). Therefore, to investigate the silencing effect of tasi78A, we generated a transgenic *M. polymorpha* expressing an *amiR-TASI78A* gene (*amiR-TASI78A*^{OE} plant) (Fig. 6A). However, no significant phenotypic alterations were observed in *amiR-TASI78A*^{OE} plants (Fig. 6A). High expression levels of amiR-tasi78A (33-35.8-fold) were detected by northern blotting (Fig. 6B), and the expression of Mp*CYP78A101* was downregulated (Fig. 6C). Consistent results were obtained when *78ARep*^{YFP} was transiently expressed in *amiR-TASI78A*^{OE} plants (Fig. 6D) by agropenetration, providing further support for the regulatory role of tasi78A in modulating the expression of Mp*CYP78A101*.

2.4.8 miR11700 may regulate Mp*CYP78A101* at the reproductive stage in *M. polymorpha*

To confirm the function of miR11700, we generated *mir11700*^{ge} mutants and transgenic *M. polymorpha* expressing the *MIR11700* gene (*MIR11700*^{OE} plants). In the

doi:10.6342/NTU202404007

mutants, changes in the secondary structure of the miR11700 precursor suggested that the generation of miR11700 was impaired (Fig. 7A). In various individual *mir11700*^{ge} mutants, the expression of miR11700 was undetectable (Fig. 7B). Notably, in the *mir11700*^{ge} mutant lines #2 and #7, an approximately 1.8-fold increase in the expression of Mp*CYP78A101* was detected (Fig. 7C). The lack of Mp*CYP78A101* upregulation in all the *mir11700*^{ge} mutants might be attributed to the persistent control of Mp*CYP78A101* by endogenous tasi78A. In the vegetative stage, the thallus phenotype of the *mir11700*^{ge} mutants was similar to that of Tak-1 plants (Fig. 7D). However, in the reproductive stage, the mutants exhibited a noticeable increase in thallus width compared to that of Tak-1 plants (Fig. 7D and Supplementary Fig. S6A).

Moreover, three distinct *MIR11700*^{OE} plants exhibited significant variation in the expression of miR11700 (20.1 to 194-fold) (Fig. 7E). Correspondingly, the expression of endogenous Mp*CYP78A101* decreased, showing variations that matched the differing overexpression levels of miR11700. These data suggested that miR11700 effectively reduces the expression of Mp*CYP78A101* (Fig. 7E and F). Additionally, these *MIR11700*^{OE} plants exhibited a vegetative growth morphology similar to that of Tak-1 plants (Fig. 7G). However, at the reproductive stage, the thalli of the *mir11700*^{ge} mutants appeared more expansive than those of the Tak-1 plants, while the number of sexual organs remained unchanged (Fig. 7D, arrowheads). In contrast, in the *MIR11700*^{OE} plants, the number of sexual organs was reduced (Fig. 7G, arrowheads; and Supplementary Fig. S6B). Using promoter-reporter assays, we found that the fluorescence of citrine-NLS expressed under the control of both the *MIR11700*^{OE} and Mp*CYP78A101* promoters was uniformly distributed throughout the entire antheridium in the transgenic plants (Appendix 2, data from Zhao-Jun Pan). These data suggested that miR11700 may regulate Mp*CYP78A101*, specifically during the reproductive stage in *M. polymorpha*.

doi:10.6342/NTU202404007

2.4.9 Evaluation of the regulatory relationships between tasi78A, miR11700, and Mp*CYP78A101* in *M. polymorpha*

Due to the lack of phenotypic alterations in the $MIR390^{OE}$ plants and $mir390^{ge}$ mutants (Supplementary Fig. S5A and B), we generated $mir390/11700^{ge}$ mutants and double transgenic *M. polymorpha* plants expressing the *MIR390* and *MIR11700* genes ($MIR390/11700^{OE}$ plants) (Fig. 8). In loss-of-function mutants, the altered secondary structure of the miR390 and miR11700 precursors suggested that the production of miR390 and miR11700 was disrupted (Fig. 8A). Northern blot analysis revealed that in the $mir390/11700^{ge}$ mutants, both the miR390 and miR11700 levels were undetectable. Conversely, $MIR390/11700^{OE}$ plants demonstrated substantial overexpression of these miRNAs, ranging from 1.6- to 8.8-fold for miR390 and miR11700 (Fig. 8B and C). No obvious phenotype was observed in the $mir390/11700^{ge}$ mutants (Fig. 8D). This absence of a phenotype could be attributed to the slight increase in Mp*CYP78A101* expression in gemmae, while its expression in thalli remains nearly unchanged (Fig. 8E and Supplementary Fig. S7). These $MIR390/11700^{OE}$ plants appeared to have normal thalli, but the number of gemma cups varied (Fig. 8F). Notably, Mp*CYP78A101* expression was significantly lower in these $MIR390/11700^{OE}$ plants (Fig. 8G, panel i), while Mp*ARF2* expression remained unchanged (Fig. 8G, panel ii). These data suggested that the disrupted development of gemma cups could be due to reduced Mp*CYP78A101* when miR390 and miR11700 are overexpressed. To further confirm the regulatory relationship between miR11700 and Mp*CYP78A101*, we conducted a reporter assay by transiently expressing $11700Rep^{YFP}$ in $mir390/11700^{ge}$ mutants and $MIR390/11700^{OE}$ plants. The results indicated that YFP fluorescence was greater in the $mir390/11700^{ge}$ mutants and significantly decreased in the $MIR390/11700^{OE}$ plants (Fig. 8H), supporting the regulated role of miR11700 in altering the expression of Mp*CYP78A101*.

doi:10.6342/NTU202404007

Considering the role of tasi78A in regulating Mp*CYP78A101* (Fig. 6D), we suggested that tasi78A and miR11700 coordinate in the RNA silencing-mediated regulation of Mp*CYP78A101*. Moreover, without NAA treatment, the epidermal cell sizes of *dcl4*^{ge} and *mir390/11700*^{ge} mutants were approximately 1.2-fold (Appendix 3, data from Zhao-Jun Pan). In contrast, the cell sizes of *mir390*^{ge} mutants and *amiR-TASI78A*^{OE} plants were comparable to those in Tak-1 plants (Appendix 3, data from Zhao-Jun Pan).

2.4.10 The *dcl4*^{ge}, *mir390*^{ge}, and *mir390/11700*^{ge} mutants display NAA less sensitive phenotype

The presence of tasiARF in miR390-mediated tasiRNAs is known to negatively regulate *ARFs* in Arabidopsis, thus influencing the auxin response. In this study, to elucidate the effects of tasiRNAs on the auxin response, plant growth and development, we treated *dcl4*^{ge}, *mir390*^{ge}, *mir390/11700*^{ge}, and *amiR-TASI78A* plants, as well as Tak-1 plants, with external NAA (1-naphthaleneacetic acid). Compared with other concentrations of NAA, 0.5 μM NAA significantly inhibited thallus growth in gemmalings derived from different plants (Fig. 9A; Supplementary Fig. S8). Conversely, in the absence of NAA, these plants did not exhibit any notable difference in thallus size (Fig. 9A and B). The mean relative thallus areas of the *dcl4*^{ge} and *mir390/11700*^{ge} mutants were greater than that of Tak-1 plants, whereas those of the *amiR-TASI78A*^{OE} plants were smaller (Fig. 9A and B).

To more accurately delineate NAA sensitivity, we classified plants with a thallus area ratio (with NAA/without NAA) less than 0.025 as extremely sensitive phenotypes, those with a ratio ranging from 0.025-0.2 as sensitive phenotypes, and those with a ratio exceeding 0.2 as less sensitive phenotypes (Fig. 9A). According to these categories, approximately 33.3% of Tak-1 gemmalings exhibited highly sensitivity to NAA, 44.4% showed sensitivity, and 22.2% presented less sensitivity (Fig. 9C). Among the various

doi:10.6342/NTU202404007

knockout mutants, only 11.1% of the gemmalings of the *dcl4*^{ge} mutant and *mir390*^{ge} mutant showed an extremely sensitive phenotype to NAA; however, most of them were classified as sensitive (11.1-55.6%) or less sensitive (33.3-88.8%) phenotypes (Fig. 9C). In contrast, a significant proportion of *amiR-TASI78A*^{OE} gemmalings #10 and #19 exhibited extremely sensitive (44.4-77.8%) or sensitive (22.2-33.3% sensitive) phenotypes (Fig. 9C). Additionally, gain-of-function of tasi78A in *amiR-TASI78A*^{OE} plants resulted in the downregulation of Mp*CYP78A101* under NAA condition (Appendix 4A, data from Zhao-Jun Pan), suggesting that the levels of Mp*CYP78A101* could alter the sensitivity of gemmalings to auxin.

We assessed the Mp*ARF2* expression in these gemmalings to investigate the morphological changes under NAA treatment. Despite a noticeable reduction in Mp*ARF2* expression in *amiR-TASI78A*^{OE} plants under NAA treatment, the decrease was not statistically significant. In contrast, other mutants exhibited no significant differences in Mp*ARF2* expression when compared to Tak-1 plants (Appendix 4B, data from Zhao-Jun Pan), suggesting that the morphological variations observed in the mutants and transgenic plants under NAA treatment may not be attributed to alterations in Mp*ARF2* expression. Instead, they are more likely related to auxin signaling regulation mediated by Mp*CYP78A101*.

2.4.11 Target sites of tasi78A and miR11700 in *CYP78* homologs during land plant evolution

By aligning the *CYP78* homologs in land plants, we identified target sites for tasi78A in the bryophyte lineage (Fig. 10, labeled with an orange circle). However, no corresponding target site was found in Mp1g14150, a paralog of Mp*CYP78A101,* or in other *CYP78* homologs of vascular plants (Fig. 10; Supplementary Fig. S9). These findings suggest that tasi78A-mediated regulation may only occur in bryophytes. We

doi:10.6342/NTU202404007

also identified the targeting site for miR11700 of Mp*CYP78A101* within land plants. Interestingly, the target site for miR11700 is present only in Mp*CYP78A101* and not in other bryophytes or vascular plants (Fig. 10, labeled with a blue square). Although fewer mismatches are observed in the base pairing between miR11700 and its target site in *Ceratodon purpureus* (Cp3G030000), *Ceratopteris richardii* (Cr1Z230800), and *Oryza sativa* (Os08g43390), these mismatches are evenly distributed (Fig. 10, labeled with an open square; Supplementary Fig. S10). This distribution suggested that miR11700 is still incapable of cleaving its target site.

2.5 Discussion

In Arabidopsis, the length of a miRNA determines whether AtAGO1 mediates RNA silencing or generates tasiRNAs. The miRNA that regulates RNA silencing is primarily 21-nt in length, whereas the miRNA that generates *TAS1* and *TAS2* tasiRNAs is 22-nt in length (Allen et al., 2005; Rajagopalan et al., 2006; Montgomery et al., 2008b; Chen et al., 2010; Cuperus et al., 2010). In the plant kingdom, the miR390/*TAS3* module is a highly conserved regulatory module, with miR390 involved in producing *TAS3* tasiRNAs from bryophytes to angiosperms (Xia et al., 2017; Lin and Bowman, 2018). Notably, miR390 in any plant species is 21-nt in length, not 22-nt. In Arabidopsis, *TAS3* is regulated explicitly by AtAGO7 and not through AtAGO1. AtAGO7 is specialized in carrying miR390 (Montgomery et al., 2008a). However, as *M. polymorpha* does not have AGO7, MpAGO1 carries miR390 to participate in Mp*TAS3* tasiRNAs generation.

Another unique regulatory phenomenon of the miR390/*TAS3* module is the "two-hit" model (Allen et al., 2005; Xia et al., 2017; Lin and Bowman, 2018). The *TAS3* transcript has two miR390 target sites that facilitate miR390-AtAGO7 binding. In Arabidopsis, the 5'-end target site only provides for miR390-AtAGO7 binding and is not cleaved, while the 3'-end target site undergoes miR390-AtAGO7 binding and

doi:10.6342/NTU202404007

cleavage (Allen et al., 2005). Thus, Arabidopsis follows a "two-hit and one-cleave" model to produce *TAS3* tasiRNAs, with AtRDR6 and AtDCL4 generating tasiRNAs starting from the 3'-end. However, both miR390 cleavage sites on *TAS3* transcripts in *M. polymorpha* are bound and cleaved by miR390-MpAGO1, suggesting a potential "two-hit and two-cleave" tasiRNA production model.

Like AtDCL4, we also confirmed that MpDCL4 is involved in tasiRNA production. *TAS3* tasiRNAs were no longer produced in the *dcl4*^{ge} mutant, making this mutant line valuable for future research on tasiRNAs or phasiRNAs. Through the small RNA profiles of tasiRNAs, we found that MpDCL4-produced tasiRNAs from double-stranded *TAS3* transcripts at 3'-end positions 2 or 1 are identical to those produced from 5'-end positions 4 or 5. These few types of tasiRNAs constitute 70% of all tasiRNAs and are the main *TAS3* tasiRNAs. We speculate that MpDCL4 may produce the main tasiRNAs either from 3'-end positions 2 or 1 or from 5'-end positions 4 or 5. According to the "two-hit and one-cleave" model, the main *TAS3* tasiRNAs in Arabidopsis are produced from the 3'-end positions 2 or 1, which is consistent with the 3'-end positions of *M. polymorpha*. Additionally, the observation of enlarged cell size in the *dcl4*^{ge} and *mir390/11700*^{ge} mutants suggested that RNA silencing plays a crucial role in cell expansion in *M. polymorpha*. However, besides tasi78A, whether other taisRNAs are also involved in cell expansion that need further investigation.

MpAGO1 plays roles in both RNA silencing and tasiRNA biogenesis. This discovery prompted an interesting question: Why does only miR390-MpAGO1 lead to tasiRNA production, while other 21-nt miRNAs loaded into MpAGO1 do not induce the production of tasiRNAs from their cleaved target RNA? We propose two potential explanations. First, this might be attributed to the "two-hit and two-cleave" model, as a typical miRNA-MpAGO1 cleaves at one position, whereas miR390-MpAGO1 cleaves at two positions. Second, the inherent characteristics of the *TAS3* sequence, such as its

doi:10.6342/NTU202404007

secondary structure, might predispose it to tasiRNA production. Regardless of which hypothesis is correct, both *M. polymorpha* and Arabidopsis can serve as valuable models for further investigations in the future. In addition to the aforementioned differences, the way in which MpAGO1 accommodates small RNA differs from that of AtAGO1. AtAGO1 prefers tasiRNAs and miRNAs that have a 5'-end 1st uridine (Mi et al., 2008). The insights from the MpAGO1-IP dataset indicate that other tasiRNAs incorporate other purines and pyrimidines at their 5'-end 1st position. This finding that MpAGO1 offers broader and more varied abilities in small RNA selection than AtAGO1.

According to the promoter-citrine-NLS assay, miR390 was distinctly expressed in the two apical notches of gemma. Mp*TAS3* expression in gemma was weaker, primarily in the gemma cup tissue. Furthermore, *MIR390/11700*^{OE} plants exhibited a variation in the number of gemma cups. The gemmae and gemma cup are specialized gametophytic organs of the *Marchantiopsida* species that are not found in angiosperms. Recent molecular research has revealed that the development of gemma and gemma cups in *M. polymorpha* shares regulatory modules common to other land plants (Kato et al., 2020). This finding implies that the miR390/Mp*TAS3*/miR11700 regulatory module also plays a crucial role in developing gemma, representing a shared component of these common regulatory pathways. Additionally, we observed that *MIR11700* and Mp*CYP78A101* were both specifically expressed in the apical notch and antheridium, indicating that the miR390-tasi78A-miR11700 regulation of Mp*CYP78A101* is closely related to apical notch development and reproductive processes in *M. polymorpha*.

The tasi78A is the most abundantly produced Mp*TAS3* tasiRNA and has the highest content in MpAGO1. The tasi78A belongs to the reversed and complemented sequence of tasiAP2, which is a highly conserved tasiRNA in non-vascular plants (Morozov et al., 2018). Hence, tasi78A is also a conserved tasiRNA in bryophytes. Our

doi:10.6342/NTU202404007

study showed that tasi78A can coordinately regulate Mp*CYP78A101* expression with miR11700. In non-vascular plants, the *CYP78* family of *M. polymorpha*, *C. purpureus*, and *P. patens* all have the tasi78A cleavage site; however, the vascular plant *CYP78* gene family does not have this cleavage site, indicating that tasi78A specifically regulates the *CYP78* gene family in non-vascular plants. However, miR11700 only specifically regulates Mp*CYP78A101*, and no miR11700 target site is found in the *CYP78* gene family of other non-vascular plants that show the unique dual regulation of Mp*CYP78A101* by tasi78A and miR11700.

To study the molecular mechanisms by which these small RNAs regulate Mp*CYP78A101*, CRISPR gene editing and gain-of-function strategies were employed. However, evolutionary analysis revealed an unreported gene, Mp1g14150, in *M. polymorpha*, which is a paralog of Mp*CYP78A101*. Therefore, morphological changes in these small RNA mutants or transgenic plants are not very pronounced, likely due to the functional redundancy of the Mp1g14150 gene, even though Mp*CYP78A101* expression is affected in those plants. Indeed, the *CYP78A* subfamily has undergone considerable duplication and expansion with functional retendering during the evolution from bryophytes to angiosperms (Ito and Meyerowitz, 2000; Wang et al., 2008; Katsumata et al., 2011; Vasav and Barvkar, 2019; Zhang et al., 2020). However, slight morphological changes in the thallus and sexual organs of the *mir11700^{ge}* mutant and *MIR11700^{OE}* plants suggest that the timing and region of miR11700 may affect genes other than Mp*CYP78A101*.

Notably, this study used two new techniques. First, amiRNA technology was used to specifically express tasi78A (Niu et al., 2006; Flores-Sandoval et al., 2015). Second, we used transient expression by agropenetration to verify that these small RNAs regulate Mp*CYP78A101*. By specifically expressing tasi78A using the miR160 precursor, we successfully reduced endogenous Mp*CYP78A101* expression, consistent

doi:10.6342/NTU202404007

with the results obtained for the *MIR390/11700*^{OE} plants. In addition, through the use of agropenetration to transiently express *78ARep*^{YFP} or *11700Rep*^{YFP} reporters in the young thalli of *amiR-TASI78A*^{OE} and *MIR390/11700*^{OE} plants, respectively, we observed reduced YFP fluorescence, which confirmed that these small RNAs are involved in the regulation of Mp*CYP78A101*.

On the other hand, we will face some challenges while overexpressing the *TAS3* locus. An excess of the *TAS3* transcript might not be cleaved entirely by the limited amount of endogenous miR390-AGO1, which is a limiting factor. Moreover, the overexpression of *TAS3* might result in the expression of additional tasiRNAs, possibly leading to side effects, which could obscure the precise regulatory relationship between tasi78A and Mp*CYP78A101*. We found that agropenetration requires a young thallus as a material and works best with the *Agrobacterium* strain GV2260. Transient fluorescence is often limited to younger tissue near the apical notch, while the mature/basal area shows slight fluorescence. This heterogeneity poses challenges for qRT-PCR quantification, so we recommend using a confocal microscope to observe specific regions as a standard and calculating fluorescence intensity to overcome these inconsistencies. Similar issues arise when observing the loss-of-function effect of tasi78A and miR11700 on Mp*CYP78A101*. The gemma is the preferred material for observing a slight increase in endogenous Mp*CYP78A101*, likely due to its localized expression in the apical notch area. In summary, amiRNA and agropenetration techniques reinforce and confirm the regulatory roles of tasi78A and miR11700 in controlling the expression of Mp*CYP78A101*.

The dual regulation of Mp*CYP78A101* by tasi78A and miR11700 in bryophytes is not unique. In *P. patens*, Ppt-tasiAP2 and Ppt-miR529 jointly regulate the expression of Pp*AP2* (Cho et al., 2012); Ppt-tasiARF and Ppt-miR1219 both regulate Pp*ARF* (Axtell et al., 2007). Together, Ppt-TAS3c tasiRNA and miR1217 control Pp*DCL1* (Arif

doi:10.6342/NTU202404007

et al., 2022). In *M. polymorpha*, miR11707.1 and miR11707.2 co-regulate Mp*AGO1* (Lin et al., 2016; Lin and Bowman, 2018). These examples demonstrate that bryophytes employ a distinctive dual regulatory mechanism to control essential genes. Thus, we speculate that Mp*CYP78A101* is also an essential gene in *M. polymorpha* development that requires precise regulation.

Moreover, observations of promoter fluorescence indicate that compared with the *MIR390* promoter construct, Mp*CYP78A101* exhibits more robust fluorescence in the apical notch, while the *MIR11700* promoter has weaker fluorescence in the apical notch. Additionally, the *MIR11700* promoter results in more noticeable phenotypes in developing thalli and sexual organs. Therefore, we cannot rule out the possibility that tasi78A and miR11700 might have temporal and spatial differences in regulating Mp*CYP78A101*.

Many studies suggest that *CYP78A* may be involved in the accumulation and distribution of auxin. Indeed, an auxin-less sensitive phenotype was observed for the *dcl4*^{ge} and *mir390/11700*^{ge} mutants treated with 0.5 μM NAA. In contrast, when treated with the same concentration of NAA, *amiR-TASI78A*^{OE} plants displayed an extremely sensitive phenotype to auxin, indicating that Mp*CYP78A101* is likely involved in the suppression of the auxin signaling pathway. Notably, we excluded the involvement of Mp*ARF2* in the morphological changes observed in these NAA-treated plants, as Mp*ARF2* did not exhibit significant differential expression in these plants. Additionally, based on the degradome and MpAGO-IP profiles, the evidence for the tasiARF-Mp*ARF* regulatory relationship in the vegetative stage is insignificant and cannot be conclusively demonstrated in this study. Nevertheless, the various Mp*TAS3*-related regulatory mutants, transgenic plants, and advanced amiRNAs used in this study provide a foundation for further investigations into the tasiARF-Mp*ARF* interaction using the amiR-tasiARF approach. Interestingly, in Arabidopsis, tasiARF derived from

doi:10.6342/NTU202404007

At*TAS3* can regulate At*ARF3* and At*ARF4*, both of which are involved in the suppression of the auxin signaling pathway (Fig. 11A). Coincidentally, in *M. polymorpha*, tasi78A produced from Mp*TAS3* can coordinately regulate the expression of Mp*CYP78A101* with miR11700, thereby modulating the auxin signaling pathway (Fig. 11B), especially in the differentiation of the apical notch. Indeed, Eklund et al. (2015) demonstrated that auxin is synthesized at the apex of the thallus through a tryptophan-dependent IPyA pathway and is transported from the apex to the base (Maravolo, 1976; Gaal et al., 1982), which regulates the development of the thallus of *M. polymorpha*. Therefore, we hypothesize that the apical notch of gemma may also contain a high content of auxin, which affects its development.

2.6 Conclusion

This study confirmed that miR390/Mp*TAS3* tasiRNA biogenesis is carried out through MpAGO1 and MpDCL4. We also discovered a new tasi78A variant that can coordinately regulate the expression of Mp*CYP78A101* with miR11700 in the apical notch meristem of gemma and sexual organ production. Unexpectedly, we found that Mp*CYP78A101* might be involved in regulating auxin signaling. In summary, miR390/Mp*TAS3* module-derived tasi78A coordinately regulates Mp*CYP78A101* with miR11700 for RNA silencing, which provides new insights into how Mp*CYP78A101* regulates auxin signaling and sexual organ production.

doi:10.6342/NTU202404007

2.7 Tables and Figures

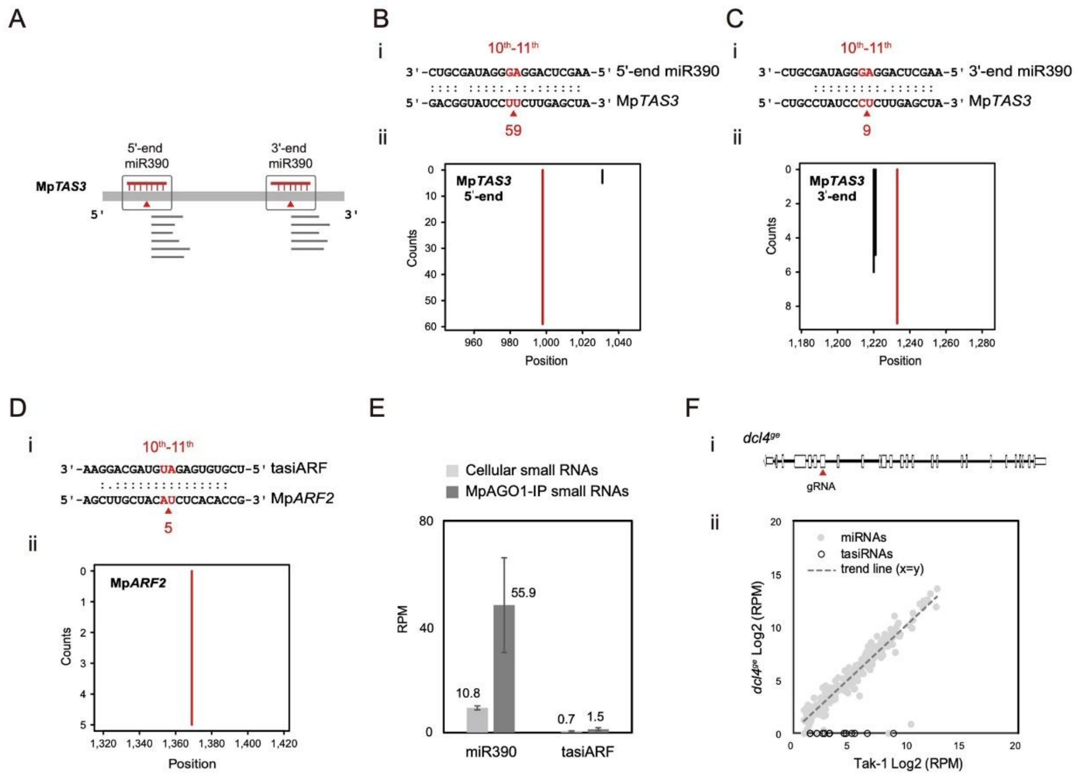

Figure 1. Target prediction of miR390 and tasiARF and the role of MpDCL4 in tasiRNA biogenesis in *M. polymorpha*.

(A) Illustration of the two-hit configuration of miR390 to Mp*TAS3*. (B) The 5'-end target site of Mp*TAS3* paired with miR390. (C) The 3'-end target site of Mp*TAS3* paired with miR390. (D) tasiARF and Mp*ARF2*. The alignments between the representative tasiRNAs or miRNAs and their target transcripts are shown below the corresponding t-plots. The arrowheads and the numbers below the arrowheads correspond to the positions of red lines and the read abundances, respectively. The x-axis of the t-plot is the position on the transcript starting from the transcription start site, and the y-axis is the number of reads detected from a position. Red lines indicate the signatures produced by tasiRNA- or miRNA-directed cleavage. (E) Bar plot of miR390 and tasiARF reads per million mapped reads (RPM) values from the cellular and MpAGO1-IP profiles. (F) miRNAs and tasiRNAs in the *dcl4*^{ge} mutant. Site of gene editing on the Mp*DCL4*

doi:10.6342/NTU202404007

genomic DNA (i). The scatter plot shows the RPM values of miRNAs (gray dots) and tasiRNAs (white dots) in Tak-1 plants and *dcl4*^{ge} mutants (ii).

doi:10.6342/NTU202404007

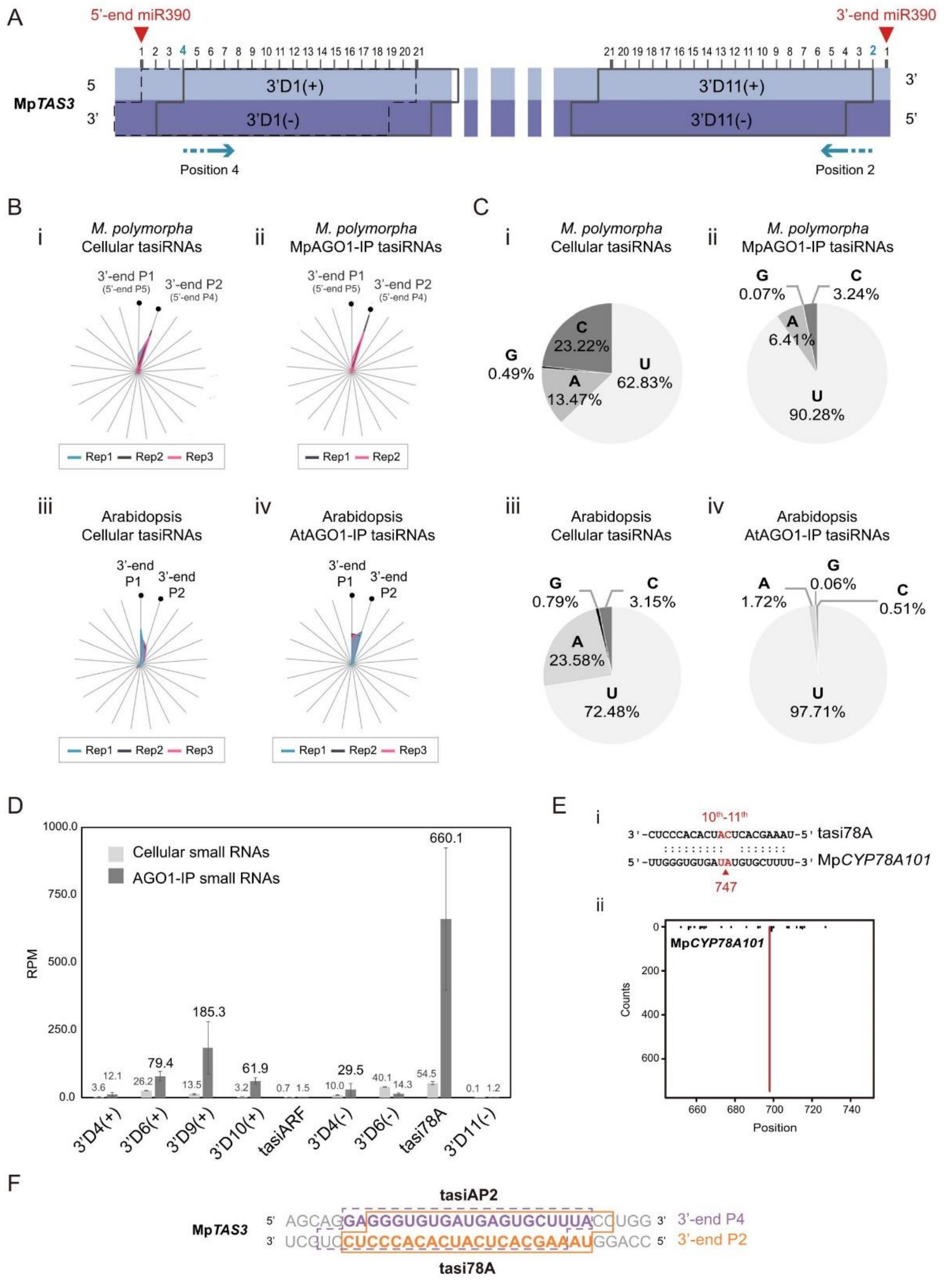

Figure 2. Mp*TAS3*-derived phased 21-nucleotide (nt) tasiRNAs and their corresponding targets in *M. polymorpha*.

(A) Illustration of the positions and orientations of the predicted DICER processing cleavage sites on Mp*TAS3*. Red arrowheads indicate the 5'-end and 3'- end miR390 cleavage sites. The Mp*TAS3*-derived tasiRNAs were named the number-phasing

doi:10.6342/NTU202404007

position. The symbols of (+) and (-) represent the tasiRNA fragments generated from the sense and antisense strands, respectively. (B) Phasing position analysis of *TAS3*-derived 21-nt tasiRNAs from cellular and AGO1-IP profiles in *M. polymorpha* and Arabidopsis. The radar plots represent the ratio of tasiRNAs from each of the 21 phasing positions. Rep-number represents the number of biological replicates. (C) The 5'-end 1st nucleotide of the tasiRNAs from the cellular and AGO1-IP profiles in *M. polymorpha* and Arabidopsis. (D) Bar plot of the reads per million mapped reads (RPM) values of tasiRNAs from 3'-end phasing position 2 in the cellular and MpAGO1-IP profiles. (E) Alignments and target plots of tasi78A and Mp*CYP78A101*. (F) Sequences of tasi78A and tasiAP2 in *M. polymorpha*.

doi:10.6342/NTU202404007

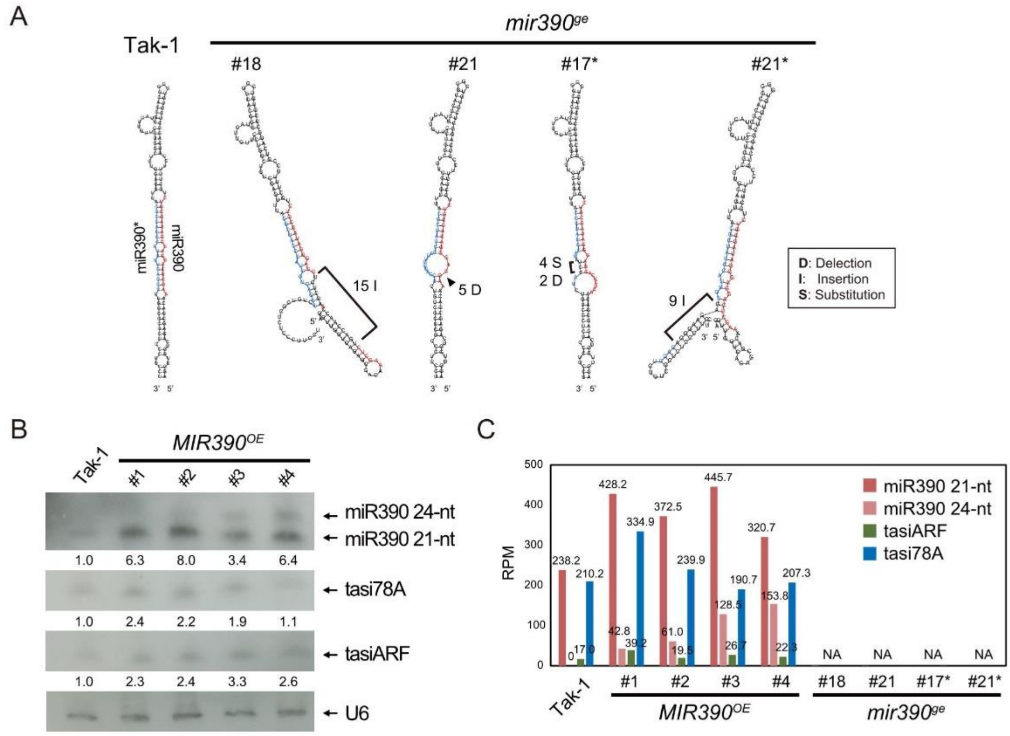

Figure 3. Small RNA expression patterns of miR390, tasiARF, and tasi78A in the *mir390ge* mutants and *MIR390OE* plants.

(A) Secondary structure prediction of the wild type and edited miR390 precursors. The mature sequence is highlighted in red, and the star sequence is highlighted in blue. (B) Northern blotting of miR390, tasiARF, and tasi78A in the *MIR390OE* plants. *U6* was used as a loading control. (C) Small RNA profiles of miR390, tasiARF, and tasi78A in the *MIR390OE* plants and *mir390ge* mutants. RPM, Reads per million mapped reads.

doi:10.6342/NTU202404007

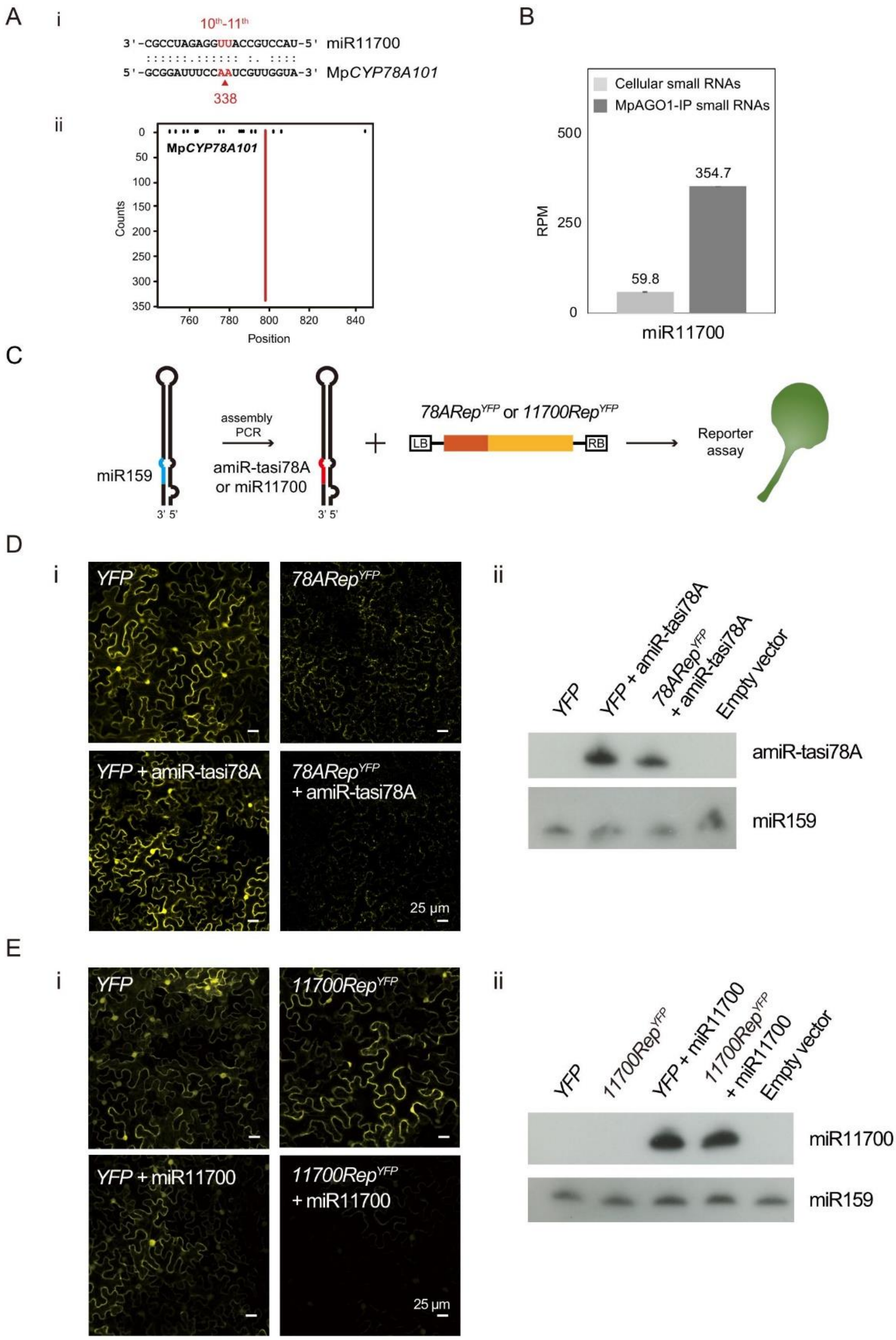

Figure 4. Target prediction of mi11700 and the reporter assays of amiR-tasi78A,

doi:10.6342/NTU202404007

miR11700, and Mp*CYP78A101* in *Nicotiana benthamiana*.

(A) Alignment and target plot of miR11700 and Mp*CYP78A101*. The alignments between the representative miRNAs and their target transcripts are shown above the t-plots. The arrowheads and the numbers below the arrowheads correspond to the positions of red lines and the read abundances, respectively. The x-axis of the t-plot is the position on the transcript starting from the transcription start site, and the y-axis is the number of reads detected from a position. Red lines indicate the signature produced by miRNA-directed cleavage. (B) Bar plot of the reads per million mapped reads (RPM) values of miR11700 from the cellular and MpAGO1-IP profiles. (C) Illustration of transient expression in *Nicotiana benthamiana* for assessing the activity of amiR-tasi78A or miR11700 alongside their reporters, *78ARep*^{YFP} and *11700Rep*^{YFP}. (D) Transient reporter assays of amiR-tasi78A and *78ARep*^{YFP} (*78ARep*^{YFP}+amiR-tasi78A) in the leaves of *N. benthamiana*. The constructs expressing YFP and amiR-tasi78A (YFP + amiR-tasi78A) were co-expressed in *N. benthamiana* as a negative control (i). Northern blotting of amiR-tasi78A in infiltrated plants. The miR159 was used as a loading control (ii). (E) Transient reporter assays of miR11700 and *11700Rep*^{YFP} (*11700Rep*^{YFP}+miR11700) in leaves of *N. benthamiana*. The constructs expressing YFP and miR11700 (YFP + miR11700) were co-expressed in *N. benthamiana* as a negative control (i). Northern blotting of miR11700 in infiltrated plants. The miR159 was used as a loading control (ii).

doi:10.6342/NTU202404007

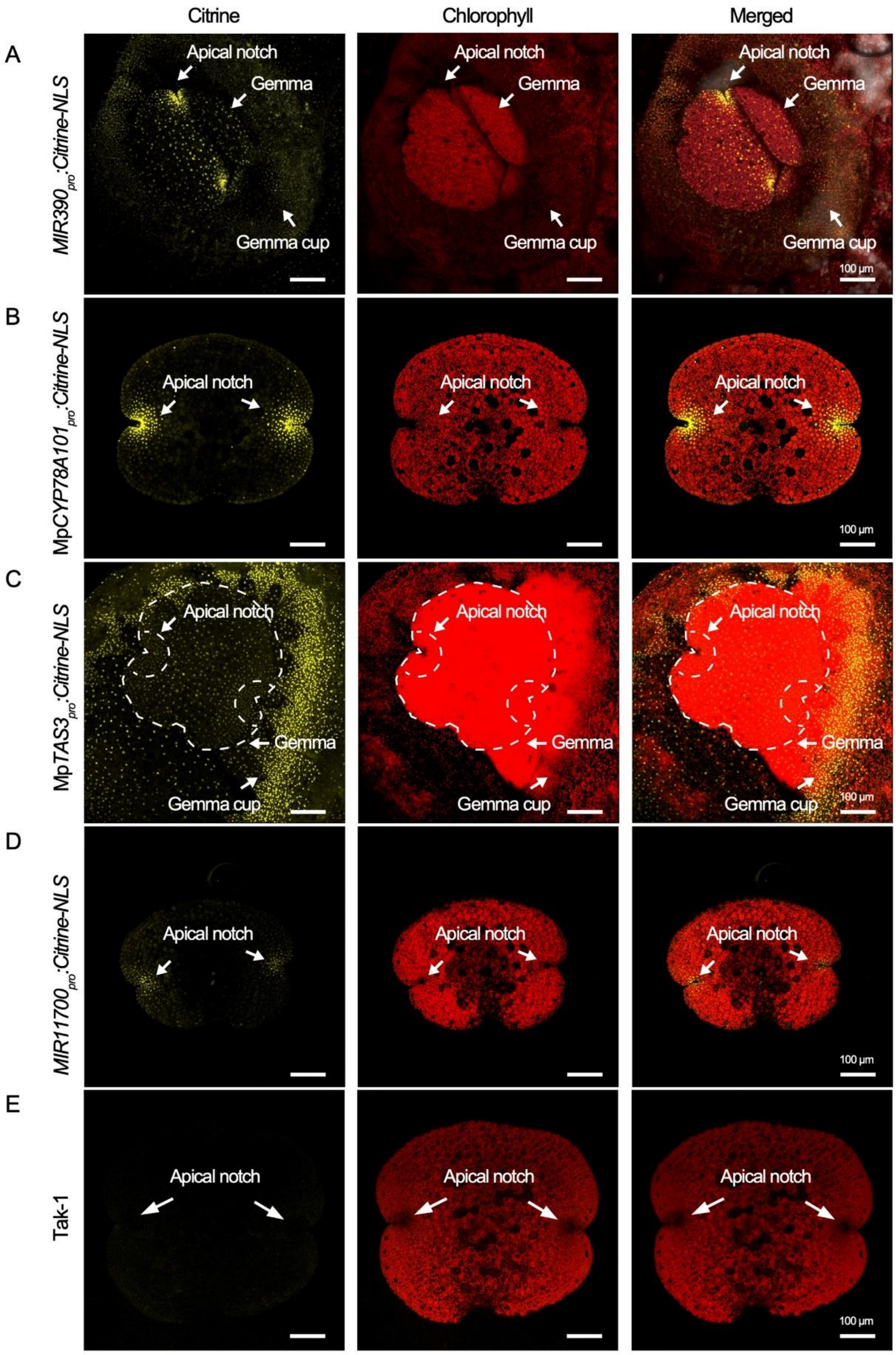

Figure 5. Expression patterns of the *MIR390*/Mp*TAS3* module, *MIR11700*, and Mp*CYP78A101* in *M. polymorpha*.

Confocal images of the *MIR390*$_{pro}$*:Citrine-NLS* (A), Mp*CYP78A101*$_{pro}$*:Citrine-NLS*

doi:10.6342/NTU202404007

(B), Mp*TAS3*$_{pro}$*:Citrine-NLS* (C), and *MIR11700*$_{pro}$*:Citrine-NLS* (D) transgenic plants during gemma development. (E) Tak-1 plant was used as a negative control.

doi:10.6342/NTU202404007

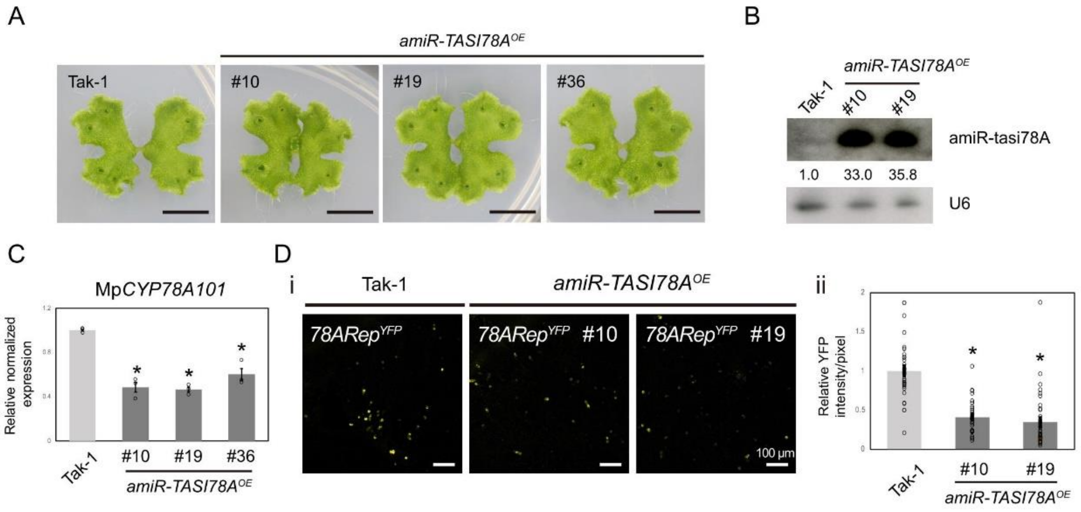

Figure 6. Phenotypic observations and reporter assays of *78ARep^{YFP}* in the a*miR-TASI78A^{OE}* plants.

(A) Vegetative growth of the 18-day-old a*miR-TASI78A^{OE}* plant G3 lines. Scale bars, 1 cm. (B) Northern blotting of amiR-tasi78A in *amiR-TASI78A^{OE}* plants. U6 served as a loading control. (C) qRT-PCR of Mp*CYP78A101* in the a*miR-TASI78A^{OE}* plants. Mp*EF1-alpha* was used as a reference gene. Error bars represent the standard error from three biological replicates. (D) YFP transient reporter assays of *78ARep^{YFP}* in the *amiR-TASI78A^{OE}* plants (i). The quantified relative YFP intensity of the data was calculated from more than 30 images captured by a fluorescence microscope (ii). Tak-1 plants were used as control. Error bars represent the standard error from three biological replicates.

doi:10.6342/NTU202404007

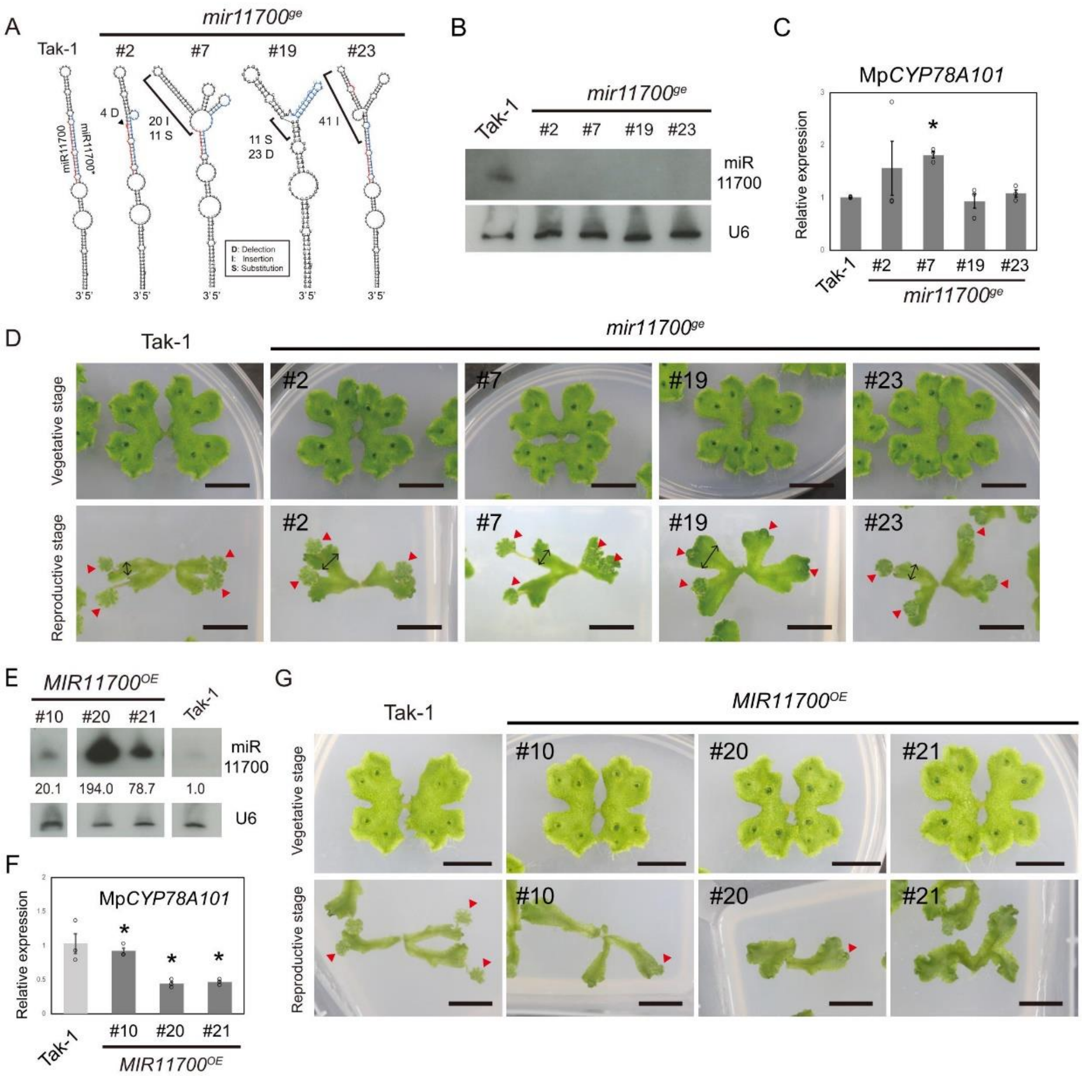

Figure 7. Phenotypic observations and expression analysis of the *mir11700^{ge}* mutants and *MIR11700^{OE}* plants.

(A) Secondary structure prediction of the wild type and edited miR11700 precursors. The mature and star sequences of miRNAs are highlighted in red and blue, respectively. (B) Northern blotting of miR11700 in the *mir11700^{ge}* mutants. (C) qRT-PCR of Mp*CYP78A101* in the *mir11700^{ge}* mutants. (D) Plant growth of the *mir11700^{ge}* mutants. (E) Northern blotting of miR11700 in the *MIR11700^{OE}* plants. (F) qRT-PCR of Mp*CYP78A101* in the *MIR11700^{OE}* plants. (G) Plant growth of the *MIR11700^{OE}* plants. U6 served as a loading control. *EF1-alpha* was used as a reference gene. Error bars represent the standard error from three biological replicates. The plants in the vegetative

doi:10.6342/NTU202404007

and reproductive stages were 2.5-week-old and 3.5-week-old plants, respectively. Scale bar, 1 cm. The bidirectional arrow indicates the width of the thallus, while the red arrowhead indicates the male sexual organs.

doi:10.6342/NTU202404007

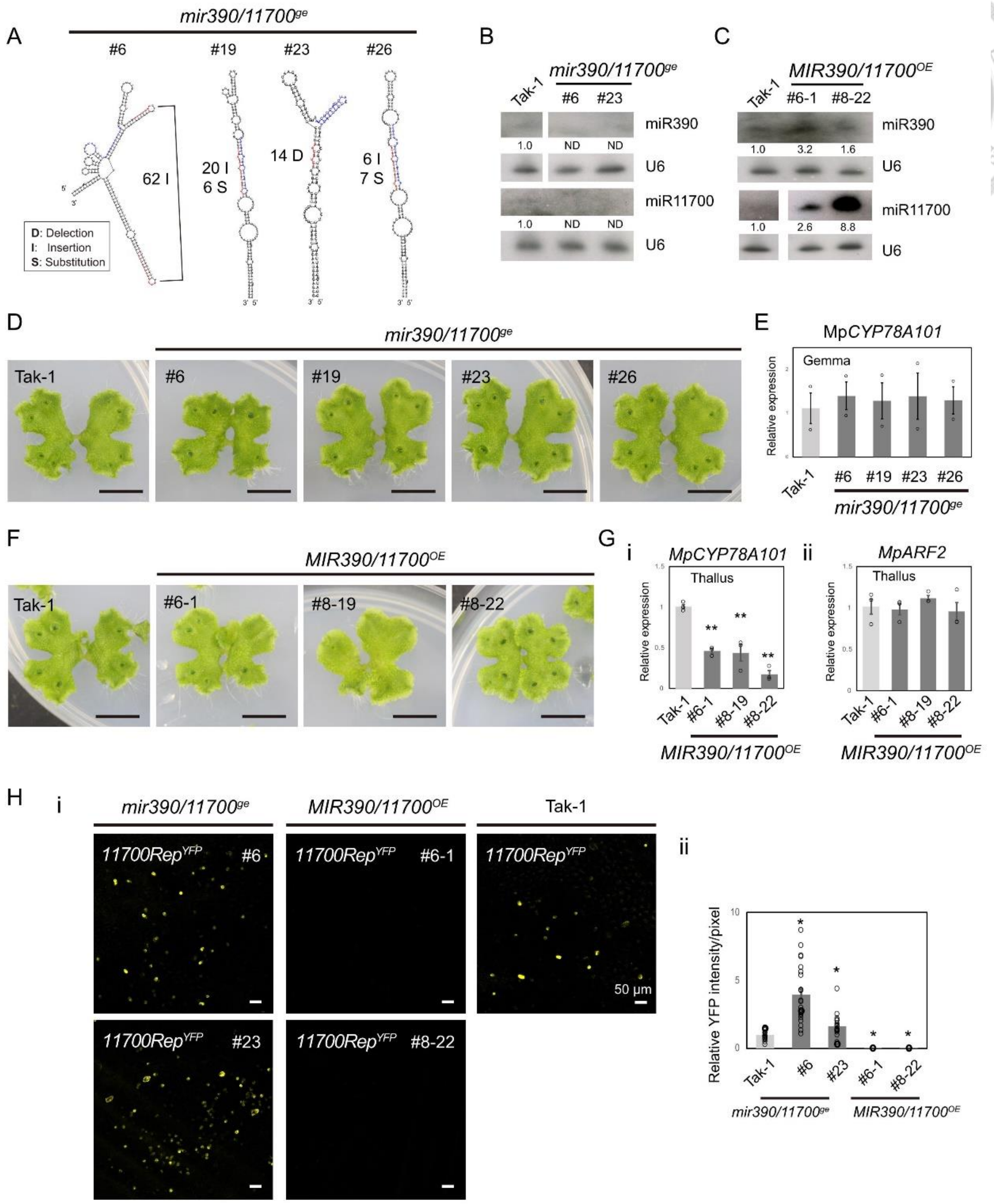

Figure 8. Phenotypic observations and reporter assays of *11700Rep*^{YFP} in the *mir390/11700*^{ge} mutants and *MIR390/11700*^{OE} plants.

(A) Secondary structure prediction of the wild type and edited miR11700 precursors. The mature sequence is highlighted in red, and the star sequence is highlighted in blue. The *mir390*^{ge} mutant was used as the genetic background to mutate miR11700. Northern blotting of miR390 and miR11700 in the *mir390/11700*^{ge} mutants (B) and

doi:10.6342/NTU202404007

MIR390/11700^{OE} plants (C), respectively. (D) Vegetative growth of the 18-day-old *mir390/11700*^{ge} mutants. Scale bars, 1 cm. (E) qRT-PCR analysis of Mp*CYP78A101* in the gemmae of the *mir390/11700*^{ge} mutants. (F) Vegetative growth of the 18-day-old *MIR390/11700*^{OE} plants. Scale bars, 1 cm. (G) qRT-PCR analysis of Mp*CYP78A101* (i) and Mp*ARF2* (ii) in the thallus of *MIR390/11700*^{OE} plants. (H) YFP transient reporter assays of *11700Rep*^{YFP} in the *mir390/11700*^{ge} mutants and *MIR390/11700*^{OE} plants (i). The YFP intensity was quantified using more than 20 images captured by a fluorescence microscope (ii). Tak-1 was used as a control. Error bars represent the standard error from three biological replicates.

doi:10.6342/NTU202404007

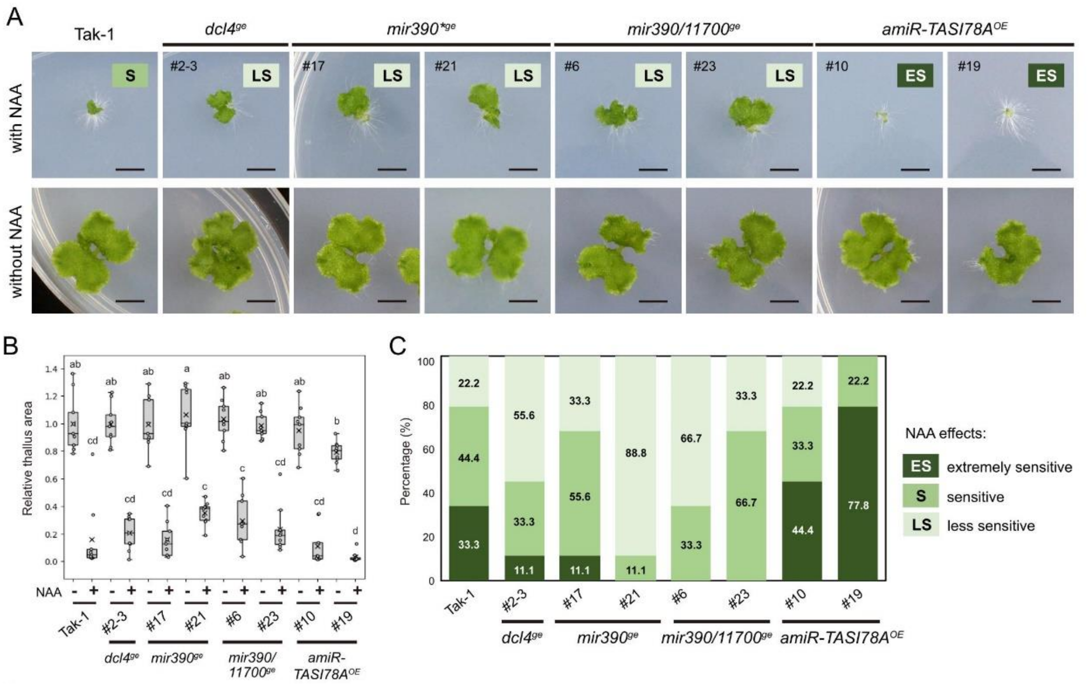

Figure 9. NAA treatment of *dcl4ge*, *mir390ge*, *mir390/11700ge* mutants, and *amiR-TASI78AOE* plants.

(A) Comparative phenotypes of Tak-1 plants, *dcl4ge*, *mir390ge*, *mir390/11700ge* mutants, and *amiR-TASI78AOE* plants ($n = 36$). These images were captured 14 days post-gemma germination on the media supplemented with 0.5 µM NAA (upper panel) and without NAA (lower panel). “ES” represents an extremely sensitive phenotype; “S” represents a sensitive phenotype; “LS” represents a less sensitive phenotype. Scale bar, 5 mm. (B) A boxplot illustrating the relative thallus area. Within each box. The horizontal band denotes the median, and the cross indicates the mean. The lower and upper edges of the box represent the first and third quartiles, respectively. Individual data points derived from a minimum of 9 independent plants are shown as dots. Statistical significance was assessed using Tukey’s honestly significant difference test, with letters above the boxplots denoting significant differences (p-value < 0.05). (C) The frequency distribution of NAA effects was classified across various plants. An area ratio (with NAA/without NAA) less than 0.025 indicated an extremely sensitive phenotype, an

doi:10.6342/NTU202404007

area ratio between 0.025 and 0.2 indicated a sensitive phenotype, and an area ratio greater than 0.2 indicated a less sensitive phenotype.

doi:10.6342/NTU202404007

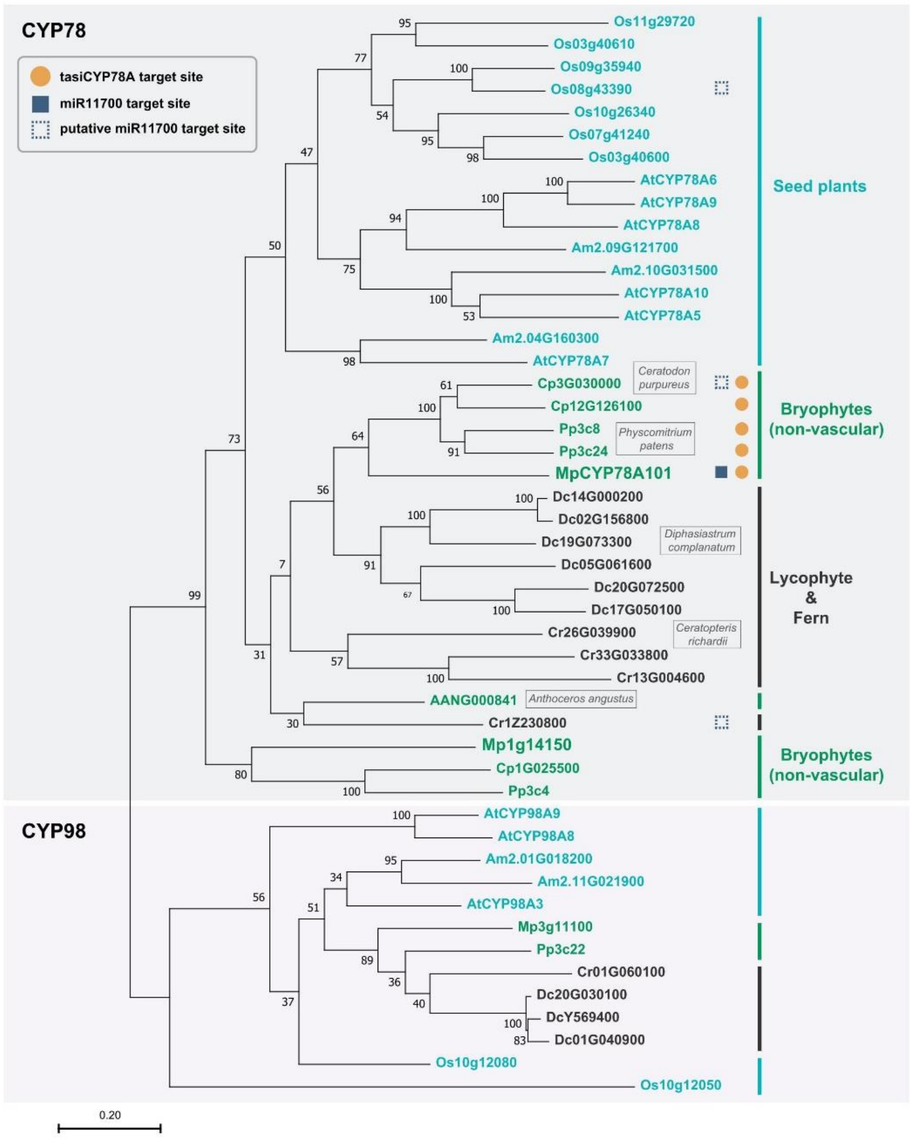

Figure 10. Phylogenetic tree of *CYP78* homologs.

CYP78 homologs in bryophytes, lycophytes, ferns and seed plants. The orange circles indicate the *CYP78* homologs with the tasi78A target site. The blue squares indicate the *CYP78* homologs with the miR11700 target site, and the open squares indicate the *CYP78* homologs with the putative miR11700 target site. Bryophytes (*Anthoceros angustus*, *Ceratodon purpureus*, *Physcomitrella patens*, and *Marchantia polymorpha*), lycophytes (*Diphasiastrum complanatum*), ferns (*Ceratopteris richardii*) and seed plants (*Arabidopsis thaliana*, *Oryza sativa*, *Amborella trichopoda*). *CYP98* homologs were used as an outgroup. The phylogenetic relationships were constructed by MEGAX using the maximum likelihood (ML) criterion with 1,000 bootstrap replicates.

doi:10.6342/NTU202404007

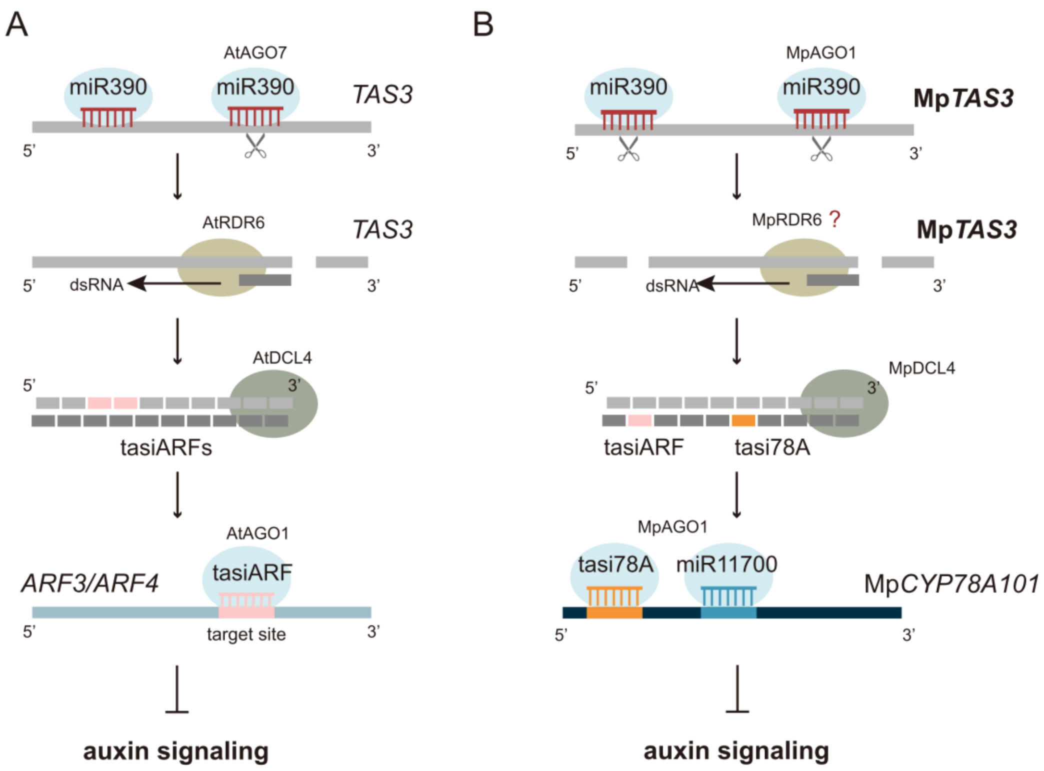

Figure 11. Illustration of the miR390/*TAS3* regulatory module in Arabidopsis and *M. polymorpha*.

doi:10.6342/NTU202404007

2.8 Supplementary Tables and Figures

Supplementary Table S1. The primer sets used for gene construction in this study

primer name	Sequence (5' to 3')	purpose	transformed method	species
Mp-pre-miR390-ox-F	caccGTACATAACGATGCCGAGG	*MIR390* overexpression	thallus transformation	*M.polymorpha*
Mp-pre-miR390-ox-R	AAAGAGGGAGGAAGGGAGAG			
Mp-miR390*-gRNA-A	ctcgGAGAGCGACAGAGCTCACAA	miR390 knockout	thallus and sporling transformation	
Mp-miR390*-gRNA-B	aaacTTGTGAGCTCTGTCGCTCTC			
Mp-pre-miR11700-ox-F	caccCGATCTTCGATTGTTGCGATGG	*MIR11700* overexpression	thallus transformation	*M.polymorpha*
Mp-pre-miR11700-ox-R	CGATCCGATTGCAACAATGCTTG			
Mp-miR11700-gRNA-A	ctcgCCAGACGCTGTACCTGCCAT	miR11700 knockout		
Mp-miR11700-gRNA-B	aaacATGGCAGGTACAGCGTCTGG			
Mp-miR390-pro-L1-F	aaggaaccaattcagtcTTTATGGGAGAAGTCAAAGGGC	promoter-repoter assay	sporling transformation	*M.polymorpha*
Mp-miR390-pro-L1-R	tagatatctcgagtgGGTTCCCCCCGGCCACCA			
Mp-TAS3-pro-F	aaggaaccaattcagtcCATAGCATCCCCTCCTTTCA			
Mp-TAS3-pro1-R	tagatatctcgagtgGGGACGATAGGGAAACGGA			
Mp-miR11700-pro-L1-F	aaggaaccaattcagtcGTTTCTATCATGACCTTGAC	promoter-repoter assay	thallus transformation	*M.polymorpha*
Mp-miR11700-pro-L1-R	tagatatctcgagtgGTCGCTCCGCCCATCTTC			
Mp-CYP78A101-pro-F	aaggaaccaattcagtcCTGACATTGCACGTTGAGAGG			
Mp-CYP78A101-pro1-R	tagatatctcgagtgTTCTTCCCAAATCCCACTC			
art-tasi78A_F1_AtmiR159	caccTTGATCTGTCGATGGA	reporter assay_AtmiR159 backbone	Agroinfiltration	*N. benthamiana*
art-tasi78A_F2_AtmiR159	AGGAGGGTGTGAACAGTGCTTTACATGAGTTGAGCAGGGT			
art-tasi78A_F3_AtmiR159	AAAGAAAAGCTGCTTAGCTATGGATCCCATAAGCCCTAAT			
art-tasi78A_F4_AtmiR159	CCTTGTAAAGTAAAAAAGGATTTGGTTATATGGATTGCAT			
art-tasi78A_F5_AtmiR159	ATCTCAGGAGCTTTAACTTGCCCTTTAATGGCTTTTACTC			

doi:10.6342/NTU202404007

art-tasi78A_F6_AtmiR159	TTCTAAAGCACTCATCACACCCTCCATCCCGGGTCAA			
art-tasi78A_R1_AtmiR159	TTGACCCGGGATGGAGGGTGTGATGAGTGCTTTAGAAGAGTAA			
art-tasi78A_R2_AtmiR159	AAGCCATTAAAGGGCAAGTTAAAGCTCCTGAGATATGCAATCCAT			
art-tasi78A_R3_AtmiR159	ATAACCAAATCCTTTTTTACTTTACAAGGATTAGGGCTTATG			
art-tasi78A_R4_AtmiR159	GGATCCATAGCTAAGCAGCTTTTCTTTACCCTGCTCAACTCA			
art-tasi78A_R5_AtmiR159	TGTAAAGCACTGTTCACACCCTCCTTCCATCGACAGATCAA			
art-tasi78A target-F	cacc**ATG**CCCCTGCTCACGAAAGGC	reporter assay_tasi78A target	Agroinfiltration and agropenetration	*N. benthamiana* and *M. polymorpha*
art-tasi78A target-R	AGGTCCAGCCCAAAACAGAAG			
Mp-pre-miR11700-ox-F	caccCGATCTTCGATTGTTGCGATGG	reporter assay	Agroinfiltration	*N. benthamiana*
Mp-pre-miR11700-ox-R	CGATCCGATTGCAACAATGCTTG			
miR11700 target-F	cacc**ATG**AACCGATTCCTGGTCCG	reporter assay_miR11700 target	Agroinfiltration and agropenetration	*N. benthamiana* and *M. polymorpha*
miR11700 target-R	CCATCAAACGCTTCGC			
miR11689 target-F	cacc**ATG**GAAGGAGATGGTGAGAGA	reporter assay_miR11689 target_internal control	Agropenetration	*M. polymorpha*
miR11689 target-R	ACGAGCTCAGAACACCTTTGGTG			
art-tasi78A_F1_MpmiR160	caccTCGACGCGACTAATTGGGGAGGCCAGACT	*amiR-TASI78A* overexpression_MpmiR160 backbone	thallus transformation	*M. polymorpha*
art-tasi78A_F2_MpmiR160	GCACTTAAAGCACTCATCACACCCTCACTGAGGAGCTCCTCAG			
art-tasi78A_F3_MpmiR160	AGACCTTGACAGGCTCCGTA			
art-tasi78A_F4_MpmiR160	GCGAGGGTCTGATGGGTGCATTAGGAGGAAG			
art-tasi78A_F5_MpmiR160	TCGCTACCTCCCGCAAGGTGCGACTA			
art-tasi78A_R1_MpmiR160	TAGTCGCACCTTGCGGGAGGTAGCGACTTC			
art-tasi78A_R2_MpmiR160	CTCCTAATGCACCCATCAGACCCTCGCTACGG			
art-tasi78A_R3_MpmiR160	AGCCTGTCAAGGTCTCTGAGGAGCTCCT			
art-tasi78A_R4_MpmiR160	CAGTGAGGGTGTGATGAGTGCTTTAAGTGCAGTCTG			
art-tasi78A_R5_MpmiR160	GCCTCCCCAATTAGTCGCGTCGA			

doi:10.6342/NTU202404007

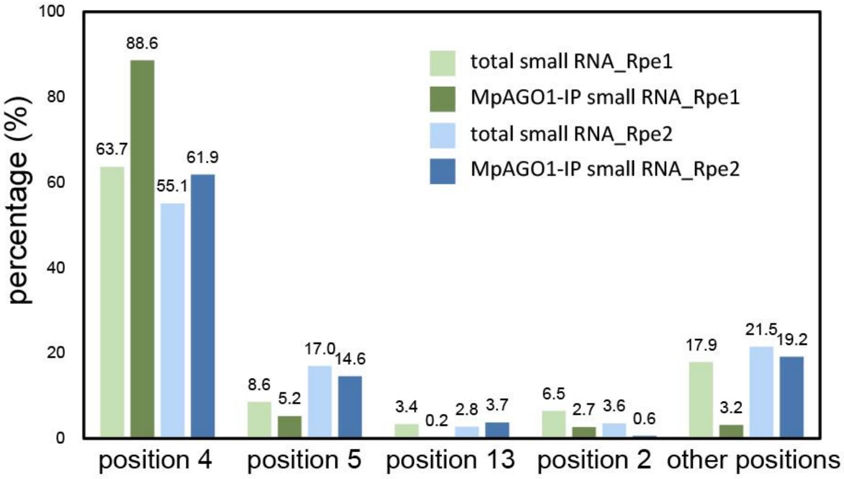

Supplementary Figure S1. Mp*TAS3*-derived phased 21-nucleotide tasiRNAs.

Percentage of the Mp*TAS3*-derived tasiRNAs from the different phasing positions in cellular and MpAGO1-IP profiles. Rep1 and Rep2 represent two biological replicates.

doi:10.6342/NTU202404007

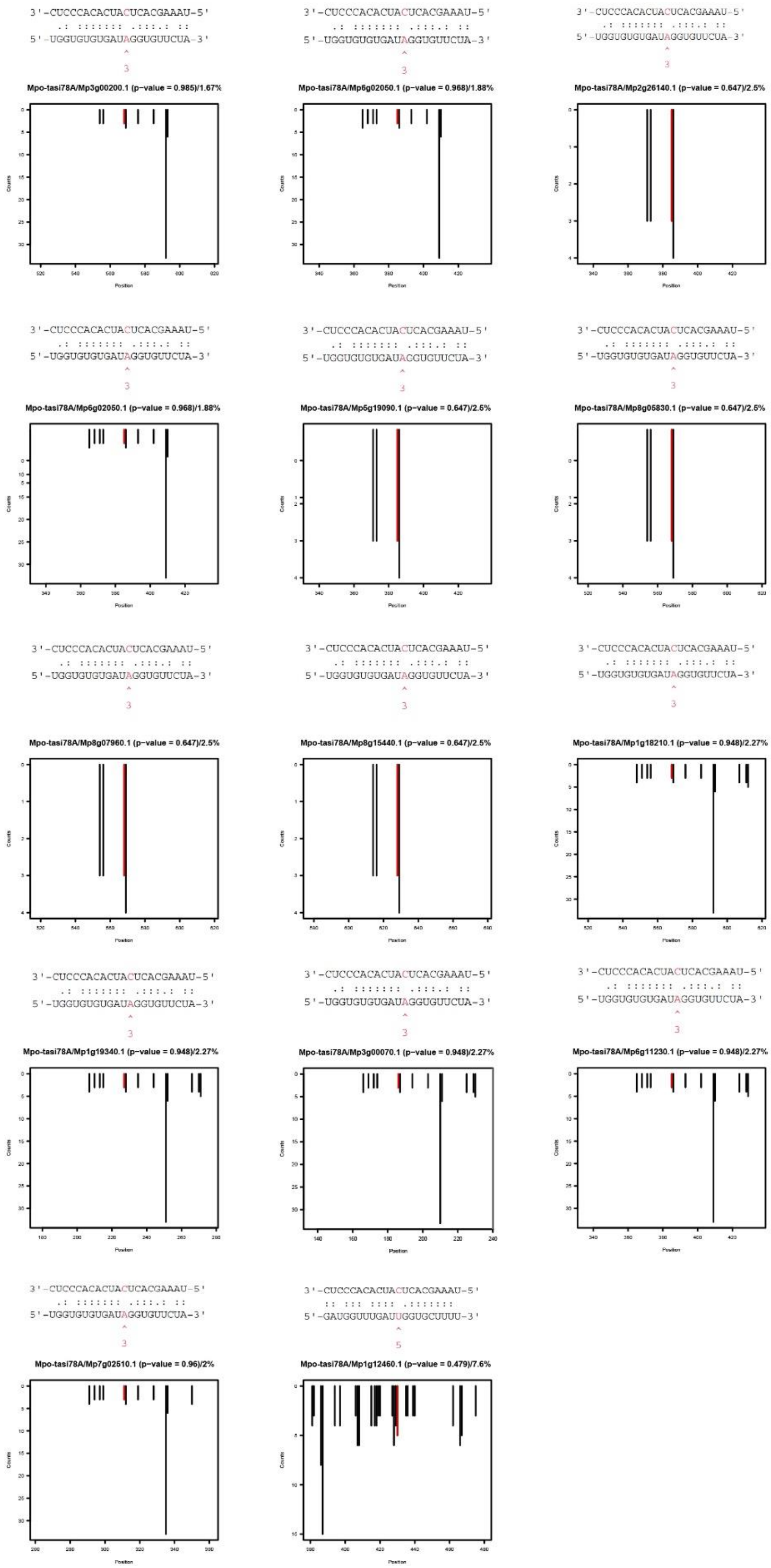

Supplementary Figure S2. Alignments and target plots of tasi78A and its targets in *M. polymorpha*.

doi:10.6342/NTU202404007

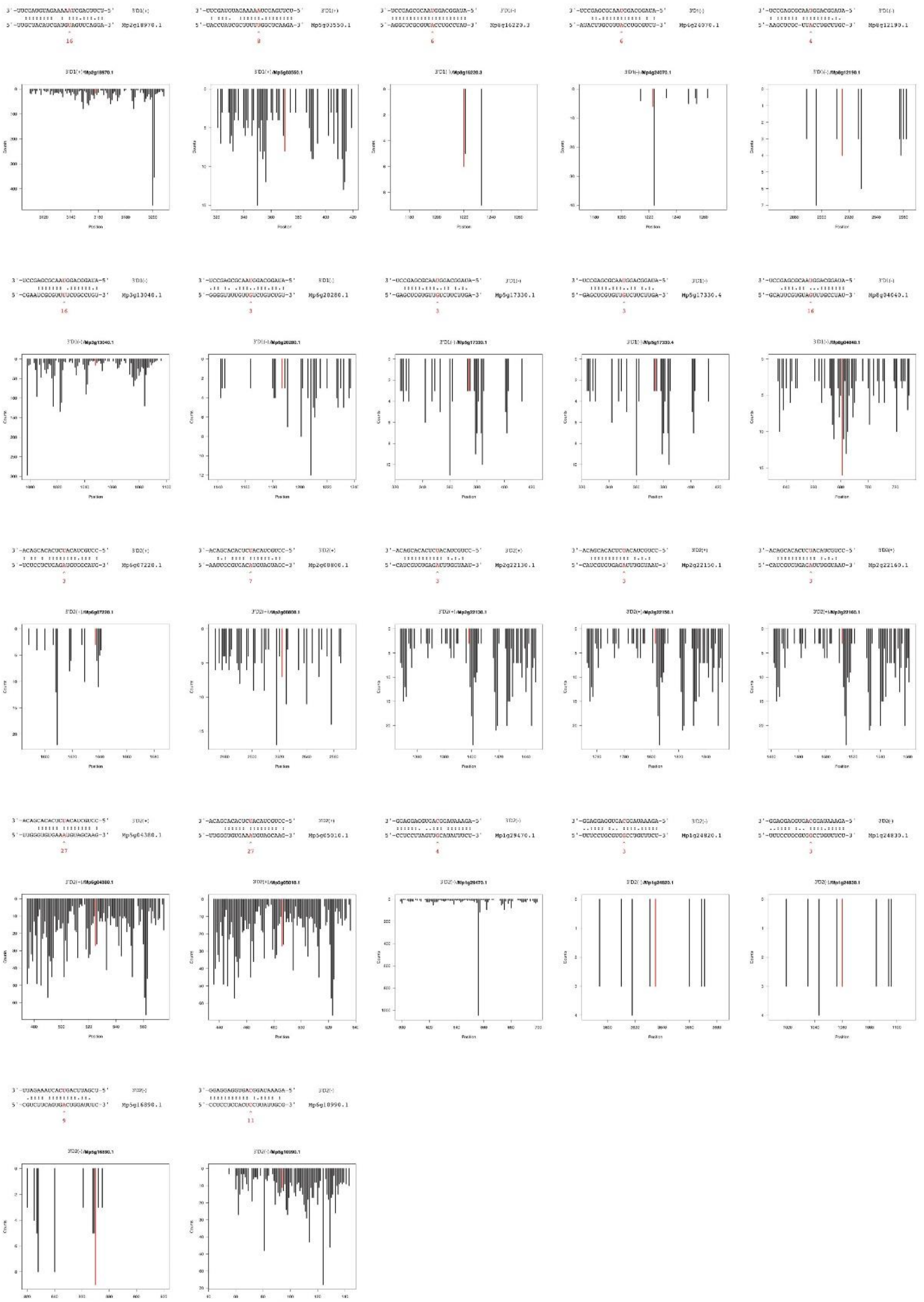

doi:10.6342/NTU202404007

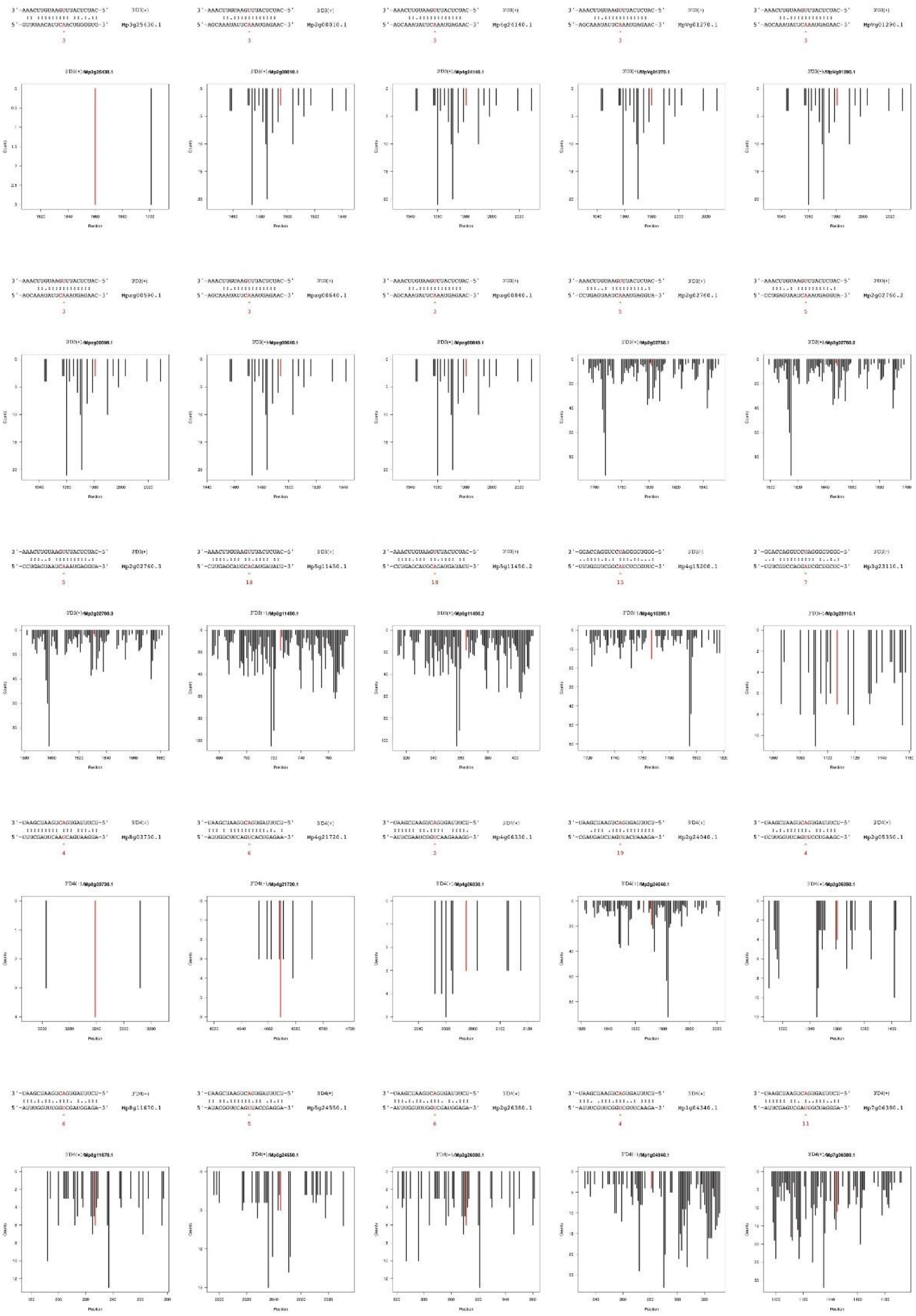

doi:10.6342/NTU202404007

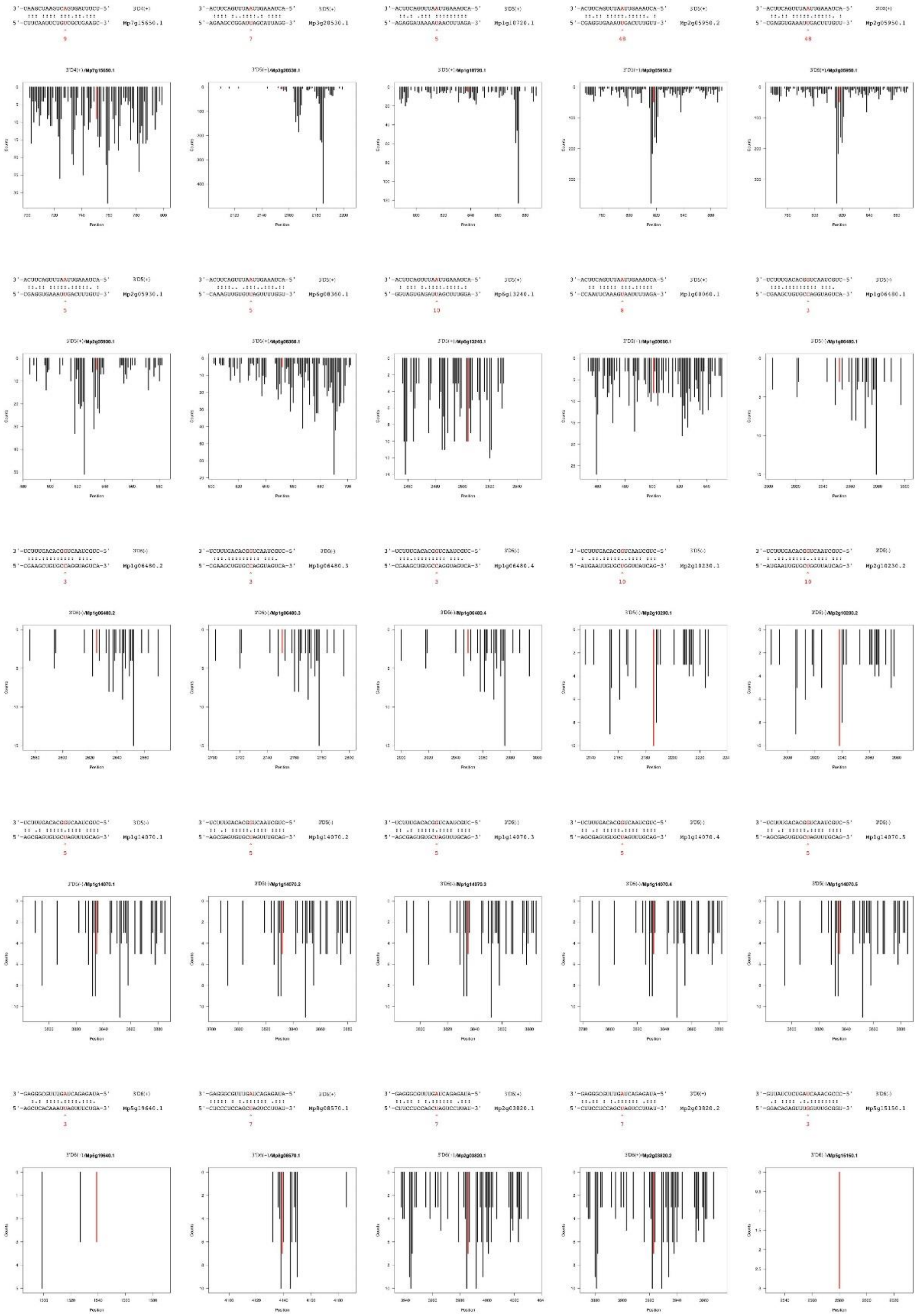

doi:10.6342/NTU202404007

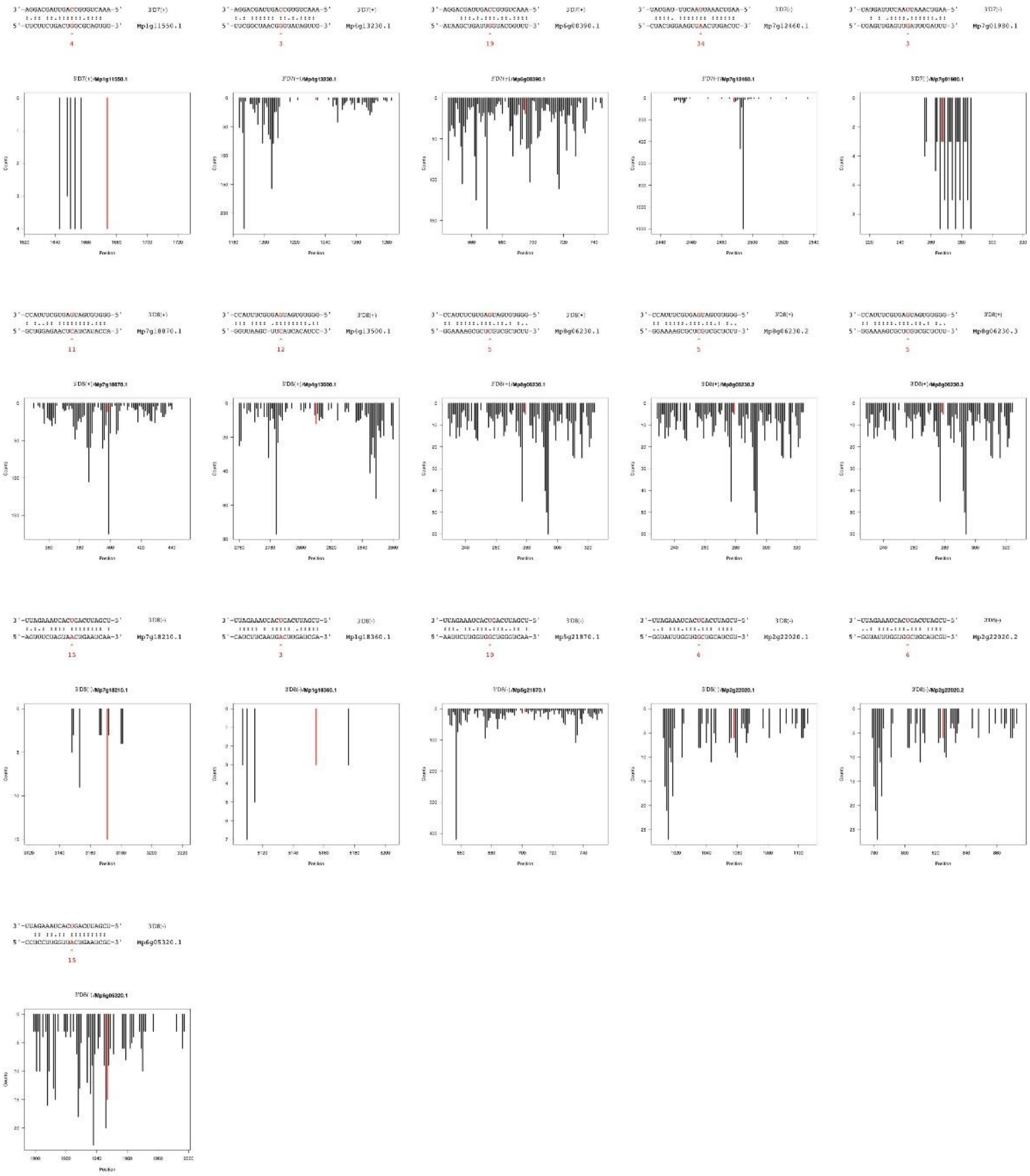

doi:10.6342/NTU202404007

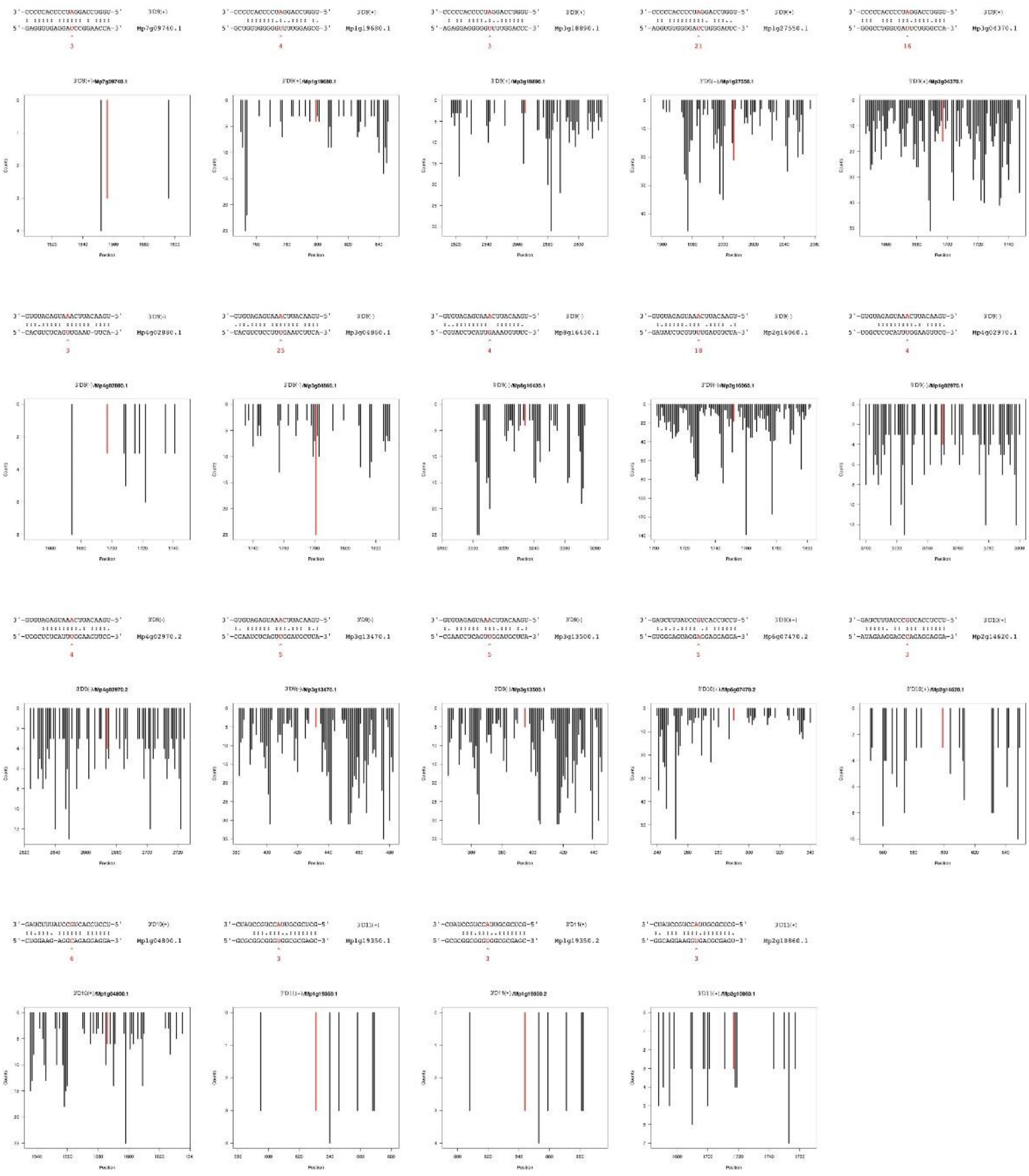

Supplementary Figure S3. Alignments and target plots of tasiRNAs from 3'-end phasing position 2 and the targets in *M. polymorpha*.

doi:10.6342/NTU202404007

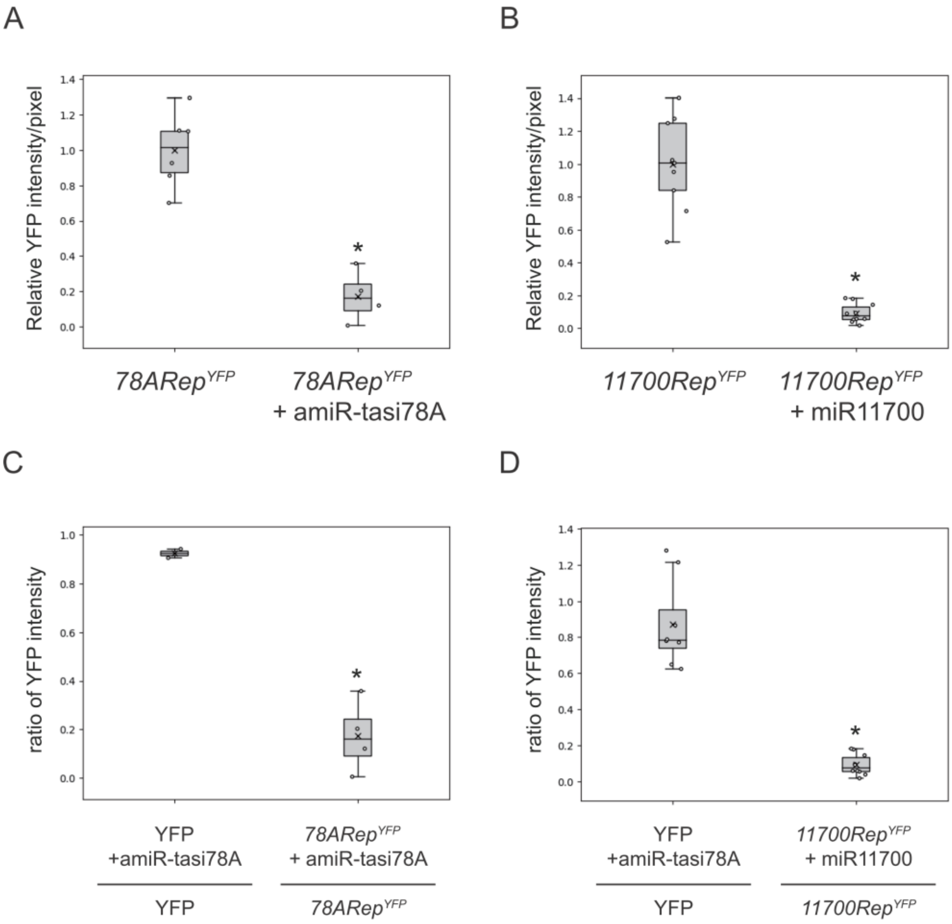

Supplementary Figure S4. Boxplot of quantified YFP intensity of the confocal images.

The relative YFP intensity of *78ARep*^{YFP} reporter and *78ARep*^{YFP} + amiR-tasi78A (A) and *11700Rep*^{YFP} reporter and *11700Rep*^{YFP} + miR11700 (B) in leaves of *Nicotiana benthamiana*. The ratio of YFP intensity of *78ARep*^{YFP} reporter and *78ARep*^{YFP} + amiR-tasi78A (C) and *11700Rep*^{YFP} reporter and *11700Rep*^{YFP} + miR11700 (D) in leaves of *N. benthamiana*. Reporter-only constructs with and without expressing small RNAs served as the numerator and denominator, respectively. The median and mean are represented by bands and crosses inside the boxes. The lower and upper hinges correspond to the first and third quartiles. Dots represent individual values from 2-10 independent images, and statistical significance was determined using Student's t-test. Boxplots labeled with '*' indicate significant differences (p-value < 0.05).

doi:10.6342/NTU202404007

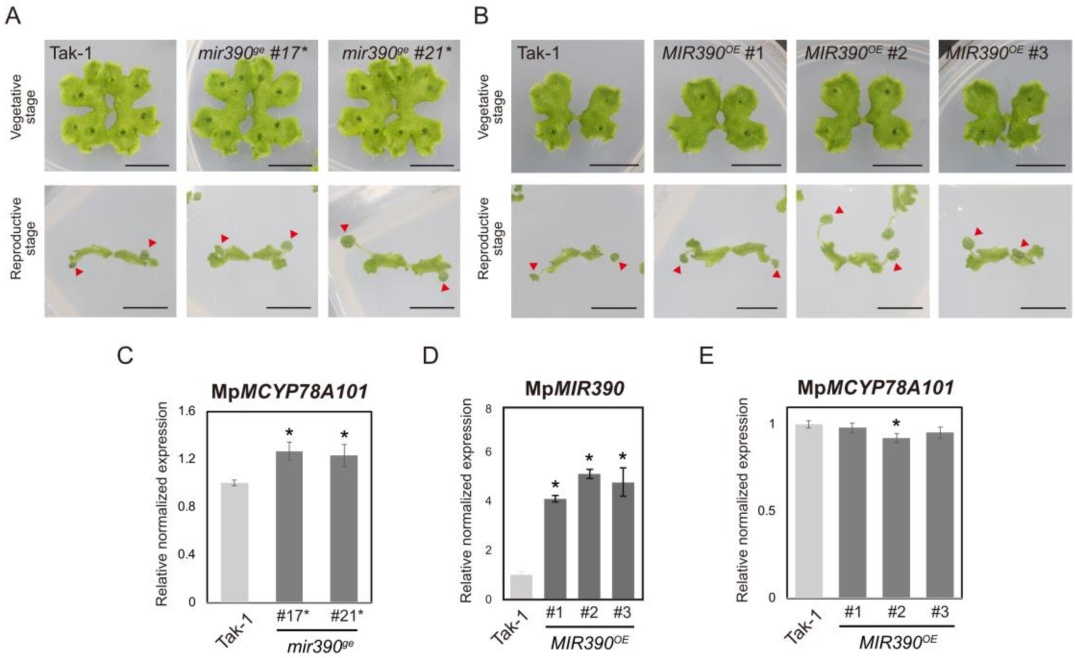

Supplementary Figure S5. Phenotypic observations and expressional analysis of the *mir390*^{ge} mutants and *MIR390* plants.

Vegetative (upper panel) and reproductive (lower panel) growth of the *mir390*^{ge} mutant G4 lines (A) and *MIR390* plant G4 lines (B). Scale bars, 1 cm. (C, D, E) Expression levels of miR390 and Mp*CYP78A101* in the *MIR390* plant and *mir390*^{ge} mutant. Stem-loop qRT-PCR of the *MIR390* in the *MIR390* plant G4 lines. *U6* was used as a loading control. qRT-PCR of Mp*CYP78A101* in the *mir390*^{ge} mutant and *MIR390* plant G4 lines. *EF1-alpha* was used as a reference gene. Error bars indicate the *SE* from three biological replicates.

doi:10.6342/NTU202404007

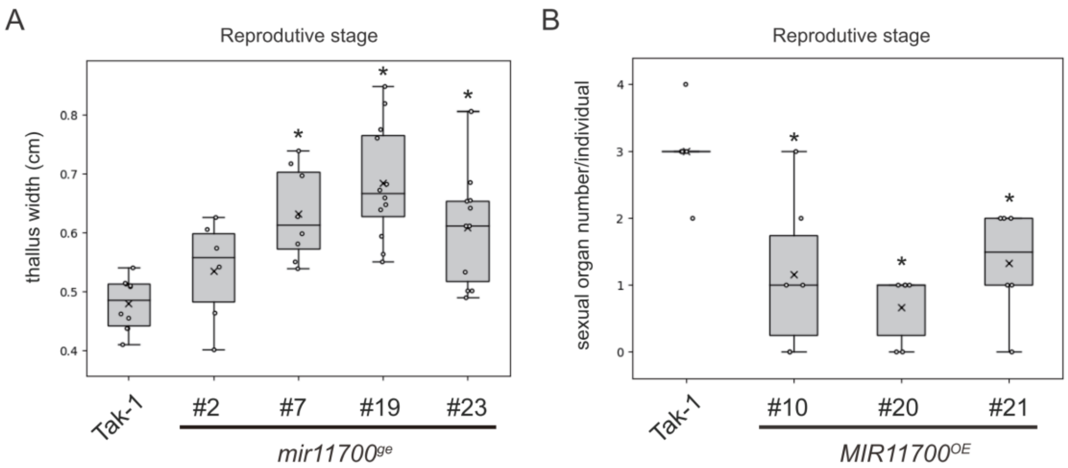

Supplementary Figure S6. Boxplot of thallus width and sexual organ number of *mir11700^{ge}* mutants and *MIR11700* plants at reproductive stage.

(A) Quantification of the thallus width. (B) Quantification of the number of sexual organs. The median and mean are represented by bands and crosses inside the boxes. The lower and upper hinges correspond to the first and third quartiles. Dots represent individual values from 6-12 independent plants, and statistical significance was determined using Student's *t*-test. Boxplots labeled with '*' indicate significant differences (p-value < 0.05).

doi:10.6342/NTU202404007

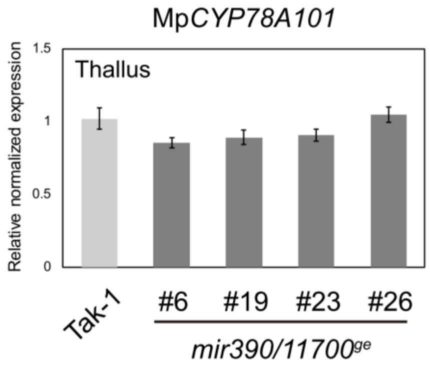

Supplementary Figure S7. qRT-PCR of Mp*CYP78A101* in the *mir390/11700^{ge}* mutants by using 2-week-old thallus.

qRT-PCR of Mp*CYP78A101* in the *mir390/11700^{ge}* mutant. *EF1-alpha* was used as a reference gene. Error bars indicate the *SE* from three biological replicates.

doi:10.6342/NTU202404007

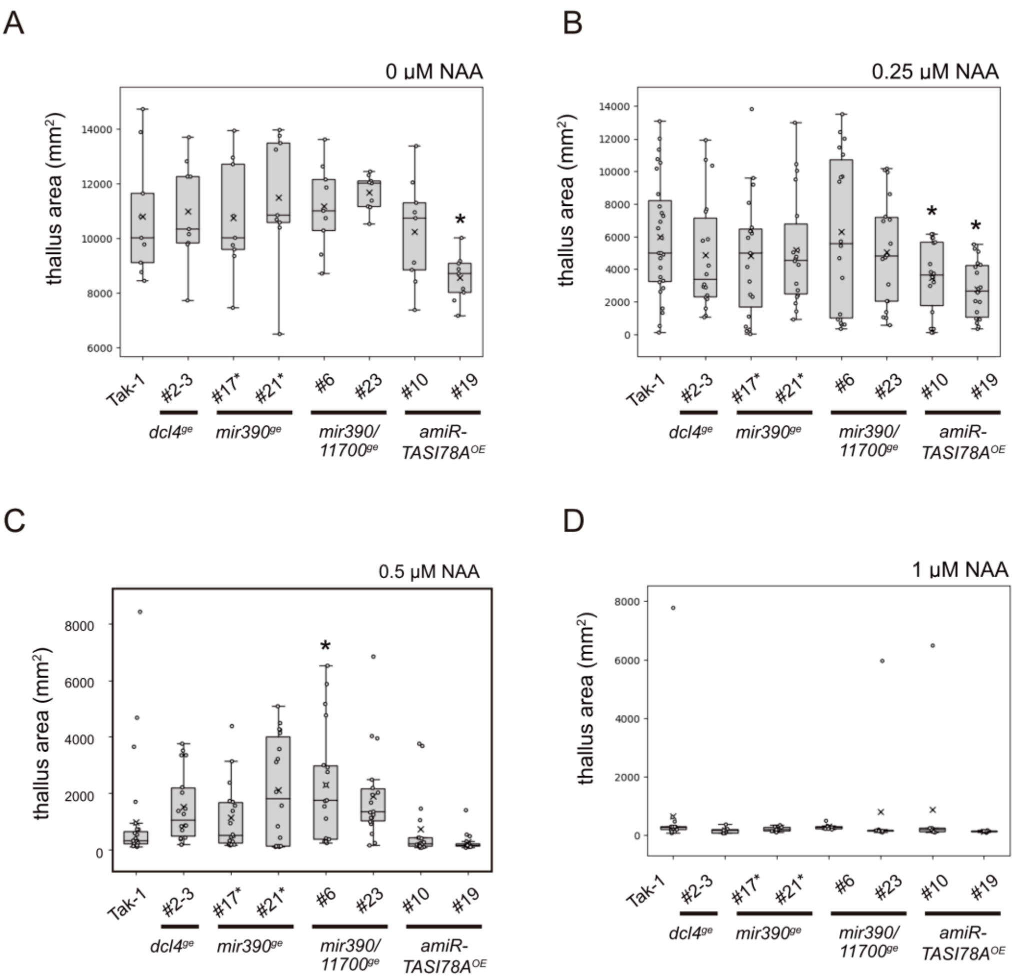

Supplementary Figure S8. Boxplot of the area of NAA-treated thallus.

The thallus area was treated with (A) 0 µM (B) 0.25 µM, (C) 0.5 µM, and (D) 1 µM NAA. The median and mean are represented by bands and crosses inside the boxes. The lower and upper hinges correspond to the first and third quartiles. Dots represent individual values from more than 9 independent gemmae, and statistical significance was determined using Student's *t*-test. Boxplots labeled with '*' indicate significant differences (p-value < 0.05).

doi:10.6342/NTU202404007

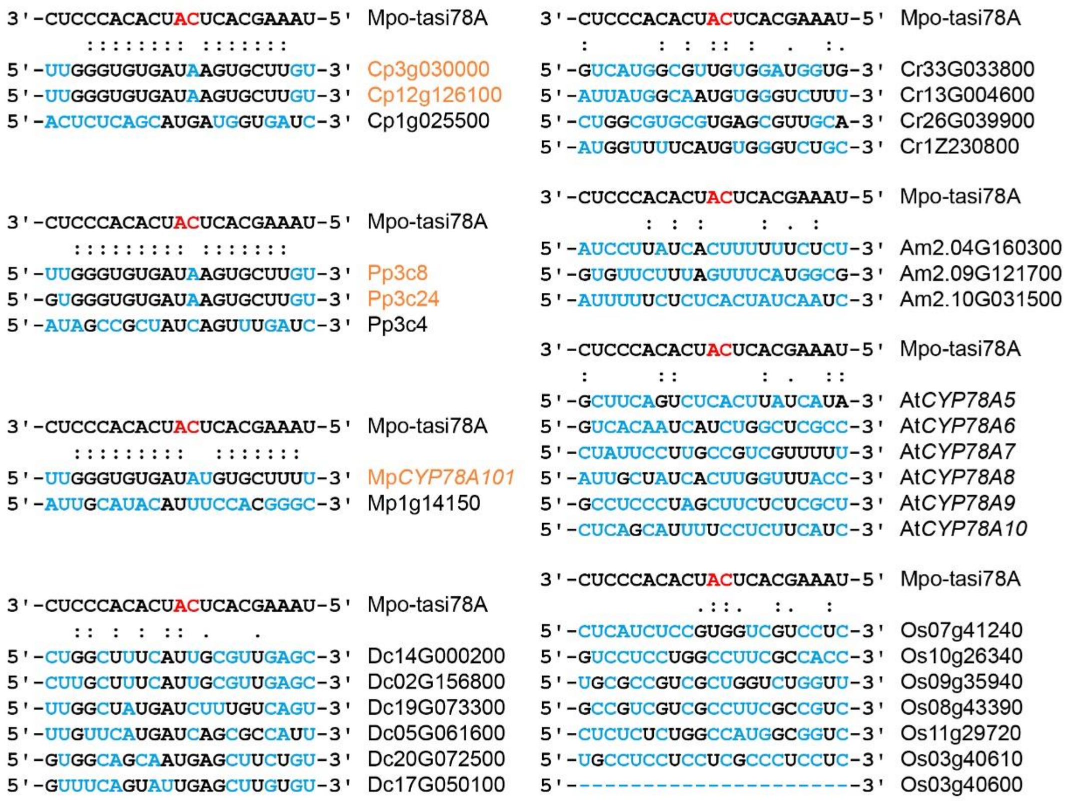

Supplementary Figure S9. Alignments of tasi78A and *CYP78* homologs.

Alignments of Mpo-tasi78A and *CYP78* homologs in land plants. Red indicates the 10th and 11th nucleotides of small RNAs. Blue represents mismatch base pairing between small RNAs and *CYP78* homologs. Sequences of *CYP78* homologs were identified from Phytozome 13.

doi:10.6342/NTU202404007

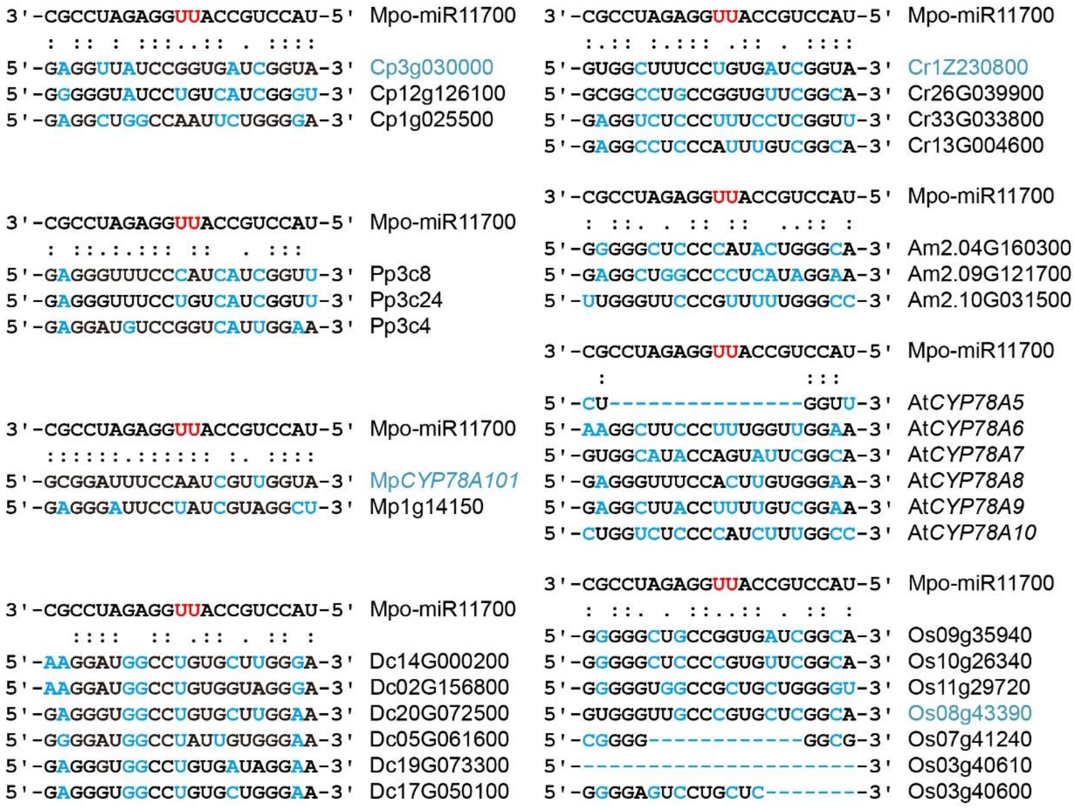

Supplementary Figure S10. Alignments of miR11700 and *CYP78* homologs.

Alignments of Mpo-miR11700 and *CYP78* homologs in land plants. Red indicates the 10th and 11th nucleotides of small RNAs. Blue represents mismatch base pairing between small RNAs and *CYP78* homologs. Sequences of *CYP78* homologs were identified from Phytozome 13.

doi:10.6342/NTU202404007

2.9 Appendix

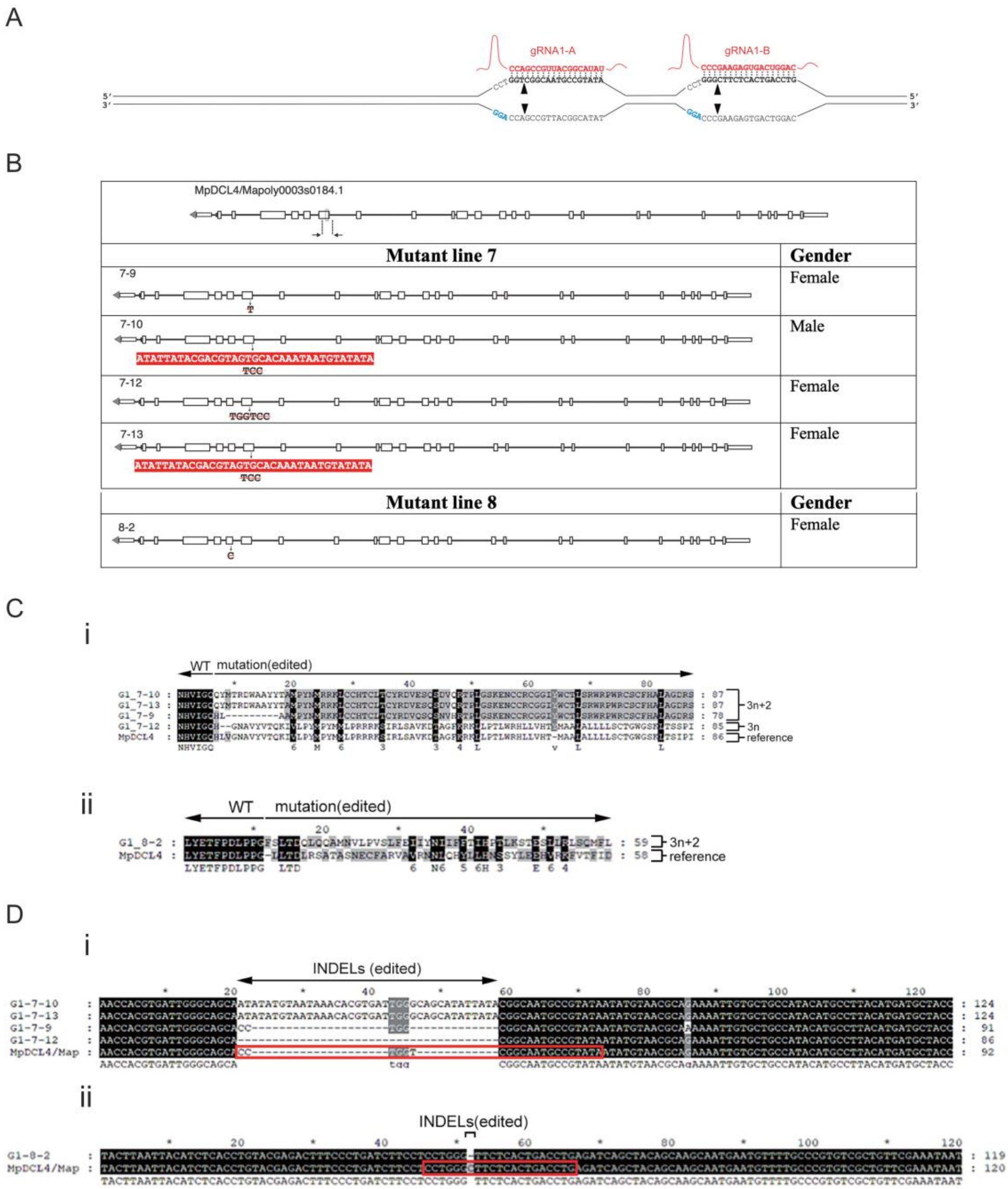

Appendix 1. CRISPR/Cas9-mediated mutation on Mp*DCL4*.

(A) Sites of two designed Mp*DCL4* gene editing gRNAs. (B) Genomic structure of *dcl4*^{ge} mutant lines with INDELs. Two small arrows that flank the small box represent forward and reverse primers, whereas the small box shows the targeted site. The red highlighter represents insertion. Crosswords represent deletion. The alignments between amino acids (C) and nucleotide (D) sequences of mutants and their references.

doi:10.6342/NTU202404007

The red box indicates the gRNA editing site. 3n+2 reading frames represent the asymmetric mutation, whereas 3n indicates symmetric or in-frame mutation.

doi:10.6342/NTU202404007

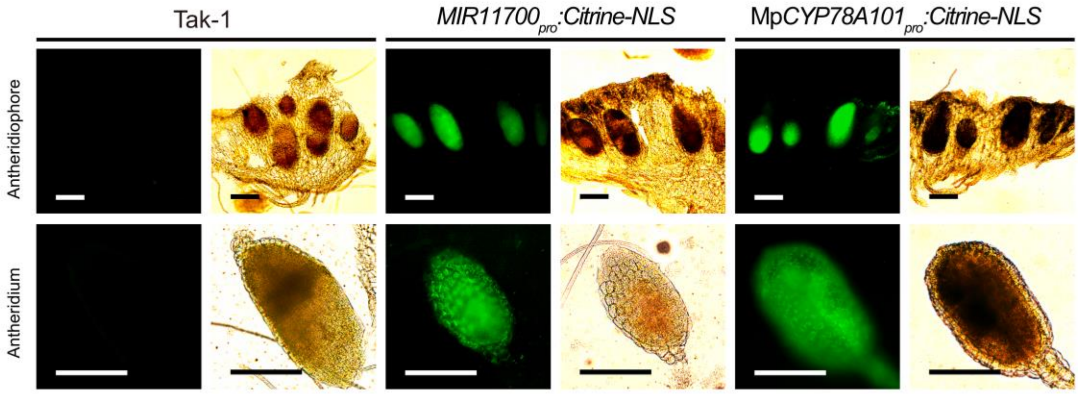

Appendix 2. Expression patterns of *MIR11700* and Mp*CYP78A101* in the male sexual organs of *M. polymorpha*.

Confocal images of the antheridiophore (upper panel) and antheridium (lower panel) of the *MIR11700*$_{pro}$*:Citrine-NLS* and Mp*CYP78A101*$_{pro}$*:Citrine-NLS* plants were obtained at the reproductive stage. Tak-1 plant was used as a negative control. Scale bars, 200 μm.

doi:10.6342/NTU202404007

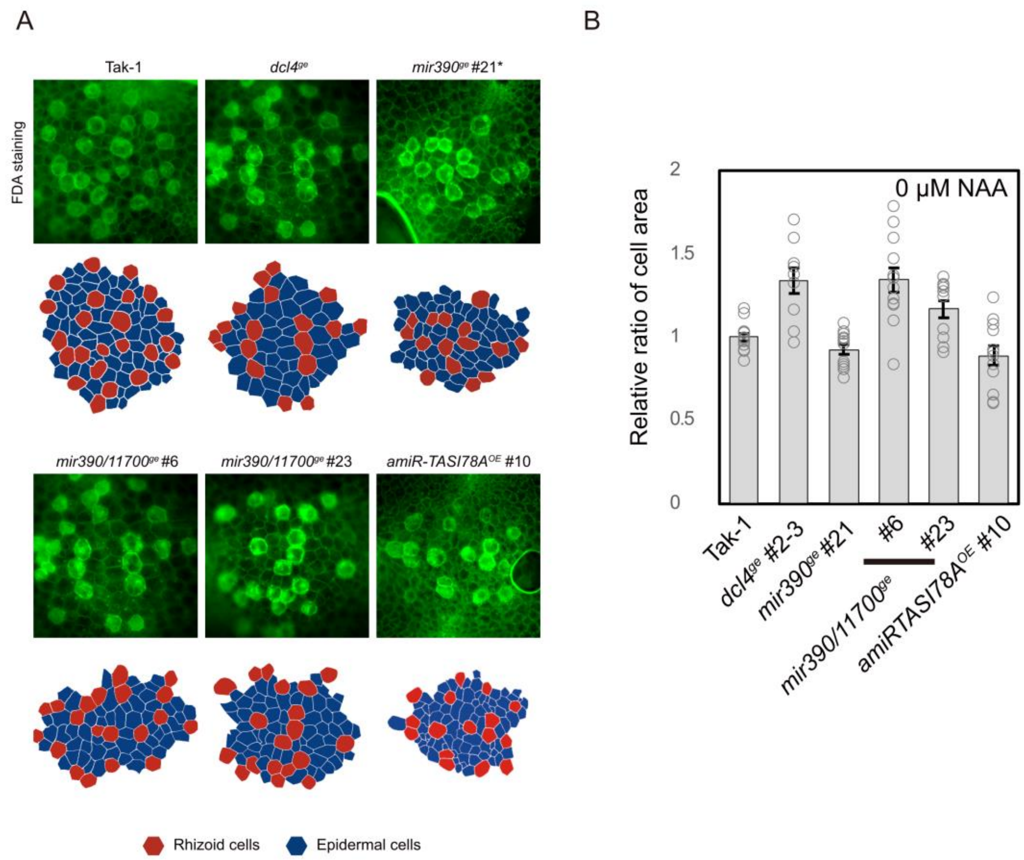

Appendix 3. Phenotypic observations of *dcl4^{ge}*, *mir390^{ge}*, *mir390/11700^{ge}* mutants, and *amiR-TASI78A^{OE}* plants

(A) The FDA staining of gemma (upper panel) and the cell size qualification (lower panel) for various plants. (B) Relative cell area ratios of various plants in response to Tak-1.

doi:10.6342/NTU202404007

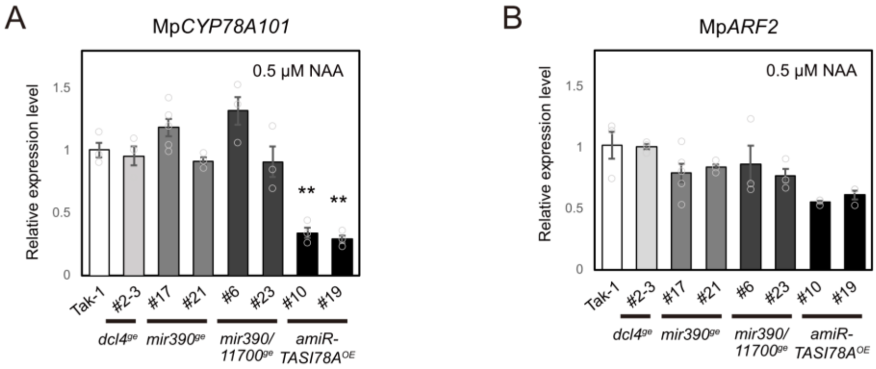

Appendix 4. NAA treatment of *dcl4^{ge}*, *mir390^{ge}*, *mir390/11700^{ge}* mutants, and *amiR-TASI78A^{OE}* plants.

qRT-PCR analysis of Mp*ARF2* (A) and Mp*CYP78A101* (B), using Mp*EF1-alpha* as the internal control. Error bars represent the standard error (*SE*) from three biological replicates.

doi:10.6342/NTU202404007

Chapter 3

Development of a petal protoplast transfection system for *Sinningia speciosa*

The data has been published in the Applications in Plant Sciences journal.

Pan, Z. J., Hung, Y. L., Chen, T. Y., Shih, Y. A., Lin, Y. C. J., & Wang, C. N. (2022). Development of a petal protoplast transfection system for Sinningia speciosa. Applications in Plant Sciences, 10(3), e11476.

doi:10.6342/NTU202404007

3.1 Abstract

Transient gene expression system offers a valuable way to study gene interactions in species where stable genetic modification methods haven't been established. To investigate the development of floral symmetry, we established and optimized a protocol for transient transfection system for petal protoplasts isolated from *Sinningia speciosa*. We achieved a high yield of protoplasts by treating petals with a specific enzyme solution with 1.5% cellulase and 0.4% macerozyme for 6 hours. A green fluorescent protein (GFP) gene was used as a marker to measure the transfection efficiency. The transformation process achieved a 41.4% efficiency by using a concentration of 40% (w/v) solution of polyethylene glycol (PEG) 4000 mixed with a sugar solution (mannitol) containing calcium chloride ($CaCl_2$), along with 10 μg of plasmid DNA. This transient transfection system shows promise as a valuable tool for studying gene regulatory interactions each other in plants from the Gesneriaceae family.

Keywords: protoplast, petal, Sinningia, transfection efficiency

doi:10.6342/NTU202404007

3.2 Introduction

Sinningia speciosa, a member of the Gesneriaceae family, is famous in horticulture for its large and diverse flowers, exhibiting both bilateral and radial symmetry, along with various floral characteristics such as color, shape, and size. While the high diversity of its flowers is known to be contributed by a single gene, *CYCLOIDEA* (*SsCYC*), a Teosinte 1/Cincinnata/Proliferating (TCP) cell factor transcription factor that regulates floral symmetry (Hsu et al., 2017; Dong et al., 2018), the reasons behind other floral diversity characteristics remain unknown. With small genome size (300 Mbp), uniform chromosomes (2n = 26), and rapid generation time (3-6 months) in *S. speciosa*, make it an ideal research model (Skog, 1984; Zaitlin and Pierce, 2010).

To investigate the roles of genes contributing to floral diversity, a stable or transient gene transformation system is necessary. Although *Agrobacterium*-mediated stable genetic transformation of *S. speciosa* has been reported (Li et al., 2013; Kuo et al., 2018), the low transfection efficiency of *Agrobacterium* in *S. speciosa* makes obtaining transgenic plants through this method challenging. Therefore, a transient transformation system is preferred to quickly validate gene relationships, protein-protein interactions, promoter assays for identifying cis-elements, subcellular localization, etc., which could facilitate studies in *S. speciosa*.

Protoplasts are plant cells whose cell walls have been removed by enzymes. Studying protoplasts offers an effective approach for observing and analyzing cellular processes involved in various biological functions. Protoplasts can be isolated from different types of plant tissues to explore cell type-specific and tissue-specific gene expression or function (Marx, 2016). Isolated protoplasts maintain their cellular identity for a certain period in vivo (Marx, 2016), facilitating the study of transient gene functions, especially in plant species lacking well-established stable genetic transformation systems. Moreover, the transient expression system of protoplasts is

doi:10.6342/NTU202404007

highly efficient and sensitive, detecting most regulatory responses within 2-10 hours after foreign gene transformation (Yoo et al., 2007). This system transfers foreign DNA without *Agrobacterium*, overcoming the challenge of infecting *S. speciosa* with *Agrobacterium*.

Our objective was to study gene regulation in flowers. Existing leaf protoplast systems may not be suitable for studying tissue-specific gene interactions in flowers, necessitating the establishment of a petal protoplast isolation and transfection system for S. speciosa. While protoplast isolation protocols for Gesneriaceae species exist, they are based on small shoot primordia regenerated from cultured leaf blade explants or young shoot lets regenerated from leaf explants. Published protoplast isolation protocols for flower tissues are scarce, especially for Gesneriaceae species.

Our goal was to investigate the gene interaction within *S. speciosa* flowers. Existing methods for isolating protoplasts from leaves might not accurately reflect flower-specific gene interactions. Therefore, we aimed to develop a system for isolating and transfecting protoplasts specifically from *S. speciosa* petals. While protocols exist for isolating protoplasts from other members of the Gesneriaceae family, these methods utilize immature tissues like shoot primordia or young shoots derived from leaf explants (Hoshino et al., 1995; Winkelmann and Grunewaldt, 1995a, b; Afkhami-Sarvestani et al., 2012). Unfortunately, there is a scarcity of published protocols for isolating protoplasts directly from floral tissues, especially in Gesneriaceae species. Therefore, distinct enzyme digestion and gene transfection treatments were tested for petal protoplast isolation and DNA transfection in this study. Here, we present an efficient protocol for isolating petal protoplasts and transforming them with exogenous DNA in *S. speciosa*. Petals harvested from flower buds provide a reliable source of protoplasts, ensuring consistent cell viability and yield. This method provides the way for future investigations into gene interactions within the floral tissues of *S. speciosa*.

doi:10.6342/NTU202404007

3.3 Material and Methods

3.3.1 Plant growth conditions

Sinningia speciosa 'Espírito Santo' (ES) plants, displaying zygomorphic flowers, were grown in a controlled-environment greenhouse under long-day conditions (16 hours light/8 hours dark) with LED lights providing 200 μmol·m^{-2}·s^{-1} light intensity. We maintained a constant temperature of 22°C to 25°C and a relative humidity of 70-80%. Under these conditions, *S. speciosa* 'ES' flowered twice annually. During non-flowering periods, the plants received a diluted water-soluble fertilizer solution (2000× dilution; 25N-5P-20K) every 1-2 weeks. To avoid compromising transfection efficiency (which can drop below 10% with frequent fertilization), fertilizer application was reduced to once every 3-4 weeks during flowering. Importantly, protoplast isolation was excluded from plants at the very beginning or end of their flowering cycle.

3.3.2 Petal protoplast isolation

All the chemicals, solutions, and equipment used in this study are listed in Appendix 1. The proposed procedures for isolating petal protoplasts were mainly modified from optimized protocols for the model plants Arabidopsis and poplar (*Populus* L.) (Yoo et al., 2007; Lin et al., 2014). 1.5 g of fresh petals from 5 to 6 pre-bloom flowers at floral bud were collected. All the sepals, stamen/staminodes, and carpels were carefully removed and discarded to ensure a pure population of petal cells. Each petal was cut into 0.5 to 1 mm strips using a new sharp scalpel blade, without crushing the petal tissue at the cutting site. The petal strips were immediately fully submerged in a freshly prepared enzyme solution. To enhance enzyme digestion, the solution undergoes vacuum infiltration (30–40 mm Hg) for 30 minutes at room temperature (23°C to 26°C) in the dark. This is followed by a 5-6 hour incubation at room temperature, also in the dark, to allow for complete cell wall digestion. Following

doi:10.6342/NTU202404007

enzymatic digestion, the solution became a distinctive purple color due to the release of purple petal protoplasts. We then examined the isolated protoplasts under a microscope, confirming their intact, round shape and a diameter of approximately 30-40 µm. A pre-cleaned nylon mesh with a pore size of 75 µm, wetted with MMG solution, was used for filtration to capture debris larger than the protoplasts. The protoplast suspension was carefully filtered through a double layer of nylon mesh. The filtrate containing the purified protoplasts was collected in a 30 mL round-bottomed tube. Finally, the suspension was centrifuged at low speed (200 × g) for 1-2 minutes using a swinging-bucket rotor. This gentle centrifugation process pelleted the protoplasts at the bottom of the tube.

The supernatant was removed using a pipette as fully as possible to harvest the protoplasts without disturbing the pellet. The pellet was then gently resuspended in a small volume of fresh MMG solution. Using a hemacytometer, we determined the protoplast concentration, which was subsequently adjusted to the desired level of 2 x 10□ protoplasts/mL using additional MMG solution. Finally, the protoplast suspension was placed on ice for at least 30 minutes. Microscopic observation revealed that the isolated protoplasts remained intact and round, with some even containing large purple vacuoles, indicating that the protoplasts were viable and healthy.

3.3.3 DNA transfection

For DNA transfections, aliquots of 100 µL protoplast suspension (containing 2×10^4 protoplasts) were transferred to 2 mL round-bottomed tubes and gently mixed with 10 µL of plasmid DNA (1 µg/µL). To optimize transformation efficiency for various gene studies, different PEG-mediated transfection solutions were tested. Freshly prepared polyethylene glycol (PEG)-$CaCl_2$ solution (110 µL) was added to the protoplast-DNA mixture and carefully mixed by tapping the tube. The mixture incubated at room

doi:10.6342/NTU202404007

temperature for 10-15 minutes before being stopped by dilution with W5 solution (440 μL) and gentle inversion. Following the transfection step, the mixture was evenly distributed into new 2 mL round-bottomed tubes. The tubes were centrifuged at 200 × g for 2 minutes at room temperature to harvest the protoplasts. The supernatant was then discarded. To prevent adherence to the culture plate, 5 mL of 5% BSA solution was briefly applied (1-2 seconds) to the wells of a 12-well plate, creating a coating buffer. The transfected protoplasts were then resuspended in 0.5 mL of WI solution, gently transferred to the coated wells, and incubated under room temperature light (daylight fluorescent) for 16-18 hours. Finally, the transfection efficiency, calculated as the ratio of transfected protoplasts to the total number of protoplasts, was determined.

3.4 Results

3.4.1 Petal protoplast isolation and protoplast yield

Enzyme concentration and digestion time are key to obtaining a high yield of petal protoplasts (Huang et al., 2013; Wu et al., 2017; Li et al., 2018). For choosing the parameters used in protoplast isolation from petals of *S. speciosa*, the protocols for protoplast isolation were sorted from different texture of material source from soft (callus) to hard (xylem) (Hoshino et al., 1995; Yoo et al., 2007; Yang et al., 2009; Lin et al., 2014; Nanjareddy et al., 2016). The range of mannitol for adjusting osmotic pressure is from 0.2 M to 0.6 M (Table 1), the middle value of this range, 0.4 M mannitol was used as the default value. Same standard is applied in digestion time, the period of 3 hr was chosen for cell wall digestion. For the enzyme combination, cellulase R-10 and macerozyme R-10 are commonly used in all species. Next, the concentration of these two enzymes is most chosen in 1.5% and 0.4% for cellulase R-10 and macerozyme R-10, respectively. Taken together, 1.5% cellulase R-10 and 0.4 % macerozyme R-10 combining with 0.4 M mannitol and 3 hr digestion time as the initial

doi:10.6342/NTU202404007

conditions (default conditions) for protoplast isolation from petals in *S. speciosa*.

As protoplasts lack cell walls, maintaining the proper osmotic pressure is essential for their health. Osmotic pressure is regulated by mannitol. To determine the optimal osmotic pressure for isolating protoplasts from Sinningia speciosa petals, we tested concentrations of mannitol at 0.3, 0.35, and 0.4 M. The highest protoplast yield was obtained at 0.3 M mannitol condition, reaching 6.5×10^5 protoplasts/g FW (Fig. 1A). The isolated protoplasts mostly remained spherical at lower osmotic pressure (Fig. 1B). In contrast, the protoplasts became wrinkling at higher osmotic pressure (Fig. 1C, red arrow). In this work, lower osmotic pressure was chosen as the optimal condition for protoplast isolation in *S. speciosa*. The optimal osmotic pressure will apply to further experiments.

When we used the default enzyme concentration (1.5% Cellulase R-10 and 0.4% Macerozyme R-10) and digestion time (3 hours), we observed a low protoplast yield ($<10^6$ protoplasts/g FW) and insufficient digestion of the petal stripes. To enhance protoplast yield, we doubled the enzyme concentration and digestion time. Extending the digestion time to six hours resulted in transparent petal stripes, indicating greater enzymatic digestion of cell walls and a noticeable purple color change in the enzyme solution. Our findings indicate that doubling the digestion time has a greater impact on protoplast yield ($>1 \times 10^6$/g FW), while doubling the enzyme concentration provides less assistance to protoplast yield (Table 2). Furthermore, with FDA staining, protoplast viability remains consistently high (>80%) across all combinations of enzyme concentrations and digestion times (Table 2). The results demonstrated that extended digest time was helpful for protoplast isolation in *S. speciosa*.

3.4.2 DNA transformation into petal protoplasts form *S. speciosa*

As we have found the optimized protoplast isolation conditions, to further test

doi:10.6342/NTU202404007

whether the protoplast can be transformed or not, the transient expression vector pUC-GFP was used. The GFP fluorescence indicates the successfully transformed petal protoplast (Fig. 2A and 2B). We calculated the transfection efficiency by dividing the number of protoplast cells displaying GFP fluorescence under a dark□field UV microscope by the total number of protoplast cells observed under a bright□field microscope.

Nanjareddy et al. noted that the choice of solvent in the transfection buffer can impact transformation efficiency (Nanjareddy et al., 2016). To investigate this, we conducted transfection experiments using combinations of MMG solution or 0.2 M mannitol for dissolving PEG, with or without the addition of 100 mM $CaCl_2$. Subsequently, we compared the resulting transfection efficiencies to identify the most effective transfection buffer. Notably, the use of a calcium-containing transfection solution yielded higher transformation efficiency. This underscores the importance of calcium in protoplast transformation (Fig. 2C). When compared with the transformation efficiency of the PEG-M-calcium and PEG-MMG-calcium transfection solution, the PEG-MMG-calcium transfection solution exhibited lower efficiency (Fig. 2C). As a result, we selected the PEG-calcium transfection solution for further experiments. For optimal transfection efficiency, careful optimization of both PEG concentration and the amount of exogenous DNA is essential (Huang et al., 2013; Nanjareddy et al., 2016; Wu et al., 2017; Li et al., 2018; Page et al., 2019); PEG facilitates the introduction of exogenous DNA (i.e., plasmids) into the targeted cell by adjusting the osmotic pressure of the cell membrane, thereby increasing its permeability. To determine the effect of PEG 4000 concentrations on transfection efficiency, the protoplasts were transfected with 40% or 50% PEG 4000 in combination with digestive enzymes (1× or 2× concentration). Following a 16-h incubation, transfection efficiencies ranged from 44.3% to 56.1% across the four combined conditions (Fig.2D). Under the combination

doi:10.6342/NTU202404007

of 50% PEG 4000 and 2× concentration conditions, the highest transfection efficiency (56.1%) was achieved. However, the digestive enzymes with 1× and 2× concentration under 40% PEG 4000 resulted in a similar high transfection efficiency (49.9% and 51.2%, respectively). Hence, 40% PEG 4000 and 1× digestive enzyme concentration was therefore used in subsequent tests.

To assess the effect of the amount of plasmid DNA on transfection, the protoplasts were transfected with different amounts of plasmid DNA. The transfection efficiencies obtained using 10, 15, and 25 μg were 49.9%, 35.9%, and 51.1%, respectively (Fig.2E). A transfection efficiency of nearly 50% was achieved using 10 μg of plasmid DNA; therefore, we used 10μg of plasmid DNA in our subsequent tests for cost-efficiency. Accordingly, the key factors required to achieve optimal transfection in *S. speciosa* petal protoplasts can be summarized as follows: a 1× concentration of digestive enzymes, 10 μg of exogenous DNA, and 40% PEG 4000.

3.5 Discussion

3.5.1 Moderate yields and transfection efficiency of *S. speciosa* petal protoplasts

The enzyme concentration and digestion time are the critical role affecting protoplast yield (Huang et al., 2013; Wu et al., 2017; Li et al., 2018). To maximize protoplast isolation from *S. speciosa* petals, we investigated the impact of these variables. We compared the yield obtained using two enzyme concentrations (1× and 2×) and various digestion times (3-6 hours). All experiments were conducted at room temperature in the dark without shaking. Our results revealed that a 6-hour digestion with a 1× enzyme concentration yielded the best outcome, producing over 2.84×10^6 protoplasts per gram of fresh weight (FW) (Table 2). This yield is comparable to, or even surpasses, the typical range of 10^5-10^6 protoplasts/g FW reported for petal protoplast isolations. Previous studies have documented a range of low to moderate

doi:10.6342/NTU202404007

protoplast yields from flower petals. Examples include 9.5×10^5/g FW for Phalaenopsis orchids (Lin et al., 2018), 2×10^5/g FW for Phaseolus vulgaris (Nanjareddy et al., 2016), and 1.5–8 × 10^6/g FW for *Petunia* hybrids (Oh and Kim, 1994). Notably, Cymbidium orchid petals yielded a significantly higher amount, reaching 3.5×10^7/g FW (Ren et al., 2020). It's important to note that petal protoplast yields generally lower than those achievable from leaves, which can reach approximately 3.0×10^7 protoplasts/g FW (Wu et al., 2009). Our optimized protocol for *S. speciosa* petals achieved moderate yields to 2.84×10^6/g FW, comparable to other petal isolations. Given this success, we opted to maintain the 6-hour digestion time and 1× enzyme concentration as the optimal conditions for subsequent experiments.

Our optimized protocol yielded *S. speciosa* petal protoplasts with an average transfection efficiency of 41.40% ± 7% (range: 30-50%). This is almost equivalent to the range reported for Arabidopsis leaf protoplasts (50%) (Yoo et al., 2007; Wu et al., 2009), a well-established system. However, it's noteworthy that recent studies have achieved significantly higher efficiencies (around 80%) for petal protoplasts from *Cymbidium* and *Phalaenopsis* orchids (Lin et al., 2018; Ren et al., 2020). This difference may be attributed to variations in the composition of the extracellular matrices or cell wall residues remaining on the protoplasts of these orchid species compared to *S. speciosa*.

doi:10.6342/NTU202404007

3.6 Tables and Figures

Table 1 Comparison of protoplast isolation condition in different species.

Species	Tissue	Mannitol	Enzyme combination	Digestion time (hr)	Protoplast yield (10^5/g)	Reference
Saintpaulia ionantha	Callus	0.2 M	2% cellulase 1% macerozyme 0.05 % pectolyase Y-23 1% driselase	4	100-300	Hoshino et al., 1995
Phaseolus vulgaris	Petal	0.4 M	1.5 % cellulase R-10 0.4 % macerozyme R-10 30 U pectinase	8-10	2	Nanjareddy et al., 2016
Rosa damascena	Petal	0.6 M	2 % cellulase R-10 1 % macerozyme R-10	3.5	NA	Yang et al., 2009
Arabidopsis thaliana	Leaf	0.4 M	1.5% cellulase R-10 0.4% macerozyme R-10	3	100	Yoo et al., 2007
Populus trichocarpa	Xylem	0.5 M	1.5% cellulase R-10 0.4% macerozyme R-10	0.33	250	Lin et al., 2014

Note: Mannitol is used for adjusting osmotic pressure.

doi:10.6342/NTU202404007

Table 2 Effect of enzyme combinations and digestion time on protoplast yield and viability from petal in *Sinningia speciosa*

Species	Mannitol	Enzyme combination	Digestion time (hr)	Protoplast yield (10^5/g FW)	Protoplast viability (%)
Sinningia speciosa	0.3 M	**1.5% Cellulase R-10 0.4% Macerozyme R-10**	3	1.3	>80%
			6	**28.4**	>80%
		3% Cellulase R-10 0.8% Macerozyme R-10	3	4.7	>80%
			6	16.5	>80%

doi:10.6342/NTU202404007

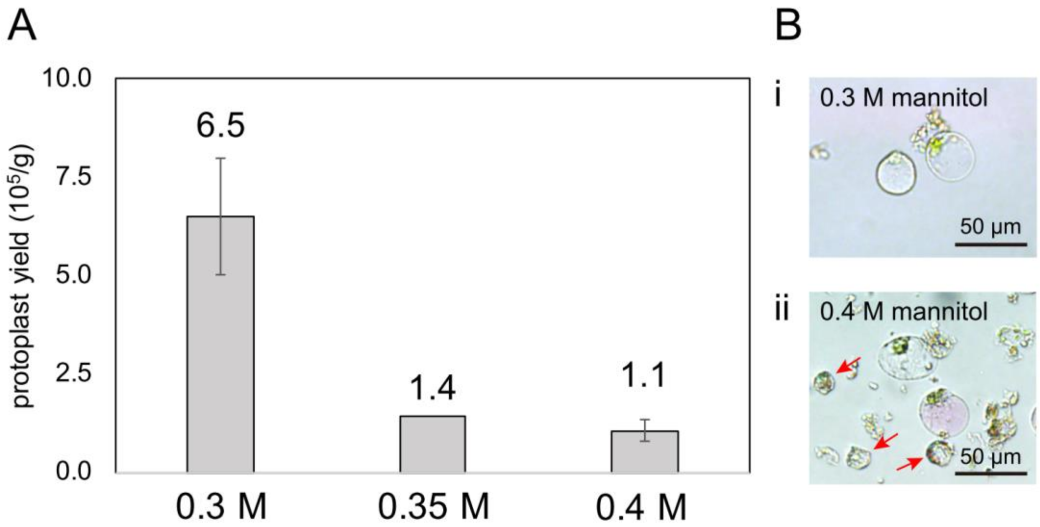

Figure 1 Effect of osmotic pressure (mannitol concentration) on protoplast yield from petal in *S. speciosa*.

(A), the protoplast yield from petal protoplast isolation in various osmotic pressure. The values are presented as mean ± SEM (n=2 or 3). (B), the morphology of isolated protoplast from petals in 0.3 M (i) and 0.4 M (ii) mannitol. The red arrow shows the wrinkling shape of protoplast.

doi:10.6342/NTU202404007

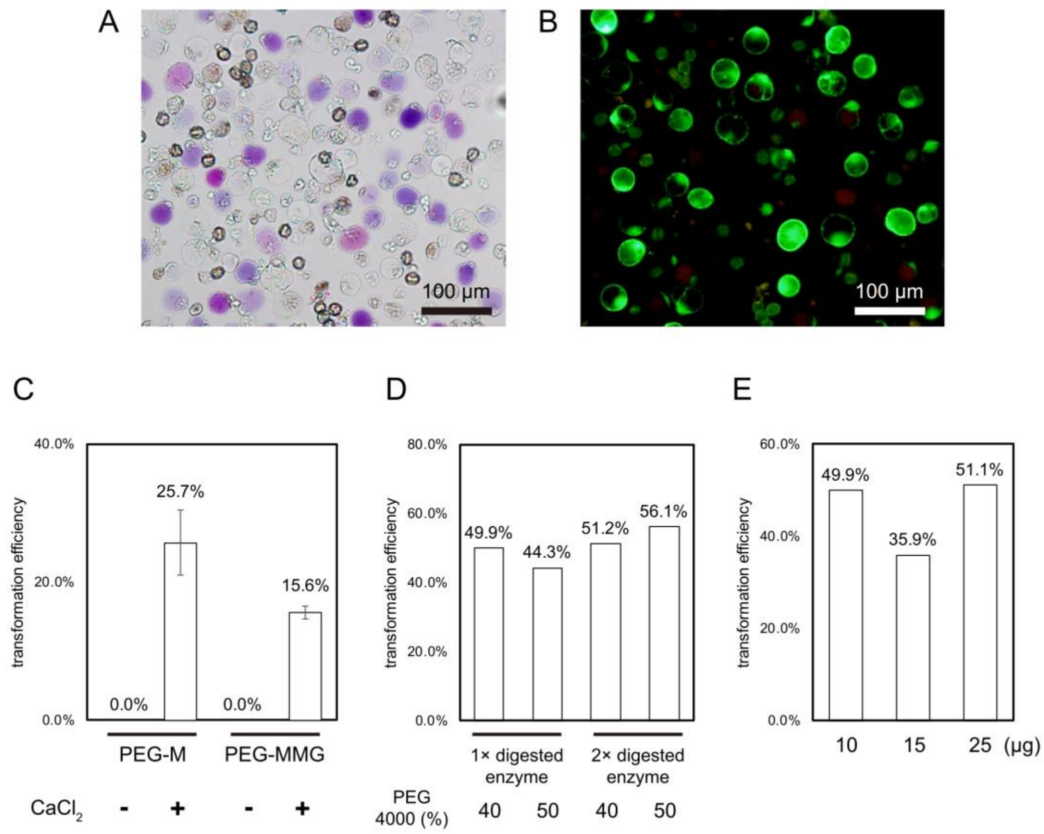

Figure 2 Transfection efficiency of transfected *Sinningia speciosa* 'ES' petal protoplasts.

(A, B) Images of GFP transfected petal protoplasts taken under (A) bright light and (B) ultraviolet light to quantify transfection efficiency. (C) Effect of different transfection solution on transfection efficiency. (D) Effect of different enzyme concentrations in combination with different PEG 4000 amounts on transfection efficiency. (E) Effect of the amount of plasmid DNA on transfection efficiency.

doi:10.6342/NTU202404007

3.7 Appendix

Appendix 1. Reagents and Equipment required to perform the isolation and transfection of *S. speciosa* petal protoplasts.

Chemicals/solutions

- **0.2M 4-morpholineethanesulfonic acid (MES)** adjust to pH 5.7 and sterilize using a 0.45-µm filter (MES monohydrate; MW 231.2; no. E169-250G, Amresco, Solon, OH, USA)
- **0.8M Mannitol** sterilize using a 0.45-µm filter (Mannitol; MW 182.17; no. M4125-500G Sigma-Aldrich, St. Louis, Missouri, USA)
- **1M $CaCl_2$** sterilize using a 0.45-µm filter ($CaCl_2$; MW 110.98; SHIMAKYU'S PURE. CHEMICALS, Osaka, Japan)
- **2M KCl** sterilize using a 0.45-µm filter (KCl; MW 74.55; no. 20598, Affymetrix/USB™, Santa Clara, CA, USA)
- **2M $MgCl_2$** sterilize using a 0.45-µm filter ($MgCl_2.6H_2O$; MW 203.3; no. 18461-500G, Affymetrix/USB™, Santa Clara, CA, USA)
- **1% BSA** (wt/vol) sterilize using a 0.45-µm filter (BSA; MW 66KDa; no. AAJ1086722, Affymetrix/USB™, Santa Clara, CA, USA)
- **5M NaCl** sterilize using a 0.45-µm filter (NCl; MW 58.44; no. 0241-1KG, Amresco, Solon, OH, USA)
- **0.1M Glucose** sterilize using a 0.45-µm filter (Glucose; MW 180.156; no. G-7520, Sigma-Aldrich, St. Louis, Missouri, USA)
- **Cellulase R10** (Yakult Pharmaceutical Ind. Co., Nishinomiya, Japan)
- **Macerozyme R10** (Yakult Pharmaceutical Ind. Co., Nishinomiya, Japan)
- **Polyethylene glycol (PEG) 4000** (PEG 4000, no. 81240-1KG, Sigma-Aldrich, St. Louis, Missouri, USA)
- **β-Mercaptoethanol** (no. M6250, Sigma-Aldrich, St. Louis, Missouri, USA)
- **Enzyme solution** The enzyme solution should be freshly prepared. Prepare 20 mM MES (pH 5.7) containing 1.5% (wt/vol) cellulase R10, 0.4% (wt/vol) macerozyme R10, 0.4 M mannitol and 20 mM KCl. Heat the solution at 55℃ for 10 min and cool to room temperature. Add 10 mM $CaCl_2$, 5 mM β-mercaptoethanol and 0.1% BSA. Filter the enzyme solution using a 0.45-µm syringe filter.
- **MMG solution** Prepare 4 mM MES (pH 5.7) containing 0.4 M mannitol and 15 mM $MgCl_2$.
- **PEG-$CaCl_2$ transfection solution** Freshly prepare. 40% (wt/vol) PEG4000 containing 0.2 M mannitol and 100 mM $CaCl_2$.

doi:10.6342/NTU202404007

- **W5 solution** Prepare 2 mM MES (pH 5.7) containing 154 mM NaCl, 125 mM $CaCl_2$, 5 mM KCl and 0.1 M Glucose.
- **WI solution** Prepare 4 mM MES (pH 5.7) containing 0.5 M mannitol and 20 mM KCl.
- **Maxi Plus Ultrapure Plasmid Extraction System (**no. GMV2002, Viogene, Sunnyvale, CA, USA)

Equipment

- **Olympus DP72 fluorescence microscope** (Olympus Corp., Tokyo, Japan)
- **Zeiss LSM 780 inverted confocal microscope** (Carl Zeiss Microscopy GmbH, Jena, Germany)
- **Sorvall™ ST 8 small benchtop centrifuge** (Thermo Fisher Scientific, Waltham, MA, USA)
- **0.45-µm sterile membrane syringe filter**
- **Nylon mesh** (75 mm, Nylon sifters)
- **Neubauer-improved counting chamber 0.1mm** (no. 0650030, Marienfeld Superior™)
- **30-ml round-bottomed tube**
- **2-ml round-bottomed microcentrifuge tube**

12-well culture dish (no. 3046, Falcon)

doi:10.6342/NTU202404007

Reference

Afkhami-Sarvestani, R., Serek, M., and Winkelmann, T. (2012). Protoplast Isolation and Culture from Streptocarpus, Followed by Fusion with Saintpaulia ionantha Protoplasts.

Alaba, S., Piszczalka, P., Pietrykowska, H., Pacak, A.M., Sierocka, I., Nuc, P.W., Singh, K., Plewka, P., Sulkowska, A., Jarmolowski, A., Karlowski, W.M., and Szweykowska-Kulinska, Z. (2015). The liverwort Pellia endiviifolia shares microtranscriptomic traits that are common to green algae and land plants. New Phytol **206,** 352-367.

Allen, E., Xie, Z., Gustafson, A.M., and Carrington, J.C. (2005). microRNA-directed phasing during *trans*-acting siRNA biogenesis in plants. Cell **121,** 207-221.

Arif, M.A., Top, O., Csicsely, E., Lichtenstern, M., Beheshti, H., Adjabi, K., and Frank, W. (2022). DICER-LIKE1a autoregulation based on intronic microRNA processing is required for stress adaptation in Physcomitrium patens. Plant J **109,** 227-240.

Arif, M.A., Fattash, I., Ma, Z., Cho, S.H., Beike, A.K., Reski, R., Axtell, M.J., and Frank, W. (2012). DICER-LIKE3 activity in *Physcomitrella patens DICER-LIKE4* mutants causes severe developmental dysfunction and sterility. Molecular Plant **5,** 1281-1294.

Axtell, M.J. (2013). Classification and comparison of small RNAs from plants. Annu Rev Plant Biol **64,** 137-159.

Axtell, M.J., and Bowman, J.L. (2008). Evolution of plant microRNAs and their targets. Trends Plant Sci **13,** 343-349.

Axtell, M.J., Snyder, J.A., and Bartel, D.P. (2007). Common functions for diverse small RNAs of land plants. Plant Cell **19,** 1750-1769.

Axtell, M.J., Westholm, J.O., and Lai, E.C. (2011). Vive la difference: biogenesis and evolution of microRNAs in plants and animals. Genome Biol **12,** 221.

Axtell, M.J., Jan, C., Rajagopalan, R., and Bartel, D.P. (2006). A two-hit trigger for siRNA biogenesis in plants. Cell **127,** 565-577.

Bak, S., Beisson, F., Bishop, G., Hamberger, B., Hofer, R., Paquette, S., and Werck-Reichhart, D. (2011). Cytochromes p450. Arabidopsis Book **9,** e0144.

Bartel, D.P. (2004). MicroRNAs: genomics, biogenesis, mechanism, and function. Cell **116,** 281-297.

Berruezo, F., de Souza, F.S.J., Picca, P.I., Nemirovsky, S.I., Martinez Tosar, L., Rivero, M., Mentaberry, A.N., and Zelada, A.M. (2017). Sequencing of small RNAs of the fern *Pleopeltis minima* (Polypodiaceae) offers insight into the

doi:10.6342/NTU202404007

evolution of the microrna repertoire in land plants. PLoS One **12,** e0177573.

Bonnet, E., Van de Peer, Y., and Rouze, P. (2006). The small RNA world of plants. New Phytol **171,** 451-468.

Bowman, J.L., Kohchi, T., Yamato, K.T., Jenkins, J., Shu, S., Ishizaki, K., Yamaoka, S., Nishihama, R., Nakamura, Y., Berger, F., Adam, C., Aki, S.S., Althoff, F., Araki, T., Arteaga-Vazquez, M.A., Balasubrmanian, S., Barry, K., Bauer, D., Boehm, C.R., Briginshaw, L., Caballero-Perez, J., Catarino, B., Chen, F., Chiyoda, S., Chovatia, M., Davies, K.M., Delmans, M., Demura, T., Dierschke, T., Dolan, L., Dorantes-Acosta, A.E., Eklund, D.M., Florent, S.N., Flores-Sandoval, E., Fujiyama, A., Fukuzawa, H., Galik, B., Grimanelli, D., Grimwood, J., Grossniklaus, U., Hamada, T., Haseloff, J., Hetherington, A.J., Higo, A., Hirakawa, Y., Hundley, H.N., Ikeda, Y., Inoue, K., Inoue, S.I., Ishida, S., Jia, Q., Kakita, M., Kanazawa, T., Kawai, Y., Kawashima, T., Kennedy, M., Kinose, K., Kinoshita, T., Kohara, Y., Koide, E., Komatsu, K., Kopischke, S., Kubo, M., Kyozuka, J., Lagercrantz, U., Lin, S.S., Lindquist, E., Lipzen, A.M., Lu, C.W., De Luna, E., Martienssen, R.A., Minamino, N., Mizutani, M., Mizutani, M., Mochizuki, N., Monte, I., Mosher, R., Nagasaki, H., Nakagami, H., Naramoto, S., Nishitani, K., Ohtani, M., Okamoto, T., Okumura, M., Phillips, J., Pollak, B., Reinders, A., Rovekamp, M., Sano, R., Sawa, S., Schmid, M.W., Shirakawa, M., Solano, R., Spunde, A., Suetsugu, N., Sugano, S., Sugiyama, A., Sun, R., Suzuki, Y., Takenaka, M., Takezawa, D., Tomogane, H., Tsuzuki, M., Ueda, T., Umeda, M., Ward, J.M., Watanabe, Y., Yazaki, K., Yokoyama, R., Yoshitake, Y., Yotsui, I., Zachgo, S., and Schmutz, J. (2017). Insights into Land Plant Evolution Garnered from the *Marchantia polymorpha* Genome. Cell **171,** 287-304 e215.

Braybrook, S.A., and Kuhlemeier, C. (2010). How a plant builds leaves. Plant Cell **22,** 1006-1018.

Carthew, R.W., and Sontheimer, E.J. (2009). Origins and Mechanisms of miRNAs and siRNAs. Cell **136,** 642-655.

Chen, H.M., Chen, L.T., Patel, K., Li, Y.H., Baulcombe, D.C., and Wu, S.H. (2010). 22-Nucleotide RNAs trigger secondary siRNA biogenesis in plants. Proceedings of the National Academy of Sciences of the United States of America **107,** 15269-15274.

Chen, X. (2009). Small RNAs and their roles in plant development. Annu Rev Cell Dev Biol **25,** 21-44.

Chitwood, D.H., Nogueira, F.T., Howell, M.D., Montgomery, T.A., Carrington, J.C., and Timmermans, M.C. (2009). Pattern formation via small RNA

doi:10.6342/NTU202404007

mobility. Genes Dev **23,** 549-554.

Cho, S.H., Coruh, C., and Axtell, M.J. (2012). miR156 and miR390 regulate tasiRNA accumulation and developmental timing in *Physcomitrella patens*. The Plant Cell **24,** 4837-4849.

Chuck, G., Candela, H., and Hake, S. (2009). Big impacts by small RNAs in plant development. Curr Opin Plant Biol **12,** 81-86.

Cuperus, J.T., Carbonell, A., Fahlgren, N., Garcia-Ruiz, H., Burke, R.T., Takeda, A., Sullivan, C.M., Gilbert, S.D., Montgomery, T.A., and Carrington, J.C. (2010). Unique functionality of 22-nt miRNAs in triggering RDR6-dependent siRNA biogenesis from target transcripts in Arabidopsis. Nat Struct Mol Biol **17,** 997-1003.

D'Ario, M., Griffiths-Jones, S., and Kim, M. (2017). Small RNAs: Big Impact on Plant Development. Trends Plant Sci **22,** 1056-1068.

de Felippes, F.F., Marchais, A., Sarazin, A., Oberlin, S., and Voinnet, O. (2017). A single miR390 targeting event is sufficient for triggering *TAS3*-tasiRNA biogenesis in *Arabidopsis*. Nucleic Acids Research **45,** 5539-5554.

Ding, B., Xia, R., Lin, Q., Gurung, V., Sagawa, J.M., Stanley, L.E., Strobel, M., Diggle, P.K., Meyers, B.C., and Yuan, Y.W. (2020). Developmental Genetics of Corolla Tube Formation: Role of the tasiRNA-ARF Pathway and a Conceptual Model. Plant Cell **32,** 3452-3468.

Dong, Y., Liu, J., Li, P.W., Li, C.Q., Lu, T.F., Yang, X., and Wang, Y.Z. (2018). Evolution of Darwin's Peloric Gloxinia (Sinningia speciosa) Is Caused by a Null Mutation in a Pleiotropic TCP Gene. Mol Biol Evol **35,** 1901-1915.

Douglas, R.N., Wiley, D., Sarkar, A., Springer, N., Timmermans, M.C., and Scanlon, M.J. (2010). ragged seedling2 Encodes an ARGONAUTE7-like protein required for mediolateral expansion, but not dorsiventrality, of maize leaves. Plant Cell **22,** 1441-1451.

Duran-Figueroa, N., and Vielle-Calzada, J.P. (2010). ARGONAUTE9-dependent silencing of transposable elements in pericentromeric regions of Arabidopsis. Plant Signal Behav **5,** 1476-1479.

Eklund, D.M., Ishizaki, K., Flores-Sandoval, E., Kikuchi, S., Takebayashi, Y., Tsukamoto, S., Hirakawa, Y., Nonomura, M., Kato, H., Kouno, M., Bhalerao, R.P., Lagercrantz, U., Kasahara, H., Kohchi, T., and Bowman, J.L. (2015). Auxin Produced by the Indole-3-Pyruvic Acid Pathway Regulates Development and Gemmae Dormancy in the Liverwort Marchantia polymorpha. Plant Cell **27,** 1650-1669.

Endo, Y., Iwakawa, H.O., and Tomari, Y. (2013). Arabidopsis ARGONAUTE7 selects miR390 through multiple checkpoints during RISC assembly. EMBO

doi:10.6342/NTU202404007

Rep **14,** 652-658.

Fei, Q., Xia, R., and Meyers, B.C. (2013). Phased, secondary, small interfering RNAs in posttranscriptional regulatory networks. The Plant Cell **25,** 2400-2415.

Flores-Sandoval, E., Eklund, D.M., and Bowman, J.L. (2015). A Simple Auxin Transcriptional Response System Regulates Multiple Morphogenetic Processes in the Liverwort *Marchantia polymorpha*. PLOS Genetics **11,** e1005207.

Gaal, D.J., Dufresne, S.J., and Maravolo, N.C. (1982). Transport of ¹⁴C-indoleacetic Acid in the Hepatic Marchantia polymorpha. The Bryologist **85,** 410-418.

Garcia, D., Collier, S.A., Byrne, M.E., and Martienssen, R.A. (2006). Specification of leaf polarity in Arabidopsis via the trans-acting siRNA pathway. Curr Biol **16,** 933-938.

Ghosh, T.K., Kaneko, M., and Takezawa, D. (2016). Transient Assays of Gemmalings of the Liverwort Marchantia polymorpha for Studies of Abscisic Acid-induced Gene Expression. 低温生物工学会誌 **62,** 57-60.

Guo, L., Ma, M., Wu, L., Zhou, M., Li, M., Wu, B., Li, L., Liu, X., Jing, R., Chen, W., and Zhao, H. (2022). Modified expression of TaCYP78A5 enhances grain weight with yield potential by accumulating auxin in wheat (Triticum aestivum L.). Plant Biotechnol J **20,** 168-182.

Han, M.H., Goud, S., Song, L., and Fedoroff, N. (2004). The Arabidopsis double-stranded RNA-binding protein HYL1 plays a role in microRNA-mediated gene regulation. Proc Natl Acad Sci U S A **101,** 1093-1098.

Hasing, T., Rinaldi, E., Manrique, S., Colombo, L., Haak, D.C., Zaitlin, D., and Bombarely, A. (2019). Extensive phenotypic diversity in the cultivated Florist's Gloxinia, Sinningia speciosa (Lodd.) Hiern, is derived from the domestication of a single founder population. Plants, People, Planet **1,** 363-374.

Heisel, S.E., Zhang, Y., Allen, E., Guo, L., Reynolds, T.L., Yang, X., Kovalic, D., and Roberts, J.K. (2008). Characterization of unique small RNA populations from rice grain. PLoS One **3,** e2871.

Henderson, I.R., Zhang, X., Lu, C., Johnson, L., Meyers, B.C., Green, P.J., and Jacobsen, S.E. (2006). Dissecting Arabidopsis thaliana DICER function in small RNA processing, gene silencing and DNA methylation patterning. Nat Genet **38,** 721-725.

Hoshino, Y., Nakano, M., and Mii, M. (1995). Plant regeneration from cell suspension-derived protoplasts of Saintpaulia ionantha Wendl. Plant Cell Rep **14,** 341-344.

Hsu, H.C., Wang, C.N., Liang, C.H., Wang, C.C., and Kuo, Y.F. (2017). Association between Petal Form Variation and CYC2-like Genotype in a Hybrid Line of

doi:10.6342/NTU202404007

Sinningia speciosa. Front Plant Sci **8,** 558.

Huang, H., Wang, Z., Cheng, J., Zhao, W., Li, X., Wang, H., Zhang, Z., and Sui, X. (2013). An efficient cucumber (Cucumis sativus L.) protoplast isolation and transient expression system. Scientia Horticulturae **150,** 206-212.

Ishizaki, K., Chiyoda, S., Yamato, K.T., and Kohchi, T. (2008). *Agrobacterium*-mediated transformation of the haploid liverwort *Marchantia polymorpha* L., an emerging model for plant biology. Plant and Cell Physiology **49,** 1084-1091.

Ishizaki, K., Nishihama, R., Ueda, M., Inoue, K., Ishida, S., Nishimura, Y., Shikanai, T., and Kohchi, T. (2015). Development of Gateway Binary Vector Series with Four Different Selection Markers for the Liverwort *Marchantia polymorpha*. PLoS One **10,** e0138876.

Ito, T., and Meyerowitz, E.M. (2000). Overexpression of a gene encoding a cytochrome P450, *CYP78A9*, induces large and seedless fruit in arabidopsis. The Plant Cell **12,** 1541-1550.

Iwakawa, H., Melkonian, K., Schluter, T., Jeon, H.W., Nishihama, R., Motose, H., and Nakagami, H. (2021). Agrobacterium-Mediated Transient Transformation of Marchantia Liverworts. Plant Cell Physiol **62,** 1718-1727.

Jiang, L., Yoshida, T., Stiegert, S., Jing, Y., Alseekh, S., Lenhard, M., Perez-Alfocea, F., and Fernie, A.R. (2021). Multi-omics approach reveals the contribution of KLU to leaf longevity and drought tolerance. Plant Physiol **185,** 352-368.

Jones-Rhoades, M.W. (2012). Conservation and divergence in plant microRNAs. Plant Mol Biol **80,** 3-16.

Kato, H., Yasui, Y., and Ishizaki, K. (2020). Gemma cup and gemma development in *Marchantia polymorpha*. New Phytologist **228,** 459-465.

Katsumata, T., Fukazawa, J., Magome, H., Jikumaru, Y., Kamiya, Y., Natsume, M., Kawaide, H., and Yamaguchi, S. (2011). Involvement of the CYP78A subfamily of cytochrome P450 monooxygenases in protonema growth and gametophore formation in the moss *Physcomitrella patens*. Bioscience, Biotechnology, and Biochemistry **75,** 331-336.

Kim, V.N. (2008). Sorting out small RNAs. Cell **133,** 25-26.

Krasnikova, M.S., Goryunov, D.V., Troitsky, A.V., Solovyev, A.G., Ozerova, L.V., and Morozov, S.Y. (2013). Peculiar evolutionary history of miR390-guided TAS3-like genes in land plants. The Scientific World Journal **2013,** 924153.

Kubota, A., Ishizaki, K., Hosaka, M., and Kohchi, T. (2013). Efficient *Agrobacterium*-mediated transformation of the liverwort *Marchantia polymorpha* using regenerating thalli. Bioscience, Biotechnology, and Biochemistry **77,** 167-172.

Kumar, S., Stecher, G., Li, M., Knyaz, C., and Tamura, K. (2018). MEGA X:

doi:10.6342/NTU202404007

Molecular Evolutionary Genetics Analysis across Computing Platforms. Mol Biol Evol **35,** 1547-1549.

Kuo, W.-H., Hung, Y.-L., Wu, H.-W., Pan, Z.-J., Hong, C.-Y., and Wang, C.-N. (2018). Shoot regeneration process and optimization of Agrobacterium-mediated transformation in Sinningia speciosa. Plant Cell, Tissue and Organ Culture (PCTOC) **134,** 301-316.

Li, J., Liao, X., Zhou, S., Liu, S., Jiang, L., and Wang, G. (2018). Efficient protoplast isolation and transient gene expression system for Phalaenopsis hybrid cultivar 'Ruili Beauty'. In Vitro Cellular & Developmental Biology - Plant **54,** 87-93.

Li, J., Yue, L., Shen, Y., Sheng, Y., Zhan, X., Xu, G., and Xing, B. (2017). Phenanthrene-responsive microRNAs and their targets in wheat roots. Chemosphere **186,** 588-598.

Li, X., Bian, H., Song, D., Ma, S., Han, N., Wang, J., and Zhu, M. (2013). Flowering time control in ornamental gloxinia (Sinningia speciosa) by manipulation of miR159 expression. Ann Bot **111,** 791-799.

Liang, C., Wang, X., He, H., Xu, C., and Cui, J. (2023). Beyond Loading: Functions of Plant ARGONAUTE Proteins. Int J Mol Sci **24**.

Lin, H.Y., Chen, J.C., and Fang, S.C. (2018). A Protoplast Transient Expression System to Enable Molecular, Cellular, and Functional Studies in Phalaenopsis orchids. Front Plant Sci **9,** 843.

Lin, P.C., Lu, C.W., Shen, B.N., Lee, G.Z., Bowman, J.L., Arteaga-Vazquez, M.A., Liu, L.Y., Hong, S.F., Lo, C.F., Su, G.M., Kohchi, T., Ishizaki, K., Zachgo, S., Althoff, F., Takenaka, M., Yamato, K.T., and Lin, S.S. (2016). Identification of miRNAs and Their Targets in the Liverwort *Marchantia polymorpha* by Integrating RNA-Seq and Degradome Analyses. Plant and Cell Physiology **57,** 339-358.

Lin, S.S., and Bowman, J.L. (2018). MicroRNAs in *Marchantia polymorpha*. New Phytologist **220,** 409-416.

Lin, Y.C., Li, W., Chen, H., Li, Q., Sun, Y.H., Shi, R., Lin, C.Y., Wang, J.P., Chen, H.C., Chuang, L., Qu, G.Z., Sederoff, R.R., and Chiang, V.L. (2014). A simple improved-throughput xylem protoplast system for studying wood formation. Nat Protoc **9,** 2194-2205.

Lin, Y.Y., Fang, M.M., Lin, P.C., Chiu, M.T., Liu, L.Y., Lin, C.P., and Lin, S.S. (2013). Improving initial infectivity of the *Turnip mosaic virus* (TuMV) infectious clone by an mini binary vector via agro-infiltration. Botanical Studies **54,** 22.

Luo, L., Yang, X., Guo, M., Lan, T., Yu, Y., Mo, B., Chen, X., Gao, L., and Liu, L. (2021). *TRANS-ACTING SIRNA3*-derived short interfering RNAs confer

doi:10.6342/NTU202404007

cleavage of mRNAs in rice. Plant Physiology.

Luo, Q.J., Mittal, A., Jia, F., and Rock, C.D. (2012). An autoregulatory feedback loop involving PAP1 and TAS4 in response to sugars in Arabidopsis. Plant Mol Biol **80,** 117-129.

Maravolo, N.C. (1976). Polarity and Localization of Auxin Movement in the Hepatic, Marchantia polymorpha. American Journal of Botany **63,** 526-531.

Marin, E., Jouannet, V., Herz, A., Lokerse, A.S., Weijers, D., Vaucheret, H., Nussaume, L., Crespi, M.D., and Maizel, A. (2010). miR390, Arabidopsis TAS3 tasiRNAs, and their AUXIN RESPONSE FACTOR targets define an autoregulatory network quantitatively regulating lateral root growth. Plant Cell **22,** 1104-1117.

Marx, V. (2016). Plants: a tool box of cell-based assays. Nat Methods **13,** 551-554.

Mi, S., Cai, T., Hu, Y., Chen, Y., Hodges, E., Ni, F., Wu, L., Li, S., Zhou, H., Long, C., Chen, S., Hannon, G.J., and Qi, Y. (2008). Sorting of small RNAs into Arabidopsis argonaute complexes is directed by the 5' terminal nucleotide. Cell **133,** 116-127.

Miyoshi, K., Ahn, B.O., Kawakatsu, T., Ito, Y., Itoh, J., Nagato, Y., and Kurata, N. (2004). PLASTOCHRON1, a timekeeper of leaf initiation in rice, encodes cytochrome P450. Proc Natl Acad Sci U S A **101,** 875-880.

Montgomery, T.A., Howell, M.D., Cuperus, J.T., Li, D., Hansen, J.E., Alexander, A.L., Chapman, E.J., Fahlgren, N., Allen, E., and Carrington, J.C. (2008a). Specificity of ARGONAUTE7-miR390 interaction and dual functionality in *TAS3 trans-acting* siRNA formation. Cell **133,** 128-141.

Montgomery, T.A., Yoo, S.J., Fahlgren, N., Gilbert, S.D., Howell, M.D., Sullivan, C.M., Alexander, A., Nguyen, G., Allen, E., Ahn, J.H., and Carrington, J.C. (2008b). AGO1-miR173 complex initiates phased siRNA formation in plants. Proceedings of the National Academy of Sciences of the United States of America **105,** 20055-20062.

Morozov, S.Y., Milyutina, I.A., Erokhina, T.N., Ozerova, L.V., Troitsky, A.V., and Solovyev, A.G. (2018). TAS3 miR390-dependent loci in non-vascular land plants: towards a comprehensive reconstruction of the gene evolutionary history. PeerJ **6,** e4636.

Nanjareddy, K., Arthikala, M.-K., Blanco, L., Arellano, E.S., and Lara, M. (2016). Protoplast isolation, transient transformation of leaf mesophyll protoplasts and improved Agrobacterium-mediated leaf disc infiltration of Phaseolus vulgaris: tools for rapid gene expression analysis. BMC Biotechnology **16,** 53.

Nelson, D.R. (2018). Cytochrome P450 diversity in the tree of life. Biochimica et Biophysica Acta - Proteins and Proteomics **1866,** 141-154.

doi:10.6342/NTU202404007

Nien, Y.-C. (2018). Global analysis of small RNAs for controlling floral symmetry in *Sinningia speciosa*. In Institute of Ecology and Evolutionary Biology (National Taiwan University).

Niu, Q.W., Lin, S.S., Reyes, J.L., Chen, K.C., Wu, H.W., Yeh, S.D., and Chua, N.H. (2006). Expression of artificial microRNAs in transgenic Arabidopsis thaliana confers virus resistance. Nat Biotechnol **24,** 1420-1428.

Oh, M.-H., and Kim, S.-G. (1994). Plant regeneration from petal protoplast culture ofPetunia hybrida. Plant Cell, Tissue and Organ Culture **36,** 275-283.

Ohyama, K. (1996). Chloroplast and mitochondrial genomes from a liverwort, Marchantia polymorpha--gene organization and molecular evolution. Biosci Biotechnol Biochem **60,** 16-24.

Ohyama, K., Fukuzawa, H., Kohchi, T., Sano, T., Sano, S., Shirai, H., Umesono, K., Shiki, Y., Takeuchi, M., Chang, Z., and et al. (1988). Structure and organization of Marchantia polymorpha chloroplast genome. I. Cloning and gene identification. J Mol Biol **203,** 281-298.

Olmedo-Monfil, V., Duran-Figueroa, N., Arteaga-Vazquez, M., Demesa-Arevalo, E., Autran, D., Grimanelli, D., Slotkin, R.K., Martienssen, R.A., and Vielle-Calzada, J.P. (2010). Control of female gamete formation by a small RNA pathway in Arabidopsis. Nature **464,** 628-632.

Page, M.T., Parry, M.A.J., and Carmo-Silva, E. (2019). A high-throughput transient expression system for rice. Plant Cell Environ **42,** 2057-2064.

Pegler, J.L., Oultram, J.M.J., Curtin, S.J., Grof, C.P.L., and Eamens, A.L. (2019). Further Disruption of the *TAS3* Pathway via the Addition of the AGO7 Mutation to the DRB1, DRB2 or DRB4 Mutations Severely Impairs the Reproductive Competence of *Arabidopsis thaliana*. Agronomy **9,** 680.

Pietrykowska, H., Sierocka, I., Zielezinski, A., Alisha, A., Carrasco-Sanchez, J.C., Jarmolowski, A., Karlowski, W.M., and Szweykowska-Kulinska, Z. (2022). Biogenesis, conservation, and function of miRNA in liverworts. J Exp Bot **73,** 4528-4545.

Plavskin, Y., Nagashima, A., Perroud, P.F., Hasebe, M., Quatrano, R.S., Atwal, G.S., and Timmermans, M.C. (2016). Ancient trans-Acting siRNAs Confer Robustness and Sensitivity onto the Auxin Response. Dev Cell **36,** 276-289.

Pratt, A.J., and MacRae, I.J. (2009). The RNA-induced silencing complex: a versatile gene-silencing machine. J Biol Chem **284,** 17897-17901.

Rajagopalan, R., Vaucheret, H., Trejo, J., and Bartel, D.P. (2006). A diverse and evolutionarily fluid set of microRNAs in *Arabidopsis thaliana*. Genes & Development **20,** 3407-3425.

Ren, R., Gao, J., Lu, C., Wei, Y., Jin, J., Wong, S.M., Zhu, G., and Yang, F. (2020).

doi:10.6342/NTU202404007

Highly Efficient Protoplast Isolation and Transient Expression System for Functional Characterization of Flowering Related Genes in Cymbidium Orchids. Int J Mol Sci **21**.

Shen, B., Zhang, W., Zhang, J., Zhou, J., Wang, J., Chen, L., Wang, L., Hodgkins, A., Iyer, V., Huang, X., and Skarnes, W.C. (2014). Efficient genome modification by CRISPR-Cas9 nickase with minimal off-target effects. Nat Methods **11,** 399-402.

Shimamura, M. (2016). Marchantia polymorpha: Taxonomy, Phylogeny and Morphology of a Model System. Plant Cell Physiol **57,** 230-256.

Skog, L.E. (1984). A REVIEW OF CHROMOSOME NUMBERS IN THE GESNERIACEAE. Selbyana **7,** 252-273.

Song, L., Han, M.H., Lesicka, J., and Fedoroff, N. (2007). Arabidopsis primary microRNA processing proteins HYL1 and DCL1 define a nuclear body distinct from the Cajal body. Proc Natl Acad Sci U S A **104,** 5437-5442.

Stemmer, W.P., Crameri, A., Ha, K.D., Brennan, T.M., and Heyneker, H.L. (1995). Single-step assembly of a gene and entire plasmid from large numbers of oligodeoxyribonucleotides. Gene **164,** 49-53.

Sugano, S.S., Nishihama, R., Shirakawa, M., Takagi, J., Matsuda, Y., Ishida, S., Shimada, T., Hara-Nishimura, I., Osakabe, K., and Kohchi, T. (2018). Efficient CRISPR/Cas9-based genome editing and its application to conditional genetic analysis in *Marchantia polymorpha*. PLoS One **13,** e0205117.

Takeda, A., Iwasaki, S., Watanabe, T., Utsumi, M., and Watanabe, Y. (2008). The mechanism selecting the guide strand from small RNA duplexes is different among argonaute proteins. Plant Cell Physiol **49,** 493-500.

Talmor-Neiman, M., Stav, R., Klipcan, L., Buxdorf, K., Baulcombe, D.C., and Arazi, T. (2006). Identification of *trans-acting* siRNAs in moss and an RNA-dependent RNA polymerase required for their biogenesis. The Plant Journal **48,** 511-521.

Tamura, K., Nei, M., and Kumar, S. (2004). Prospects for inferring very large phylogenies by using the neighbor-joining method. Proc Natl Acad Sci U S A **101,** 11030-11035.

Tsuboyama-Tanaka, S., and Kodama, Y. (2015). AgarTrap-mediated genetic transformation using intact gemmae/gemmalings of the liverwort Marchantia polymorpha L. J Plant Res **128,** 337-344.

Tsuboyama, S., and Kodama, Y. (2014). AgarTrap: a simplified Agrobacterium-mediated transformation method for sporelings of the liverwort Marchantia polymorpha L. Plant Cell Physiol **55,** 229-236.

Tsuzuki, M., Nishihama, R., Ishizaki, K., Kurihara, Y., Matsui, M., Bowman, J.L.,

doi:10.6342/NTU202404007

Kohchi, T., Hamada, T., and Watanabe, Y. (2016). Profiling and Characterization of Small RNAs in the Liverwort, Marchantia polymorpha, Belonging to the First Diverged Land Plants. Plant Cell Physiol **57,** 359-372.

Vasav, A.P., and Barvkar, V.T. (2019). Phylogenomic analysis of cytochrome P450 multigene family and their differential expression analysis in *Solanum lycopersicum* L. suggested tissue specific promoters. BMC Genomics **20,** 116.

Vaucheret, H., Vazquez, F., Crete, P., and Bartel, D.P. (2004). The action of ARGONAUTE1 in the miRNA pathway and its regulation by the miRNA pathway are crucial for plant development. Genes Dev **18,** 1187-1197.

Vazquez, F., Vaucheret, H., Rajagopalan, R., Lepers, C., Gasciolli, V., Mallory, A.C., Hilbert, J.L., Bartel, D.P., and Crete, P. (2004). Endogenous *trans*-acting siRNAs regulate the accumulation of *Arabidopsis* mRNAs. Molecular Cell **16,** 69-79.

Voinnet, O. (2008). Use, tolerance and avoidance of amplified RNA silencing by plants. Trends Plant Sci **13,** 317-328.

Wang, J.W., Schwab, R., Czech, B., Mica, E., and Weigel, D. (2008). Dual effects of miR156-targeted *SPL* genes and *CYP78A5/KLUH* on plastochron length and organ size in *Arabidopsis thaliana*. The Plant Cell **20,** 1231-1243.

Westermann, J., Koebke, E., Lentz, R., Hulskamp, M., and Boisson-Dernier, A. (2020). A Comprehensive Toolkit for Quick and Easy Visualization of Marker Proteins, Protein-Protein Interactions and Cell Morphology in Marchantia polymorpha. Front Plant Sci **11,** 569194.

Williams, L., Carles, C.C., Osmont, K.S., and Fletcher, J.C. (2005). A database analysis method identifies an endogenous trans-acting short-interfering RNA that targets the *Arabidopsis ARF2*, *ARF3*, and *ARF4* genes. Proceedings of the National Academy of Sciences of the United States of America **102,** 9703-9708.

Willmann, M.R., and Poethig, R.S. (2007). Conservation and evolution of miRNA regulatory programs in plant development. Curr Opin Plant Biol **10,** 503-511.

Winkelmann, T., and Grunewaldt, J. (1995a). Genotypic variability for protoplast regeneration in Saintpaulia ionantha (H. Wendl.). Plant Cell Rep **14,** 704-707.

Winkelmann, T., and Grunewaldt, J. (1995b). Analysis of protoplast-derived plants of Saintpaulia ionantha H. Wendl. Plant Breeding **114,** 346-350.

Wu, F.H., Shen, S.C., Lee, L.Y., Lee, S.H., Chan, M.T., and Lin, C.S. (2009). Tape-Arabidopsis Sandwich - a simpler Arabidopsis protoplast isolation method. Plant Methods **5,** 16.

Wu, J.-Z., Liu, Q., Geng, X.-S., Li, K.-M., Luo, L.-J., and Liu, J.-P. (2017). Highly efficient mesophyll protoplast isolation and PEG-mediated transient gene expression for rapid and large-scale gene characterization in cassava (Manihot

doi:10.6342/NTU202404007

esculenta Crantz). BMC Biotechnology **17,** 29.

Xia, R., Xu, J., and Meyers, B.C. (2017). The Emergence, Evolution, and Diversification of the miR390-*TAS3-ARF* Pathway in Land Plants. The Plant Cell **29,** 1232-1247.

Xie, Z., Allen, E., Fahlgren, N., Calamar, A., Givan, S.A., and Carrington, J.C. (2005). Expression of Arabidopsis MIRNA genes. Plant Physiol **138,** 2145-2154.

Yan, J., Cai, X., Luo, J., Sato, S., Jiang, Q., Yang, J., Cao, X., Hu, X., Tabata, S., Gresshoff, P.M., and Luo, D. (2010). The REDUCED LEAFLET genes encode key components of the trans-acting small interfering RNA pathway and regulate compound leaf and flower development in Lotus japonicus. Plant Physiol **152,** 797-807.

Yang, L., Liu, Z., Lu, F., Dong, A., and Huang, H. (2006). SERRATE is a novel nuclear regulator in primary microRNA processing in Arabidopsis. Plant J **47,** 841-850.

Yang, M., Lu, H., Xue, F., and Ma, L. (2019). Identifying High Confidence microRNAs in the Developing Seeds of *Jatropha curcas*. Scientific Reports **9,** 4510.

Yang, Z., Sakai, M., Sayama, H., Shimeno, T., Yamaguchi, K., and Watanabe, N. (2009). Elucidation of the biochemical pathway of 2-phenylethanol from shikimic acid using isolated protoplasts of rose flowers. J Plant Physiol **166,** 887-891.

Yoo, S.D., Cho, Y.H., and Sheen, J. (2007). Arabidopsis mesophyll protoplasts: a versatile cell system for transient gene expression analysis. Nat Protoc **2,** 1565-1572.

Yoshikawa, M., Peragine, A., Park, M.Y., and Poethig, R.S. (2005). A pathway for the biogenesis of trans-acting siRNAs in *Arabidopsis*. Genes & Development **19,** 2164-2175.

You, C., Cui, J., Wang, H., Qi, X., Kuo, L.Y., Ma, H., Gao, L., Mo, B., and Chen, X. (2017). Conservation and divergence of small RNA pathways and microRNAs in land plants. Genome Biol **18,** 158.

Zaitlin, D., and Pierce, A.J. (2010). Nuclear DNA content in Sinningia (Gesneriaceae); intraspecific genome size variation and genome characterization in S. speciosa. Genome **53,** 1066-1082.

Zhang, B., Pan, X., Cannon, C.H., Cobb, G.P., and Anderson, T.A. (2006). Conservation and divergence of plant microRNA genes. Plant J **46,** 243-259.

Zhang, J., Fu, X.X., Li, R.Q., Zhao, X., Liu, Y., Li, M.H., Zwaenepoel, A., Ma, H., Goffinet, B., Guan, Y.L., Xue, J.Y., Liao, Y.Y., Wang, Q.F., Wang, Q.H.,

doi:10.6342/NTU202404007

Wang, J.Y., Zhang, G.Q., Wang, Z.W., Jia, Y., Wang, M.Z., Dong, S.S., Yang, J.F., Jiao, Y.N., Guo, Y.L., Kong, H.Z., Lu, A.M., Yang, H.M., Zhang, S.Z., Van de Peer, Y., Liu, Z.J., and Chen, Z.D. (2020). The hornwort genome and early land plant evolution. Nature Plants **6,** 107-118.

Zhou, M., Peng, H., Wu, L., Li, M., Guo, L., Chen, H., Wu, B., Liu, X., Zhao, H., Li, W., and Ma, M. (2022). TaKLU Plays as a Time Regulator of Leaf Growth via Auxin Signaling. Int J Mol Sci **23**.

doi:10.6342/NTU202404007

Appendix

Results in chapter 2 have been published as the article entitled, Yu-Ling Hung, Syuan-Fei Hong, Wei-Lun Wei, Shiuan Cheng, Jia-Zhen Yu, Veny Tjita, Qian-Yuan Yong, Ryuichi Nishihama, Takayuki Kohchi, John Bowman, Yuan-Chi Chien, Yen-Hsin Chiu, Ho-Chun Yang, Mei-Yeh Jade Lu, Zhao-Jun Pan, Chun-Neng Wang, and Shih-Shun Lin. 2024. Dual regulation of cytochrome P450 gene expression by two distinct small RNAs, a novel tasiRNA and miRNA, in *Marchantia polymorpha*. Plant and Cell Physiology, 65:1115-1134. (First author)

Results in chapter 3 have been published as the article entitled, Zhao-Jun Pan, Yu-Ling Hung, Tsun-Ying Chen, Yu-An Shih, Ying-Chung Jimmy Lin, and Chun-Neng Wang. 2022. Development of a petal protoplast transfection system for *Sinningia speciosa*. Applications in Plant Sciences. 10:e11476. (Co-first author).

doi:10.6342/NTU202404007